



People's and Democratic Republic of Algeria  
Ministry of Higher Education and Scientific Research  
Med Khider University of Biskra



Faculty of Exact Sciences and Nature and Life

Department of Matter Sciences

Thesis

Presented to obtain the degree of

Doctorate

Speciality : Physics of Materials

**Study of Thin Layers of Indium Oxide ( $\text{In}_2\text{O}_3$ ) Elaborated by  
Chemical Means**

Presented by:

**Adel Bouhdjer**

**To the Jury composed by:**

<b>A. Zerarka</b>	Professor	University Med Khider of Biskra	President
<b>A. Attaf</b>	Professor	University Med Khider of Biskra	Reporter
<b>S. Rahmane</b>	Professor	University Med Khider of Biskra	Examiner
<b>A. Chala</b>	Professor	University Med Khider of Biskra	Examiner
<b>M.S. Aida</b>	Professor	University of Constantine 1	Examiner
<b>N. Attaf</b>	Professor	University of Constantine 1	Examiner

Academic Year: 2015-2016

## Acknowledgements

Firstly, I thank GOD the whole powerful for having agreed his infinite kindness, courage, the force and patience to complete this modest work.

After that, I make a point of profoundly thanking to my supervisor Mister **Attaf Abdallah**, Professor at the Department of sciences of matter at Faculty of Exact Sciences and Sciences of Nature and Life in Mohamed Khider University of Biskra, for his help, support, guidance and encouragement. He has been a great support on all fronts and made my doctorat dissertation journey a memorable experience.

My first thanks and my heartfelt acknowledgments go to all the members of the jury:

**Zerarka Abdelouahab** Professor at the Department of sciences of matter at Faculty of Exact Sciences and Sciences of Nature and Life in Mohamed Khider University of Biskra, for the honor that makes to me by accepting the presidency of this jury.

**Saad Rahmane** Professor at the Department of sciences of matter at Faculty of Exact Sciences and Sciences of Nature and Life in Mohamed Khider University of Biskra, who agreed to accept to belong to the jury and to examine my work.

**Chala Abdelouahad** Professor at the Department of sciences of matter at Faculty of Exact Sciences and Sciences of Nature and Life in Mohamed Khider University of Biskra, who agreed to accept to belong to the jury and to examine my work.

**Mohamed Salah Aida** Professor at the University of Constantine 1, who agreed to accept to belong to the jury and to examine my work.

**Nadir Attaf** Professor at the University of Constantine 1, who agreed to accept to belong to the jury and to examine my work.

# ***TABLE OF CONTENTS***

<b>Generale Introduction</b> .....	1
------------------------------------	---

## **CHAPTER I: Indium oxide, properties and deposition techniques**

<b>I.1 Indium Oxide properties</b> .....	4
<b>I.1.1 Structural properties</b> .....	4
<b>I.1.2 Electrical properties</b> .....	5
I.1.2.1 Formation of oxygen vacancies.....	5
<b>I.1.3 Optical properties</b> .....	6
<b>I.1.4 Application of In<sub>2</sub>O<sub>3</sub></b> .....	7
<b>II.1 Thin film growth process</b> .....	8
<b>II.2 Thin film deposition processes</b> .....	9
<b>II.2.1 Physical processes</b> .....	12
II.2.1.1 Pulsed laser deposition.....	13
II.2.1.2 Molecular beam epitaxy.....	13
II.2.1.3 Sputtering.....	14
<b>II.2.2. Chemical deposition techniques</b> .....	14
II.2.2.1. Sol-Gel process.....	15
II.2.2.2. Electrodeposition.....	16
II.2.2.3. Plasma-assisted chemical vapor deposition.....	17
II.2.2.4. Spray pyrolysis.....	17
II.2.2.4.1. Advantages of spray pyrolysis.....	18
II.2.2.4.2. Fundamental aspects of spray pyrolysis.....	18

## **CHAPTER II: Technical preparation and characterization**

<b>II.1. In<sub>2</sub>O<sub>3</sub> thin films prepared by ultrasonic spray</b> .....	22
<b>II.1.2. Experimental conditions</b> .....	22
<b>II.1.3. Used substrates</b> .....	24
<b>II.1.4. Cleaning of the substrates</b> .....	24
<b>II.1.5. Preparation of the solutions</b> .....	25
<b>II.1.6. Used Montage</b> .....	26

<b>II.2. Characterization methods of <math>\text{In}_2\text{O}_3</math></b> .....	28
<b>II.2.1 X-ray diffraction</b> .....	28
<b>II.2.2. Determination of the grains size</b> .....	28
<b>II.2.3. Determination of the lattice parameters</b> .....	29
<b>II.2.4. Strain Determination</b> .....	29
<b>II.2.5. Determination of the dislocation density ( )</b> .....	29
<b>II.2.6. Scanning electron microscopy (SEM)</b> .....	29
<b>II.2.7. Measurement of film thickness by SEM</b> .....	31
<b>II.2.8. Energy Dispersive X-ray analysis(EDX)</b> .....	32
<b>II.2.9. Infrared Spectroscopy</b> .....	32
<b>II.2.10. Optical characterization</b> .....	33
<b>II.2.11. Optical Gap</b> .....	35
<b>II.2.12. Disorder calculating</b> .....	36
<b>II.2.13. Refractive index</b> .....	37
<b>II.2.14. Four-point probe resistivity measurements</b> .....	37

### **CHAPTER III: Deposition times influence on indium oxide thin films properties**

<b>III.1. Introduction</b> .....	40
<b>III.2. Growth rate</b> .....	40
<b>III.3. XRD analysis</b> .....	41
<b>III.4. Morphological properties</b> .....	47
<b>III.5. optical properties</b> .....	51
<b>III.6. Electrical properties</b> .....	54
<b>III.7. Conclusion</b> .....	56

### **CHAPTER IV: Solution flow rate influence on properties of indium oxide thin films**

<b>IV.1. Growth rate</b> .....	58
<b>IV.2. Structural properties</b> .....	59
<b>IV.3. Morphological properties</b> .....	63
<b>IV.4. optical properties</b> .....	66
<b>IV.5. Electrical properties</b> .....	71
<b>IV.6. Conclusion</b> .....	72

**CHAPTER V:Influence of the Surface Substrate and annealing temperature on indium oxide thin films properties**

**V.I.1. Introduction.....74**

**V.I.2.Surface Substrate affects on indium oxide thin films properties.....74**

**V.I.2.1.Growth rate.....74**

**V.I.2. 2. Structural properties.....75**

**V.I.2.3. Morphological properties.....81**

**V.I.2.4. optical properties.....82**

**V.I.2.5. Electrical properties.....84**

**V.I.2.6. Conclusions.....85**

**V.II. Effects of annealing temperature on indium oxide thin films properties.....86**

**V.II.1. Structural properties.....86**

**V.II.2. Optical properties.....89**

**V.II.3. Electrical properties.....91**

**V.II.4. Conclusions.....91**

**General conclusionand perspectives.....92**

**References.....94**

**Publications produced through this work.....101**

# General Introduction

Transparent Conductive Oxide (TCO) thin films are technologically important due to their high optical transparency, in the visible region, wide band gap and good electrical conductivity. Furthermore, among them, indium oxide ( $\text{In}_2\text{O}_3$ ) thin film has received much attention. It is a wide band-gap semiconductor and has a band gap of 3.5–3.75 eV, a cubic (Ia3) structure of lattice constant 1.0117 nm, dielectric constant of 8.9, and refractive index 2.0–2.1[1]. This unique combination of electrical and optical properties has led numerous researchers to a thorough investigation of the growth and characterization of thin semiconducting indium oxide films. It is frequently used for photovoltaic devices, transparent windows, liquid crystal displays (LCD), light emitting diodes (LED), solar cell, gas sensors and anti-reflecting coatings [2].

To date, there are numerous deposition techniques that have been demonstrated to grow  $\text{In}_2\text{O}_3$  films such as spray pyrolysis [3], vacuum evaporation [4], rf and dc sputtering [5,6], sol gel [7], pulsed laser ablation [8], molecular beam epitaxy (MBE) [9] and metal organic chemical vapor deposition (MOCVD) [10]. However, the properties of  $\text{In}_2\text{O}_3$  films depend strongly by the used deposition technique; each deposition method yields films with varied properties. In this work we will focus on the spray ultrasonic technique which is a method suitable for large-scale production. It has several advantages in producing nanocrystalline thin films, such as, relatively homogeneous composition, inexpensive and reproducible, commercially viable.

Several published literatures show that the film's properties are dependent from the film deposition parameters such as: substrate–nozzle distance (SND) [11] substrate temperature [12,13] and doping [14]. The aim of this thesis is to study the structural, morphological, optical and electrical properties of  $\text{In}_2\text{O}_3$  films prepared by spray ultrasonic technique. To this end, we want to fix the optimal parameters which are represented in deposition time, solution flow rate, substrate nature, and annealing temperature. These parameters make the thin films of  $\text{In}_2\text{O}_3$  applicable for optoelectronic and photovoltaic applications (gas sensors, solar cells...etc).

The thesis is divided into 5 chapters. In the first chapter, we present fundamental physical properties of indium oxide with their applications. In addition, we explain various depositions techniques used to develop  $\text{In}_2\text{O}_3$  films. The second chapter is devoted about the experimental condition and methods which have been used in this thesis for the growth and characterization of the  $\text{In}_2\text{O}_3$  films.

In the chapter III, influence of the deposition time on the structural, morphological, optical and electrical properties of sprayed  $\text{In}_2\text{O}_3$  films is presented; and we evaluated the relationship

between these properties in general. The fourth chapter is devoted about effect of the solution flow rate on the sprayed  $\text{In}_2\text{O}_3$  thin films properties. In the chapter V, influence of the surface substrate and annealing temperature on indium oxide thin films properties are presented.

Finally, we report general conclusion about the results obtained in this work.

# Chapter I

## Indium Oxide, properties and deposition techniques

In this chapter we will present the fundamental physical properties of indium oxide thin film. In addition, we explain various deposition techniques used to develop  $\text{In}_2\text{O}_3$  films.

## I.1 Indium oxide properties:

We will present the fundamental physical properties such as the structural, optical and electrical properties.

### I.1.1 Structural properties:

It is known that indium oxide crystallizes in two different structures as body centered cubic and hexagonal. The body centered cubic structure is a bixbyite  $\text{Mn}_2\text{O}_3$  type, also called C-type rare earth oxide structure [15,16]. The bixbyite structure can be obtained by removing one fourth of the anions from the fluorite structure and allowing for small shifts of the ions. 32 cations occupy the 8 b and 24 d positions (see Figure I.1). Each cation resides at the center of a distorted cube, with six corners occupied by oxygen anions. All 8 b cations are coordinated to six oxygen anions at a distance of  $2.18\text{\AA}$  and to 2 oxygen interstitial positions, which lie along a body diagonal of the cube. The 24 d cations exhibit less symmetry as they are coordinated to six oxygen anions at three distances and to 2 oxygen interstitial sites along a face diagonal of the cube. The 48 oxygen anions are coordinated to four cations [17].

The hexagonal type is a high-pressure type phase obtained at 68 K bar and at a temperature 800-1500 °C [18]. The structure is of the corundum, or  $\text{Al}_2\text{O}_3$  type, and has 6 molecules per unit cell.

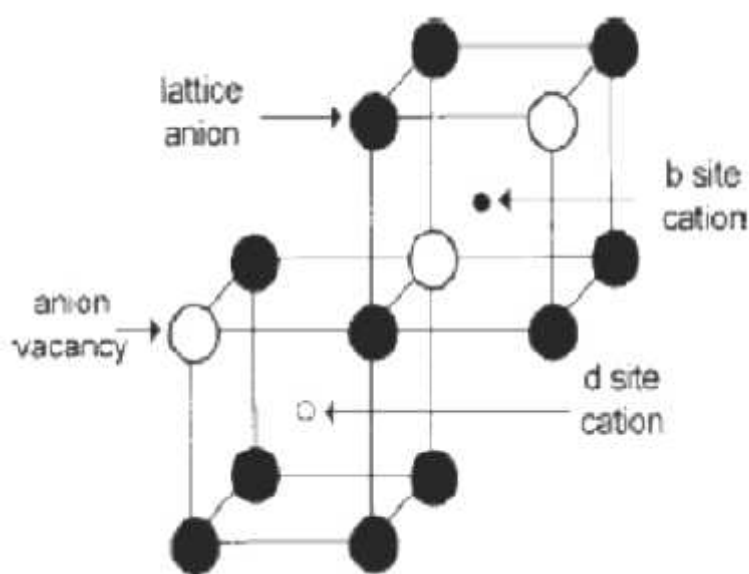


Figure.I.1 Cubic bixbyite structure showing the anion vacancy [17]

## I.1.2 Electrical properties:

Conduction in indium oxide films is attributed to oxygen vacancies and interstitial doping atoms in the indium oxide crystal lattice. Instead of the stoichiometric structure  $(\text{In}^{3+})_2(\text{O}^{2-})_3$ , oxygen deficiency creates a nonstoichiometric, or substoichiometric structure. The conduction mechanism for the indium oxide system is typically explained by its defect chemistry [19]. The undoped non-stoichiometric indium oxide film can be expressed as



where  $x$  represents the number of doubly charged oxygen vacancies,  $(\text{V}_\text{O})$ , and is typically less than 1%, depending on the oxidation state [20], and the  $e'$  represents the electrons needed for charge neutrality. This results in n-type conduction in the films. Charge carrier concentrations for indium oxide films are reported to be approximately  $10^{19}$ - $10^{20} \text{ cm}^{-3}$ . At low temperatures the conduction is strongly related to the oxygen vacancies since the band gap, of approximately 3.75 eV for  $\text{In}_2\text{O}_3$ , is too large to allow significant thermal excitation for intrinsic conduction to have an effect. The intrinsic conduction mechanism involves direct excitation of electrons from the valance band to the conduction band. At temperatures of approximately 800°C intrinsic conduction has been shown to dominate [21].

### I.1.2.1 Formation of oxygen vacancies:

In a crystal of an ionic compound the atoms are charged, and the cations and anions may be attributed with a definite valence. In the case of oxides, the oxygen ions in the regular sites are considered to have a valence of -2. The cations have a positive valence, so that the sum of all the positive and negative charges in the compound becomes equal to zero. This charge of the atoms in normal sites is termed the actual charge of the atom. The point defects may be neutral or charged. However, the charge on the defects is considered relative to the perfect crystal. This relative charge is termed the effective charge of the defect.

If a crystal is to be electrically neutral, the sum of all effective positive charges must be equal with the sum of all effective negative charges:

$$\text{pos. effective charges} = \text{neg. effective charges} \quad (\text{I.2})$$

This principle of electroneutrality forms one of the basic equations and conditions to treat defect equilibria and to evaluate defect concentrations in crystals.

When vacancies are present and thus when atoms in normal sites are missing, part or all of the actual charge of the missing atom may be absent from the vacant site. The process of the formation of an oxygen vacancy in a binary metal oxide has been described in detail by Kofstad [22]. An oxygen vacancy is formed when an oxygen atom in a normal site is removed. In this process, the two negative actual charges, i.e. two electrons, of the oxygen ion are left in the crystal. If both of these two electrons are localized at the oxygen vacancy, the oxygen vacancy has two negative actual charges and the charge is the same as in a perfect crystal. In this case, the oxygen vacancy has zero effective charge. Such vacancies are neutral. If one or both of the localized electrons are excited and transferred away from the neighborhood of the oxygen vacancy, the oxygen vacancy becomes singly or doubly ionized, respectively. Since electrons are removed, the ionized oxygen vacancies will have an effective positive charge with respect to the perfect crystal. The charged oxygen vacancy becomes an electron trapping site but in this process one or two electrons are available for conduction. For the conduction to be efficient, it is clear, that the volume fraction of traps must be small. Typical free electron concentrations observed in binary oxides are in the region  $10^{17} - 10^{21} \text{cm}^{-3}$ . Even at an electron concentration of  $10^{21} \text{cm}^{-3}$ . The oxides used as transparent conductors are all chemically unstable. Therefore, they are relatively easy to oxidise and reduce.

### I.1.3 Optical properties:

The previous sections showed that the conduction mechanism in the undoped and doped films of indium oxide is related to the oxygen content of the film. An oxygen deficiency generates charge carriers in indium oxide. In tin doped indium oxide the oxygen content effects conduction in the film through the generation of traps and tin oxide complexes. Generally, a lower oxygen content in the films corresponds to a higher conductivity.

However, oxygen deficient films tend to be less transparent than films with an oxygen surplus. This trade of between a large number of charge carriers needed for conduction and a limited number needed for low absorption illustrates the need to critically control the oxygen content in the films.

An electromagnetic wave interacting with these layers will be completely absorptive by this one if energy associated with the electromagnetic wave is able to transfer from the electrons of the valence band to the band from conduction.

The index of refraction in the visible area extends between 1.9 and 2.08. Muller brought back an effective mass  $m^*=0,3 m_e$  for the electrons of conduction [23].

### I.1.4 Application of $\text{In}_2\text{O}_3$ :

Unique transparent and conducting properties of indium oxide thin films ( $\text{In}_2\text{O}_3$ ) lead them for numerous optoelectronic applications such as:

#### 1- Gas sensors

There is no commonly accepted definition for sensor. However, in order to make clear what is designated here by sensor, it will be adopted one of the commonly accepted definitions. For this purpose, it was chosen a definition given by Jacob Fraden in the Handbook of modern sensors [24], which states that “a sensor is a device that receives a signal or stimulus and responds with an electrical signal”. The reason for the output of a sensor to be limited to electrical signals is related to the present development of signal processing, that is almost exclusively performed using electronic devices. Given this definition a sensor should be a device that receives a physical, chemical or biological signal and converts it into an electric signal, which should be compatible with electronic circuits. This definition may also be supported from the etymological origin of the word sensor. Sensor seems to come from the word sense given that usually sensor devices try to mimic or reproduce human senses' characteristics. In the biological senses the output is also an electrical signal that is transmitted to the nervous system. Recently a sufficient amount of work has been reported on materials like  $\text{In}_2\text{O}_3$  and Indium Tin Oxide (ITO) to detect hydrocarbon gases, ozone, nitric oxide gases etc. [25.26].

#### 2- Transparent Electrodes for Photovoltaics (TCO)

Transparent conducting oxide materials (TCO) underpin the photovoltaic industry by providing the transparent electrodes for thin film solar cells, amorphous silicon solar cells, dye sensitized solar cells (DSSC) and polymer based solar cells [27.28].

Traditional crystalline silicon solar cells have very high electron mobilities within the core layer, owing to the large crystal grains and relatively few imperfections in the silicon. This high mobility means that traditionally a grid of thin metal wires have been utilized as the top electrode of solar cells. Where the metal grid functions to collect the current, but it covers a low enough surface area to still let in the light. However, with the next generation of thin film materials which are based on polycrystalline or amorphous materials, the electron mobility is much lower [29]. This reduced mobility means that lateral resistance across the surface of the solar cell is too high to use metal grids. As-such, third generation thin film solar cells use highly conductive, transparent conducting thin films as the top layer contact electrode on solar cells, where They prevent lateral resistive losses across the top electrode surface whilst maintaining high transmittance of the

light into the absorbing layer of the solar cell stack [30]. Several work revealed that indium oxide can be used as electrodes in solar cell [31.32].

## II.1 Thin film growth process :

Any thin-film deposition process involves three main steps:

- 1- Production of the appropriate atomic, molecular, or ionic species.
- 2- Transport of these species to the substrate through a medium.
- 3- Condensation on the substrate, either directly or via a chemical and/or electrochemical reaction, to form a solid deposit.

The formation of thin film is carried out by a combination of nucleation and growth process. The sequences of the growth can be presented as follows:

- 1- The unit species, at the time of the impact on the substrate, lose their velocity component normal to the substrate and are physically adsorbed on the substrate surface.
- 2- The adsorbed species are not in thermodynamic balance with the substrate, and thus move over the substrate surface. In this process they interact among themselves, forming bigger clusters.
- 3- The clusters or the nuclei, as they are called, are thermodynamically unstable and may tend to desorb in time, depending on the deposition parameters. If the deposition parameters are such that a cluster collides with other adsorbed species before getting desorbed, it starts growing in size. After reaching a certain critical size, the cluster becomes thermodynamically stable and the nucleation barrier is said to have been overcome. This step involving the formation of stable, chemisorbed, critical-sized nuclei is called the nucleation stage.
- 4- The small islands continue to grow in a number and dimension until they reach a density of nucleation known as saturation. This density of nucleation and the average dimension of the small islands depend on several parameters such as energy on the incidental species, their quantity by unit of time and surface, energies of activation, absorption, desorption, the thermal diffusion, the temperature, the topology and the chemical nature of the substrate. A small island can grow parallel to the surface of the substrate by surface diffusion of the absorptive species or perpendicular by direct impact of the incidental species on the small island. In general, the speed of side growth is much larger than the speed of growth perpendicular.

- 5- The following step in the process of formation of the thin layer is the coalescence stage, in which the small islands start coalescing with each other in an attempt to reduce the substrate surface area. This step can be accelerated by increasing in mobility of surface of the species adsorbed, for example by increasing the temperature of the substrate. In some cases, formation of new nuclei may occur on areas freshly exposed as a consequence of coalescence.
- 6- Larger islands grow together, leaving channels and holes of uncovered substrate. The structure of the films at this stage changes from discontinuous island type to porous network type. Filling of the channels and holes forms a completely continuous film.

One can thus summarize the process of growth of a thin layer by saying that it is one statistical continuation of nucleation, and then a growth by diffusion of surface and formation of small islands, then a formation of islands of greater dimensions, and finally formation of a layer continue by filling of species between these islands. Depending on the thermodynamic parameters of the deposit and the substrate surface, the initial nucleation and growth stages may be described as (a) island type, called Volmer-Weber type, (b) layer type, called Frank-van der Merwe type, and (c) mixed type, called Stranski-Krastanov type. This is illustrated in Fig. I.2. In almost all practical cases, the growth takes place by island formation.

## II.2 Thin Film Deposition Processes:

The vast varieties of thin film materials, their deposition processing and fabrication techniques, spectroscopic characterization and optical characterization probes that are used to produce the devices. It is possible to classify these techniques in two ways [33, 34].

- Physical Process
- Chemical Process

Physical method covers the deposition techniques which depends on the evaporation or ejection of the material from a source, i.e. evaporation or sputtering, whereas chemical methods depend on physical properties. Structure-property relationships are the key features of such devices and basis of thin film technologies. Underlying the performance and economics of thin film components are the manufacturing techniques on a specific chemical reaction [35]. Thus chemical reactions may depend on thermal effects, as in vapour phase deposition and thermal growth. However, in all these cases a definite chemical reaction is required to obtain the final film.

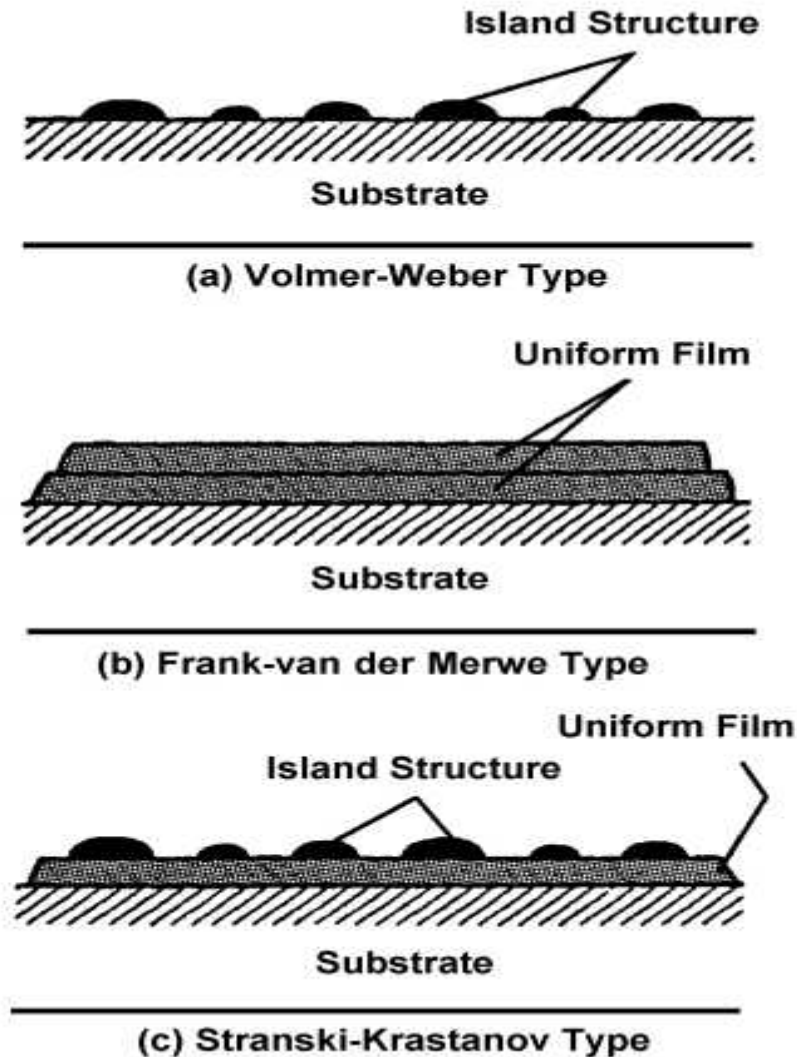


Figure.I.2 Three modes of thin film growth processes.

When one seeks to classify deposition of films by chemical methods, one finds that they can be classified into two classes. The first of these classes is concerned with the chemical formation of the film from medium, and typical methods involved are electroplating, chemical reduction plating and vapour phase deposition. A second class is that of formation of this film from the precursor ingredients e.g. iodization, gaseous iodization, thermal growth, sputtering ion beam implantation, CVD, MOCVD and vacuum evaporation.

The methods summarized in table.I.1. are often capable of producing films defined as thin films, i.e.  $1\ \mu\text{m}$  or less and films defined as thick films, i.e.  $1\ \mu\text{m}$  or more. However, there are certain techniques which are only capable of producing thick films and these include screen printing, glazing, electrophoretic deposition, flame spraying and painting.

**Thin Film Deposition Techniques**

<b>PHYSICAL</b>		<b>CHEMICAL</b>	
		Gas Phase	Liquid Phase
Sputtering	Evaporation	Chemical vapour Deposition	Electro-deposition
Glow discharge DC sputtering	Vacuum Evaporation	Laser Chemical vapour deposition	Chemical bath deposition (CBD) / Arrested Precipitation Technique (APT)
Triode sputtering	Resistive heating Evaporation	Photo-chemical vapour deposition	Electro less deposition
Getter sputtering	Flash Evaporation	Plasma enhanced vapour deposition	Anodisation
Radio Frequency sputtering	Electron beam Evaporation	Metal-Organo Chemical Vapour Deposition (MOCVD)	Liquid phase Epitaxy
Magnetron sputtering	Laser Evaporation		Sol- gel
			Spin Coating
			Spray-pyrolysis technique (SPT)
A.C. Sputtering	R. F. Heating		Ultrasonic (SPT)

Table.I.1 Thin film deposition processes.

### II.2.1 Physical Processes:

Evaporation or sublimation techniques are widely used for the preparation of thin layers. A very large number of materials can be evaporated and, if the evaporation is undertaken in vacuum system, the evaporation temperature will be very considerably reduced, the amount of impurities in the growing layer will be minimised. Two types of thermal evaporation processes are shown in Fig. I.3.

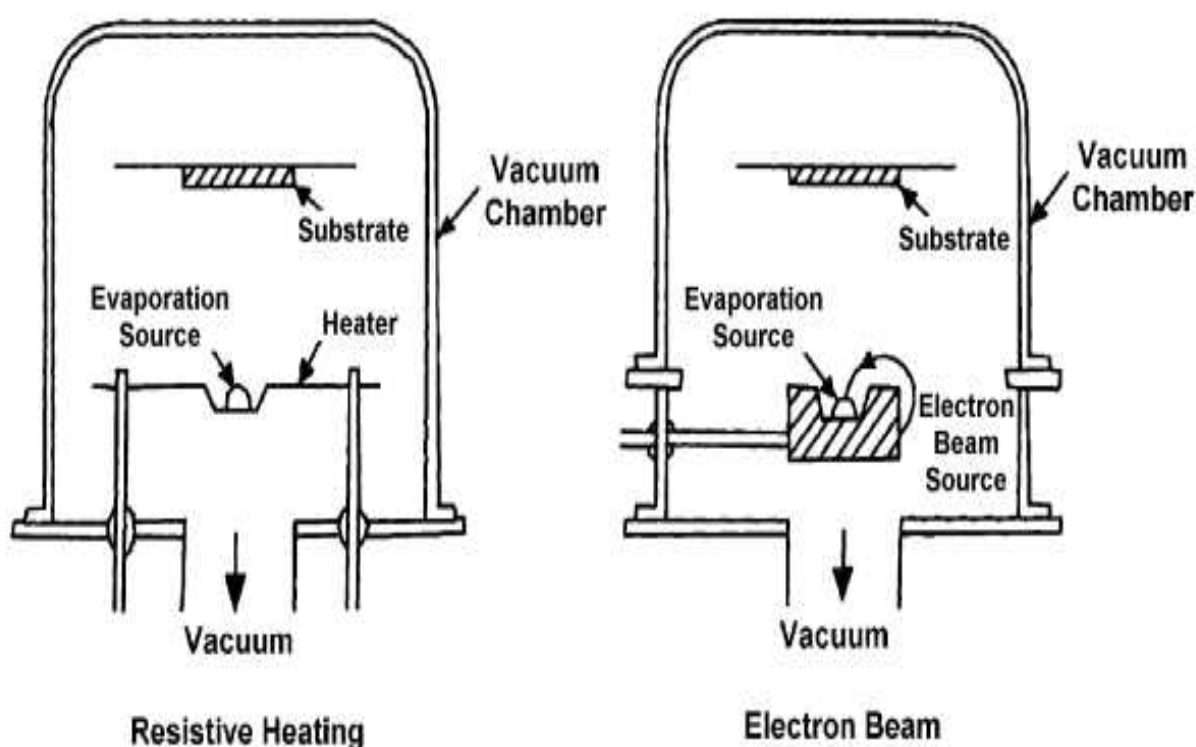


Figure.I.3 Thermal evaporation process.

Resistive heating is most commonly used for the deposition of thin films. The source materials are evaporated by a resistively heated filament or boat, generally made of refractory metals such as W, Mo, or Ta, with or without ceramic coatings. Crucibles of quartz, graphite, alumina, beryllia, boron-nitride, or zirconia are used with indirect heating. The refractory metals are evaporated by electron-beam deposition since simple resistive heating cannot evaporate high melting point materials.

### II.2.1.1 Pulsed laser deposition :

(PLD) is an improved thermal process used for the deposition of alloys and/or compounds with a controlled chemical composition. The principle of the deposit of thin layers by laser ablation (Pulsed Laser Deposition) is relatively simple. An impulse laser beam (more often nanosecond) is focused on a massive target, placed in one enclosure ultra-high vacuum. Under certain conditions of interaction, a quantity of matter target is ejected, and can be collected on a substrate placed in opposite. The nature and the quality of the deposit depend on many parameters (energy of the laser, nature and pressure of residual gas in the enclosure ...). In all the cases, it is necessary to control the transport of the species of the target until the substrate.

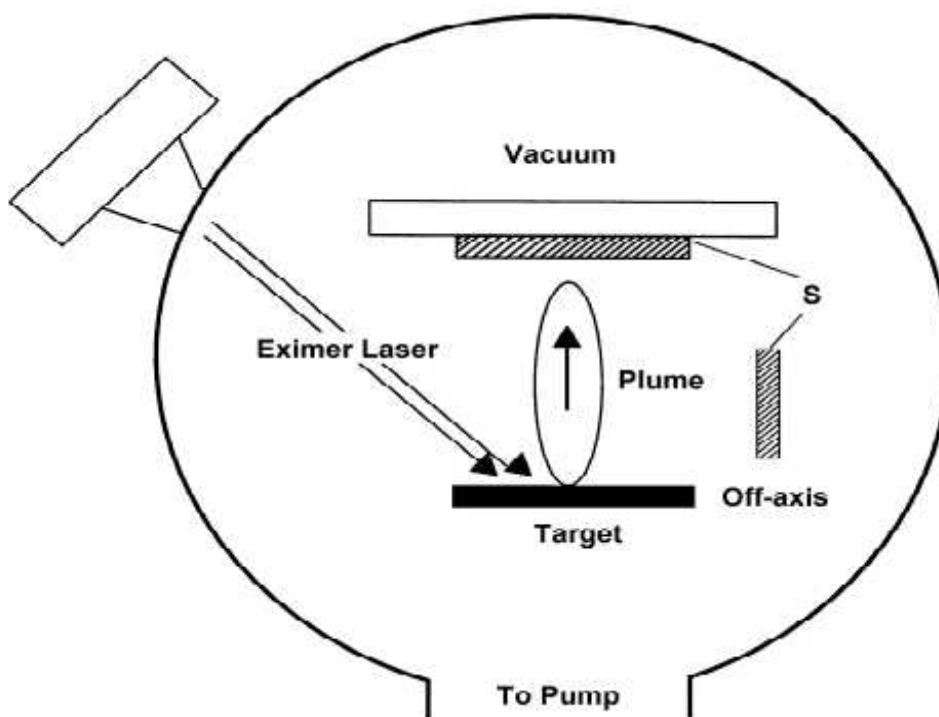


Figure. I.4. Pulsed laser deposition (PLD) uses a laser to ablate the source material from a target. The material is collected on substrates (S) in the form of thin films.

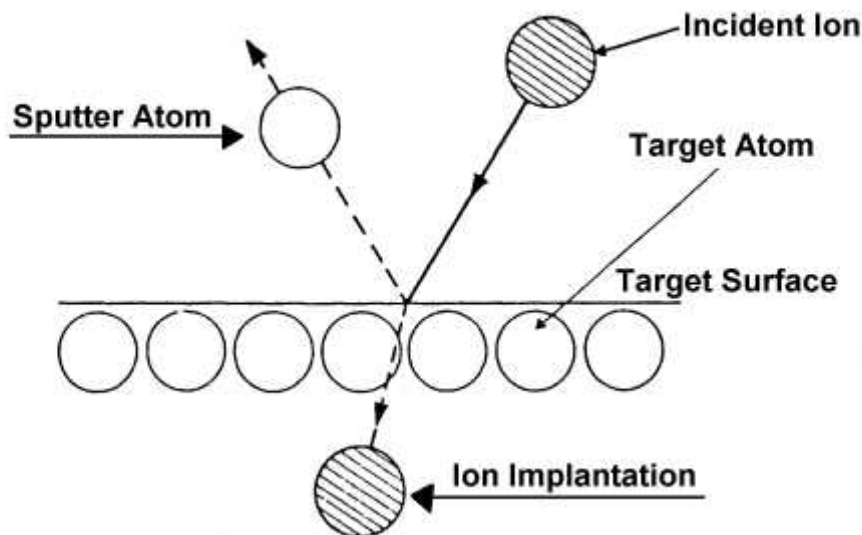
### II.2.1.2 Molecular Beam Epitaxy (MEB):

MBE is a sophisticated, finely controlled method for growing single-crystal epitaxial films in a high vacuum ( $10^{-11}$  torr). The films are formed on single-crystal substrates by slowly evaporating the elemental or molecular constituents of the film from separate Knudsen effusion source cells (deep crucibles in furnaces with cooled shrouds) onto substrates held at a temperature appropriate for chemical reaction, epitaxy, and re-evaporation of excess reactants. The furnaces produce atomic

or molecular beams of relatively small diameter, which are directed at the heated substrate, usually silicon or gallium arsenide. Fast shutters are interposed between the sources and the substrates. By controlling these shutters, one can grow superlattices with precisely controlled uniformity, lattice match, composition, dopant concentrations, thicknesses, and interfaces down to the level of atomic layers.

### II.2.1.3 Sputtering:

When a solid surface is bombarded with energetic particles such as accelerated ions, surface atoms of the solid are scattered backward due to collisions between the surface atoms and the energetic particles, as shown in Fig. I.5. this phenomenon is called back-sputtering, or simply sputtering. When a thin foil is bombarded with energetic particles, some of the scattered atoms transmit through the foil. The phenomenon is called transmission sputtering. The word “spluttering” is synonymous with “sputtering.” Cathode sputtering, cathode disintegration, and impact evaporation are also used in the same sense.



Figur I.5. The physical sputtering processes.

### II.2.2. Chemical Deposition Techniques:

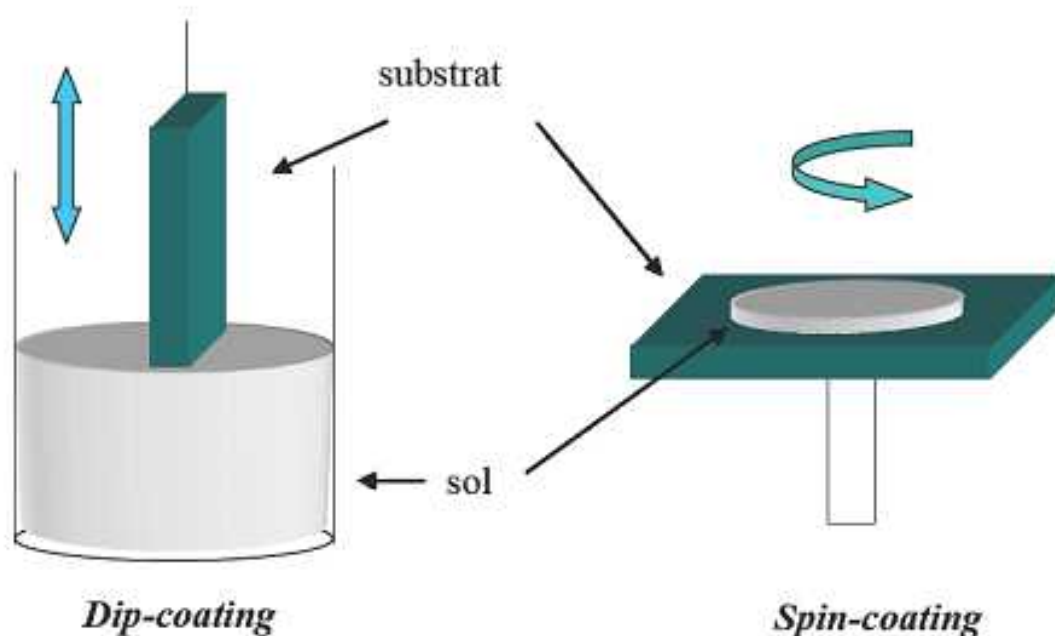
A deposition technique, in which chemical components react on the surface of the substrate to form a solid film is called chemical deposition technique [36].

### II.2.2.1. Sol-Gel Process:

two types of processes can be used to form thin films:

**Dip Coating:** Dip coating or immersion coating is a simple old way of thin film deposition by immersing a substrate in the solution of the coating material at a constant speed (preferably judder free). Film thickness is set by the competition among viscous force, capillary (surface tension) force and gravity. Thickness and uniformity can be sensitive to flow conditions of the substrate in the liquid bath and gas overhead. The withdraw speed of the substrate, the thicker of the film deposited. Theoretical prediction of process performance is more difficult, and the control of the process more demanding [37].

**Spin Coating:** Spin coating process consists of putting the drops of liquid precursor on the surface of a spinning substrate. The film formed on the substrate results from two balancing forces: the centrifugal force (due to spinning) which drives the viscous sol radially outwards and viscous force (due to friction) which acts radially inwards. Spin coating is the cheapest film production method in silicon technology. However, thinner films (<100 nm) are hard to make and can waste 98% of the process materials [38].

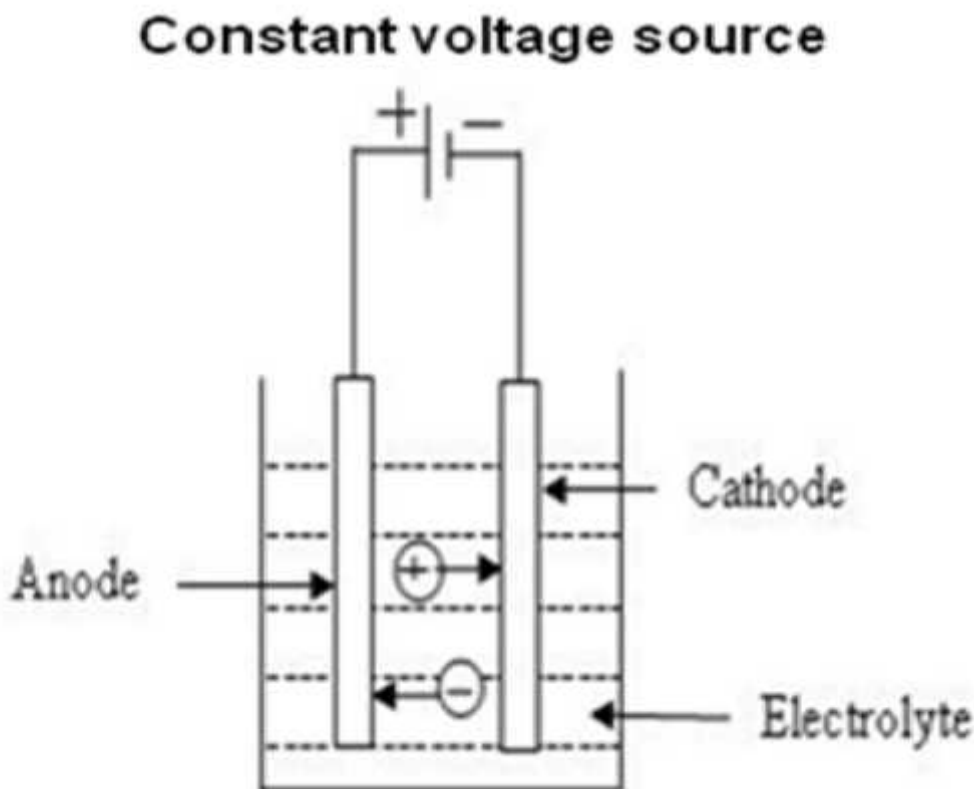


Figur I.6. Sol-gel process.[39]

### II.2.2.2. Electrodeposition:

Electrodeposition, also known as electrochemical deposition or electro crystallization, it is one of the most useful techniques for preparing thin films on the surface of conducting substrate. Besides advantages such as low temperature, the electrodeposition is the simplest of the chemical methods, and it has many advantages like [34]:

- Toxic gaseous precursors need not to be used (unlike gas phase methods).
- Deposition on complex shapes is possible.
- Structurally and compositionally modulated alloys and compounds can be deposited which are not possible with other deposition techniques.
- In most of the cases the deposition can be carried out at room temperature enabling to form the semiconductor junctions without interdiffusion.
- The deposition process can be controlled more accurately and easily.



Figur I.7. Schematic diagram explaining the electrodeposition

### II.2.2.3. Plasma-Assisted Chemical Vapor Deposition (PACVD):

Is one of the modifications of the conventional CVD process. In the PACVD system, electric power is supplied to the reactor to generate the plasma. The power is supplied by an induction coil from outside of the chamber, or directly by diode glow-discharge electrodes. Usually the working pressure is in the range of 10 to 100 Pa. In the plasma, the degree of ionization is typically only  $10^{-4}$ , so the gas in the reactor consists mostly of neutrals. Ions and electrons travel through the neutrals and get energy from the electric field in the plasma. The average electron energy is 2 to 8 eV, which corresponds to electron temperatures of 23,000 to 92,800 K. In contrast, the heavy, much more immobile, ions cannot effectively get enough coupling energy from the electric field. The ions in the plasma show slightly higher energy than the neutral gas molecules at room temperature. Typically the temperature of the ions in plasma is around 500 K.

### II.2.2.4. Spray Pyrolysis:

In this deposition technique, liquid precursors are sprayed on substrates maintained at elevated temperatures. The sprayed micro-droplets reaching the hot substrate surface undergo pyrolytic decomposition and form a cluster of crystallites the sprayed materials. In this deposition technique the Droplets are generated by tow way: the solution containing the precursors is carried by a relatively pressurized air flow; the atomization into droplets is formed at the nozzle orifice. This method is called the pneumatic spray (PS) (ii) the solution is atomized by an ultrasonic wave generator (see figure I.8); this is so called ultrasonic spray (USP). The droplet size is more uniform and finer in ultrasonic spray jet than in pneumatic spray. Moreover, the droplet velocity are relatively low in USP than in PS, these differences may have an influence in films growth in these two methods.

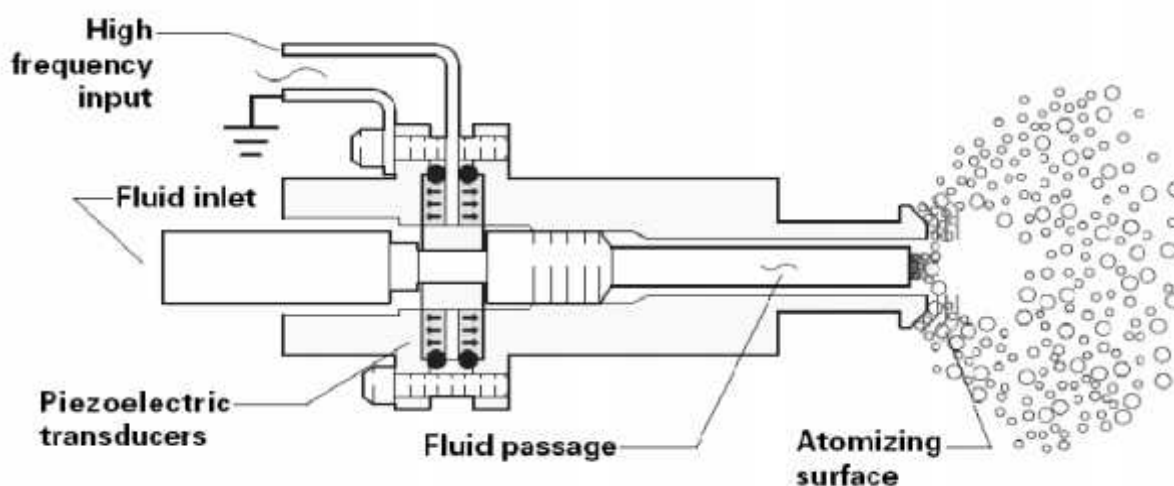


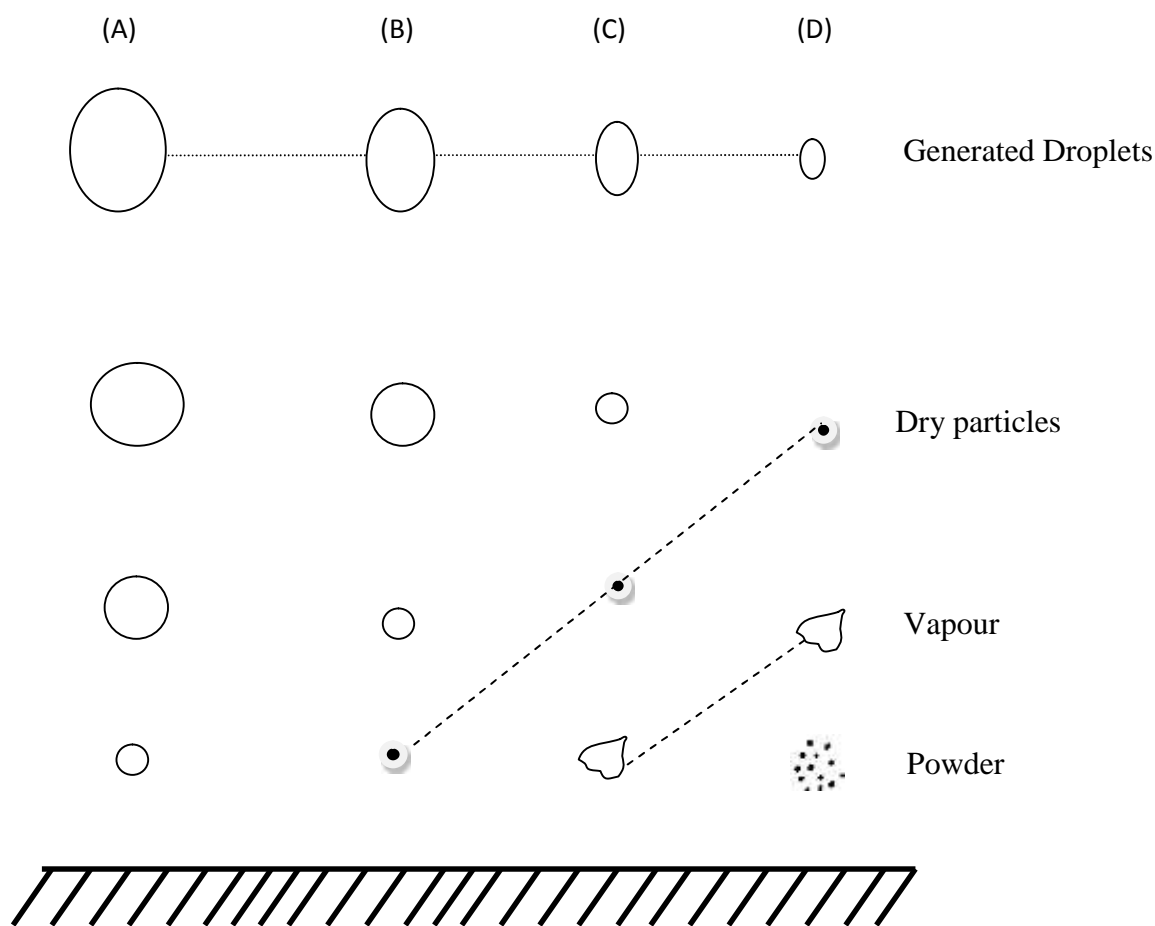
Figure I.8 Schematic of an ultrasonic atomizer.

#### **II.2.2.4.1. Advantages of Spray Pyrolysis:**

It has several advantages in producing nanocrystalline thin films, such as, relatively homogeneous composition, inexpensive and permits easy deposition in the atmospheric condition. a simple and deposition on glass substrate because of the low substrate temperatures involved, It is possible to alter the mechanical, electrical, optical and magnetic properties of  $\text{In}_2\text{O}_3$  nanostructures. One of the major advantages of spray pyrolysis over the vapor-phase routes is the possibility of producing multicomponent particles with exact desirable stoichiometry in the final product. Depending on the substrate temperature, precursor type, and the nozzle-to-substrate distance the droplets can evaporate or decompose completely before reaching the substrate, resulting in a process resembling to CVD, or the liquid is deposited without evaporation.

#### **II.2.2.4.2. Fundamental aspects of spray pyrolysis :**

The chemical reaction that provides the basis for the spray pyrolysis technique is the thermal decomposition of the initial material. Then the oxidation of the decomposition products and the formation of the desired layer material will ensue. To ensure that pyrolysis will only take place at the earliest directly in front of the substrate surface, it is necessary to keep the temperature of the initial material below the decomposition temperature. This can be achieved by dissolving the initial material in a solvent, atomizing it into fine droplets and carrying these droplets to the hot substrate with a carrier gas. During the continuous vaporization of the solvent, the temperature of the dissolved initial material is held almost at the boiling point of the solvent until the solvent is entirely vaporized. Firstly the solvent has to cool the starting material and thus prevents the material from decomposing too soon. Secondly it is possible to obtain the desired particle size for the optimum chemical reaction at the substrate surface by using a well-defined composition and atomization of the solution. The ideal transportation to the substrate will be when the droplet approaches the substrate just as the solvent is vaporized entirely. However, since in the generation of droplets a uniform droplet size cannot be attained and the thermal behaviour of the droplets depends on their mass, there will be different deposition processes depending on the size of the droplets. Figure.I.9. shows the various deposition processes that occur above the required decomposition temperature depending on the droplet size.



Figur I.9 Deposition processes in relation to the droplet size  
(modified from the work of Viguik and Spitz [40] ).

In process (A) the droplet is so large that the heat absorbed from the surroundings will not be sufficient to vaporize entirely the solvent on the way to the substrate. The droplet hits the substrate, where the solvent is entirely vaporized leaving a dry precipitate; the temperature has now increased above the boiling point of the solvent and decomposition occurs. Because the vaporization of the solvent locally removes a lot of heat, the substrate temperature decreases at this point. This affects adversely the kinetics of the reaction, i.e. equalization of the particle concentrations does not occur. The surface becomes rough and the transmission decreases markedly.

Process (B) is distinguishable in that the droplet dries up entirely before reaching the substrate and then hits the surface in a statistical distribution. Some of the particles evaporate and condense in the gaps between the particles where the surface reaction starts. In this process

also, the vaporization of the particle locally removes a lot of heat, but not to the same extent as in process (A).

Process (C) includes the classical chemical vapour deposition process leading to the optimum film properties. In this process the solvent is entirely vaporized short of the substrate. Before the particle reaches the substrate, there is sufficient time for it to warm up to ambient temperature.

The behaviour of the smallest droplets is shown in process (D). In this process the solvent is already completely vaporized far away from the substrate. The particle melts and vaporizes (or sublimates) and a chemical reaction will occur in the vapour phase. This is a homogeneous reaction, because all reactant molecules and product molecules are in the vapour phase. The molecules condense as micro-crystallites, which form a powdery precipitate on the substrate. This powder disturbs the formation of the layer and leads to a reduction in transmission. In addition the homogeneous reaction diminishes the deposition efficiency of this procedure.

## Chapter II

# Technical preparation and characterization

This chapter will be devoted on the experimental conditions and the characterization methods which are used to prepare and characterize the indium oxide thin films ( $\text{In}_2\text{O}_3$ ).

## II.1. $\text{In}_2\text{O}_3$ thin films prepared by ultrasonic spray

$\text{In}_2\text{O}_3$  thin films prepared by this technique depend on the preparation substrate and starting solution. Substrate elevator is placed above the resistance which is connected to temperature regulator. To avoid thermal shock of the substrates, the elevator is gradually heated from room temperature to the chosen temperature for deposition.

When the heating is done, we fix and/or change the solution sprayed on the substrate by (Syringe pump PHOENIX D-CP) and the amplitude of the sound wave is fixed at 40%. So Fine droplets are sprayed onto the heated substrate. Finally, the chemical reaction between the compounds takes place on the substrate due to the temperature which activates this reaction.

### II.1.2. Experimental conditions

The experimental conditions change with the change of the deposition parameter studied. In our study of deposition indium oxide by ultrasonic spray we investigate effect of the:

- 1- Deposition time.
- 2- Solution flow rate.
- 3- Surface substrate.
- 4- Annealing temperature.

So for the first parameter we take these conditions which are summarized in the table II.1.

Deposition time (min)	Solution flow rate (ml/h)	Temperature (°c)	Distance spray nozzle–substrate (cm)	Concentration of the solution (mol/h)
4	50	400	5	0.1
7	50	400	5	0.1
10	50	400	5	0.1
13	50	400	5	0.1

Table II.1. The experimental conditions for the first parameter (deposition time)

For the second parameter we take these conditions which are summarized in the table II.2.

Deposition time (min)	Solution flow rate (ml/h)	Temperature (°c)	Distance spray nozzle–substrate (cm)	Concentration of the solution (mol/h)
4	25	400	5	0.1
4	40	400	5	0.1
4	55	400	5	0.1

Table II.2. The experimental conditions for the second parameter (solution flow rate)

For the third parameter we take these conditions which are summarized in the table II.3.

Deposition time (min)	Solution flow rate (ml/h)	Temperature (°c)	Distance spray nozzle–substrate (cm)	Concentration of the solution (mol/h)	Substrates
4	25	550	5	0.1	glass
4	25	550	5	0.1	KCl single Crystal
4	25	550	5	0.1	Si single Crystal

Table II.3. The experimental conditions for the third parameter (Surface substrate)

For the fourth parameter we take these conditions which are summarized in the table II.4.

Deposition time (min)	Solution flow rate (ml/h)	Annealing temperature (°c)	Distance spray nozzle–substrate (cm)	Concentration of the solution (mol/h)
4	40	300	5	0.1
4	40	500	5	0.1

Table II.4. The experimental conditions for the last parameter (Annealing temperature)

\* For the annealing temperature the as-deposited film deposited on glass substrate heated at 150 °C.

### II.1.3. Used substrates

Indium oxide thin films deposited on glass substrate when we studied effect of the deposition times, solution flow rate and Annealing temperature on the structural, morphological, optical and electrical properties of these films. However, for the third parameters we prepared the  $\text{In}_2\text{O}_3$  thin films on glass, single crystalline Si (400) wafer and KCL single crystal substrates. The Si single crystal substrate was used for investigates the structural properties of  $\text{In}_2\text{O}_3$  films.

### II.1.4. Cleaning of the substrates

The quality of Indium oxide thin films depends on purity and surface state of the used substrate. The process of cleaning surface for the glass and Si single crystal substrates is as follows:

- 1- Firstly using a pen with diamond point to cut the substrates.
- 2- Rinsing with the water distilled and then with acetone during 5 min.
- 3- Rinsing with distilled water.
- 4- Washing in methanol at ambient temperature in a bath with the Ultrasound for to eliminate the traces from greases and impurities stuck to surface of substrate then they are to clean in a water bath distilled with the Ultrasound.
- 5- Drying using a drier.

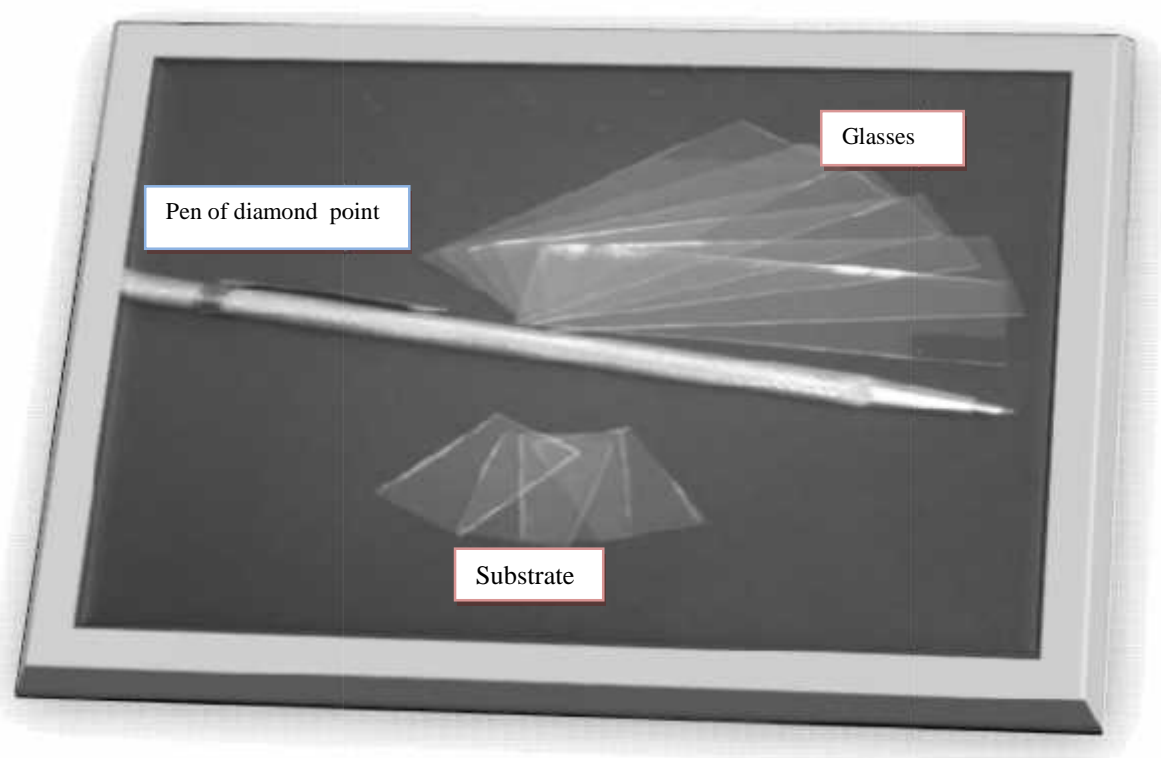


Fig.II.1. Glasses substrates and diamond pen used.



Fig.II.2: Photograph of a KCl single crystal substrate.

For the KCL single crystal we don't use the chemical cleaning due to the sensibility of this substrate, The KCl single crystal prepared using the Czochralski (Cz) method is cleaved parallel to the (100) plane with the required size. Figure II.2. Displays a photograph of a KCl single crystal substrate.

### II.1.5. Preparation of the solutions:

Indium Oxide thin films were prepared by spraying a solution containing a 0.1M of indium chloride  $\text{InCl}_3$  in absolute volume of ethanol ( $\text{C}_2\text{H}_5\text{OOH}$ ) as a solvent. We give the various properties of Indium chloride and Ethanol.

#### 1- indium chloride:

- Purity: 99.99%
- Aspect: white crystal (dissolve in water)
- Density: 3.46g/cm<sup>3</sup>
- Melting point: 586 °C



Figure. II.3: InCl<sub>3</sub> powder

## 2 Ethanol:

- Aspect: liquid
- Color: colorless
- PH: neutral (20°C)
- Melting point: – 117°C
- Boiling point: 78°C
- Dynamic viscosity: (20°C) 1,2 mPa\*s
- Temperature of auto combustion: 425°C
- Point flash: 12°C
- Vapor pressure: (20°C) 59 mbar
- Density: 0,79 g/cm<sup>3</sup>

### II.1.6. Used Montage:

The ultrasonic spray technique was used to deposit Indium oxide (In<sub>2</sub>O<sub>3</sub>) thin films has the following shape and characteristics:

- 1: ultrasonic generator with 40 KHz frequency permits to generate the ultrasonic waves and submit them to the atomizer.
- 2: resistance to heat the substrate.
- 3: substrate holder.
- 4: temperature regulator related to a thermocouple to control the temperature.
- 5: syringe pump Model PHOENIX D-CP (GF-FOURES) to control the flow rate
- 6: atomizer to decompose the solution to fine droplets.
- 7: syringe contains the solution.
- 8: thermocouple.



Fig.II.4. montage of ultrasonic spray technique

**II.2. Characterization methods of  $\text{In}_2\text{O}_3$ :** In this section we present the technical characterizations of indium oxide thin films.

### II.2.1 X-ray diffraction

X-ray diffraction was used to determine the crystalline structure, preferential orientation of the crystallites average crystalline size and stress in the films. X-ray diffraction spectra were acquired using a D8 ADVANCE diffractometer ( $\lambda = 1.5405 \text{ \AA}$ ). The basic law involved in the diffraction method of structural analysis is the Bragg's law which is given by the relation [41]:

$$n \lambda = 2d \sin \theta \quad (\text{II.1.})$$

Where:  $n$  is the order of diffraction.  $\lambda$  is the wavelength of the x-rays,  $d$  is the spacing between consecutive parallel planes.

### II.2.2. Determination of the grains size:

The average grains size  $D$  of  $\text{In}_2\text{O}_3$  is estimated using Scherrer's formula [42]:

$$D = \frac{0.9 \lambda}{\cos \theta \Delta 2\theta} \quad (\text{II.2.})$$

Where  $\theta$  is the Bragg's angle and  $\Delta 2\theta$  is the full width at half maximum (FWHM) of the peak,  $\lambda$  is the X-ray wavelength.

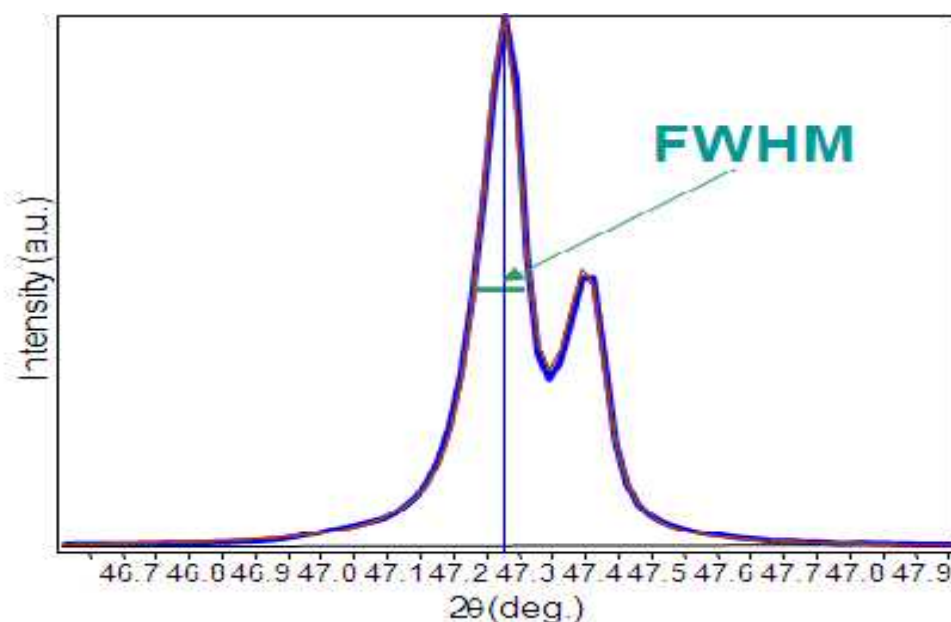


Fig.II.5: determination of

### II.2.3. Determination of the lattice parameters

The lattice parameters ( $a = b = c$ ) have been determined by equation [43]:

$$a = d \sqrt{h^2 + k^2 + l^2} \quad (II.3)$$

where  $d$  is the lattice spacing of the crystal planes ( $h k l$ ).

### II.2.4. Strain Determination:

The strain ( $\epsilon$ ) is calculated using the relation [44]:

$$\epsilon = \frac{\cos^2 \theta}{4} \Delta \theta \quad (II.4)$$

Where  $\theta$  is the Bragg's angle and  $\Delta \theta$  is the full width at half maximum (FWHM) of the peak.

### II.2.5. Determination of the dislocation density ( $\rho$ ).

The dislocation density ( $\rho$ ) is calculated using the formula [45]:

$$\rho = \frac{1}{D^2} \quad (II.5)$$

The structural parameters like lattice parameters, strain and the dislocation density of preferred growth orientation are calculated by these relations.

### II.2.6. Scanning Electron Microscopy (SEM):

The electronic microscope (SEM) is based on the analysis of the interactions electron/matter during the bombardment of the sample by a beam of electrons.

The basic steps involved in all SEM are the following: A stream of electrons is formed in high vacuum (by electron guns). This stream is accelerated towards the specimen (with a positive electrical potential) while is focused using metal apertures and electromagnetic lenses. In the final lens, the SEM contains extra sets of coils that allow it to deflect the electron beam back and forth across the sample.

A large number of interactions occur when a focused electron beam strikes the surface of a solid [46]. Among the signals produced are secondary electrons, backscattered electrons, characteristic

and continuum x-rays, Auger electrons and photons of various energies. The primary effects on the electrons of an electron beam striking the sample are elastic scattering (change of direction with negligible energy loss) and inelastic scattering (energy loss with negligible change in direction). Elastic scattering is mainly caused by interactions with the nuclei of the atoms and results in significant deviations from the direction of the incident beam. Inelastic scattering is caused by two mechanisms, inelastic interaction with the atomic nucleus and inelastic interaction with the bound electrons. If inelastic scattering occurs through interaction with the atomic nucleus, the moving electron loses energy in the Coulomb field of the nucleus and emits white or continuum x-ray radiation. If inelastic scattering occurs between a loosely bound electron on an outer shell of the atom and an electron of the incident beam, energy is lost from the beam electron and transferred to the loosely bound electron which is ejected. The electrons ejected through this process are called secondary electrons. However, these electrons are strongly absorbed, and if they are produced much below of the surface of the sample the probability of escaping is extremely small. A schematic illustration of the signals emerging from a solid struck by an electron beam is shown in Fig.II.6. Inelastic scattering can result in a variety of ionization processes, such as the emission of characteristic x-rays and the ejection of Auger electrons.

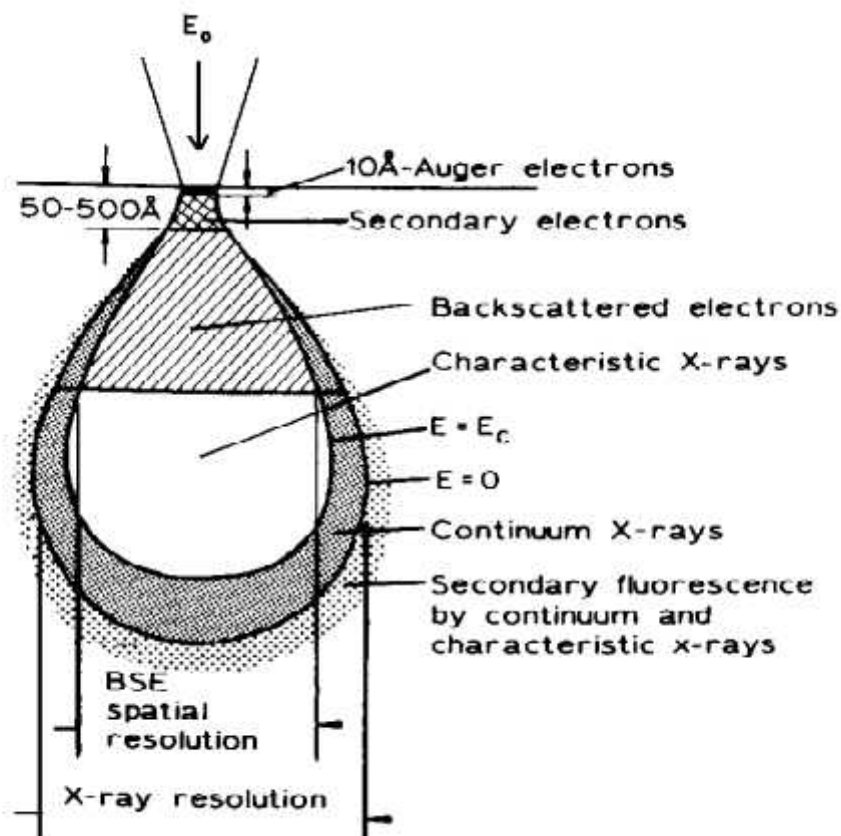
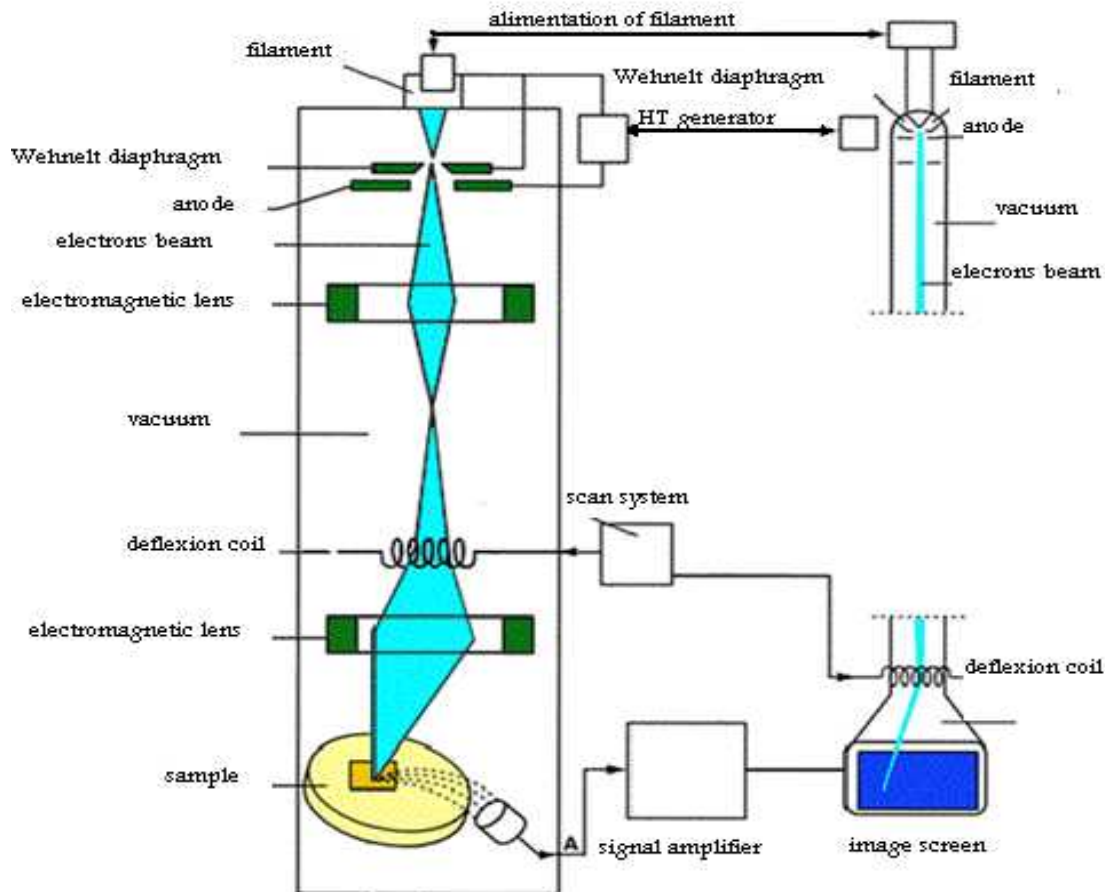


Fig.II.6: Electron and photon signals emerging from a solid struck by an electron beam [46].

The most common imaging mode collects low-energy (<50 eV) secondary electrons that are ejected from the k-orbital of the specimen atoms by inelastic scattering interactions with beam electrons. Due to their low energy, these electrons originate within a few nanometers from the sample surface.



**Figure II.7:** schematic representation of scanning electronic microscopy [46].

### II.2.7. Measurement of film thickness by SEM:

We can measure the film thickness directly by the Cross-sectional images of the  $\text{In}_2\text{O}_3$  thin films obtained by the SEM (Jeol, model JSM 6301F scanning microscopy), using a program called Visiometer.

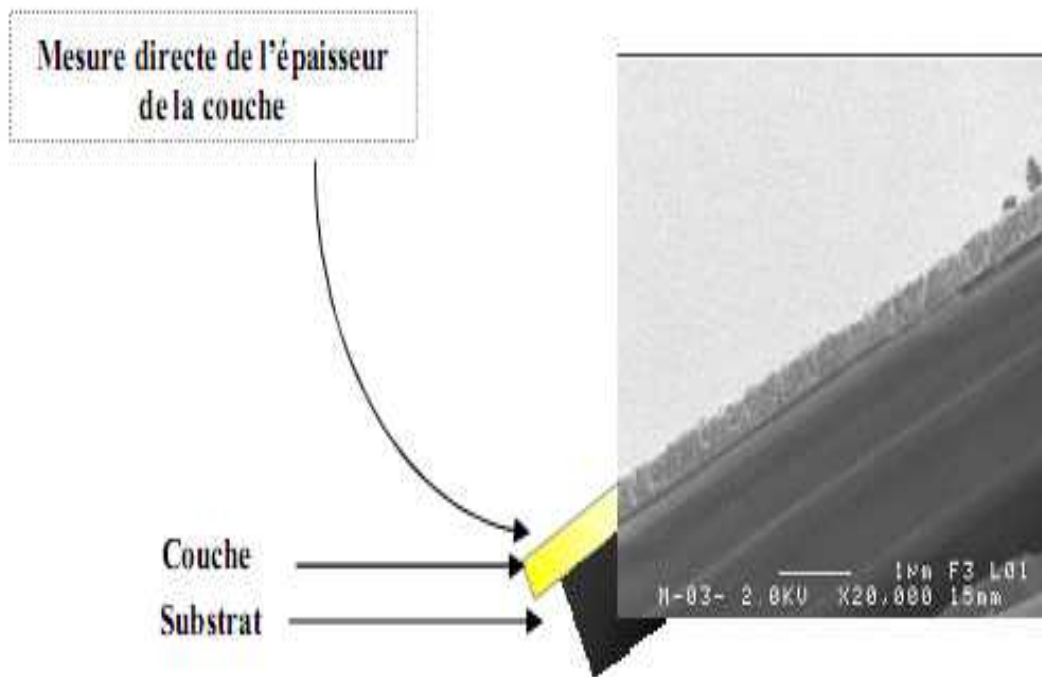


**Figure II.8:** Direct measurement thickness of a film from picture obtained by SEM.

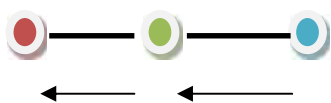
### II.2.8. Energy Dispersive X-ray analysis (EDX):

EDX is an analytical technique which utilizes x-rays that are emitted from the specimen when bombarded by the electron beam to identify and quantify the elemental composition of the specimen. The energy dispersive x-ray analysis system is usually attached to a scanning electron microscope system (SEM).

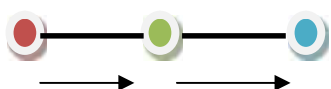
### II.2.9. Infrared Spectroscopy:

Spectroscopy is the study of matter and its interaction with electromagnetic radiation. All matter contains molecules; these molecules have bonds that are continually vibrating and moving around. These bonds can vibrate with stretch motions or bend motions. Imagine two balls attached by a spring, representing a diatomic molecule. The movement of each ball toward or away from the other ball along the line of the spring represents a stretching vibration (fig. II.9.1). Stretching can either be symmetric or asymmetric. A molecule with three or more atoms can experience a bending vibration, a vibrational mode where the angle between atoms changes (fig. II.9.2). In the following examples, imagine a triatomic molecule ABC.

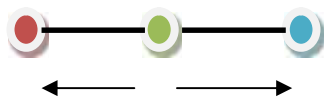
Symmetric Stretch: allows molecule to move through space



OR



Asymmetric Stretch: leads to an increase or decrease in bond length



OR

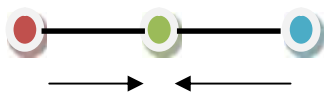


Figure. II.9.2: Bending Vibrations

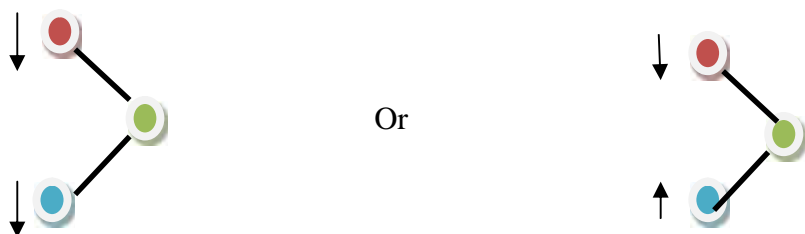


Figure. II.9.1: Stretching Vibrations

### II.2.10. Optical characterization:

The ratio of the transmitted light intensity  $I$  to the incident light intensity  $I_0$ , when light is passed through an absorbing film, is given by Beer-Lambert relation:

$$I = I_0 \exp -\alpha d \quad (\text{II. 6})$$

Where  $\alpha$  is the absorption coefficient and  $d$  the thickness of the film.

The transmittance  $T$  (quantity of the transmitted light) can be directly measured, where:  $T (\%) = I / I_0 \cdot (100)$ . and thus, for a film of known thickness, the absorption coefficient can be calculated from the transmission data.

$$\alpha = \frac{1}{d} \ln \frac{100}{T \%} \quad (\text{II. 7})$$

We measured the sample transmittance spectra with dual beam UV-VIS-NIR scanning spectrophotometer of type SHIMADZU UV-3101 PC, its operation principle is represented in figure II.9. Spectra obtained give the variation of transmittance expressed as a percentage according to their wavelength.

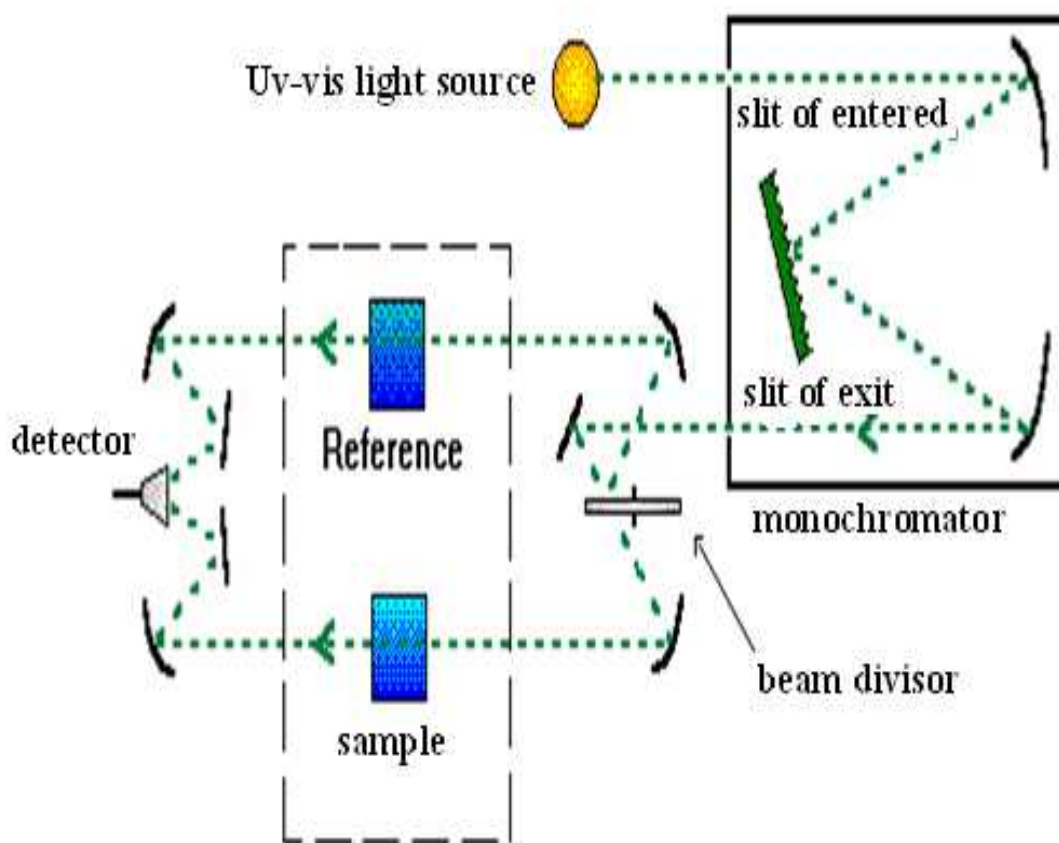


**Figure II.10:** schematic representation of scanning electronic microscopy [46].

### II.2.11. Optical Gap:

The fundamental absorption is related to the band-to-band transitions in a polycrystalline semiconductor, i.e., to the excitation of an electron from the valence band to the conduction band. Therefore, the fundamental absorption can be used to determine the energy gap of the semiconductor.

The optical band gap of  $\text{In}_2\text{O}_3$  films is estimated from Tauc relationship [47.48]:

$$\alpha(h\nu)^2 = A(h\nu - E_g) \quad (\text{II. 8})$$

Where  $\alpha$  is absorption coefficient, A is the constant independent of photon energy ( $h\nu$ ), h is the Planck constant and  $E_g$  is the optical band gap. The values of the optical band gap are obtained by extrapolating the tangential line of the data to the abscissa axis in the plot of  $\alpha(h\nu)^2$  as a function of  $h\nu$  as shown in Figure II.11.

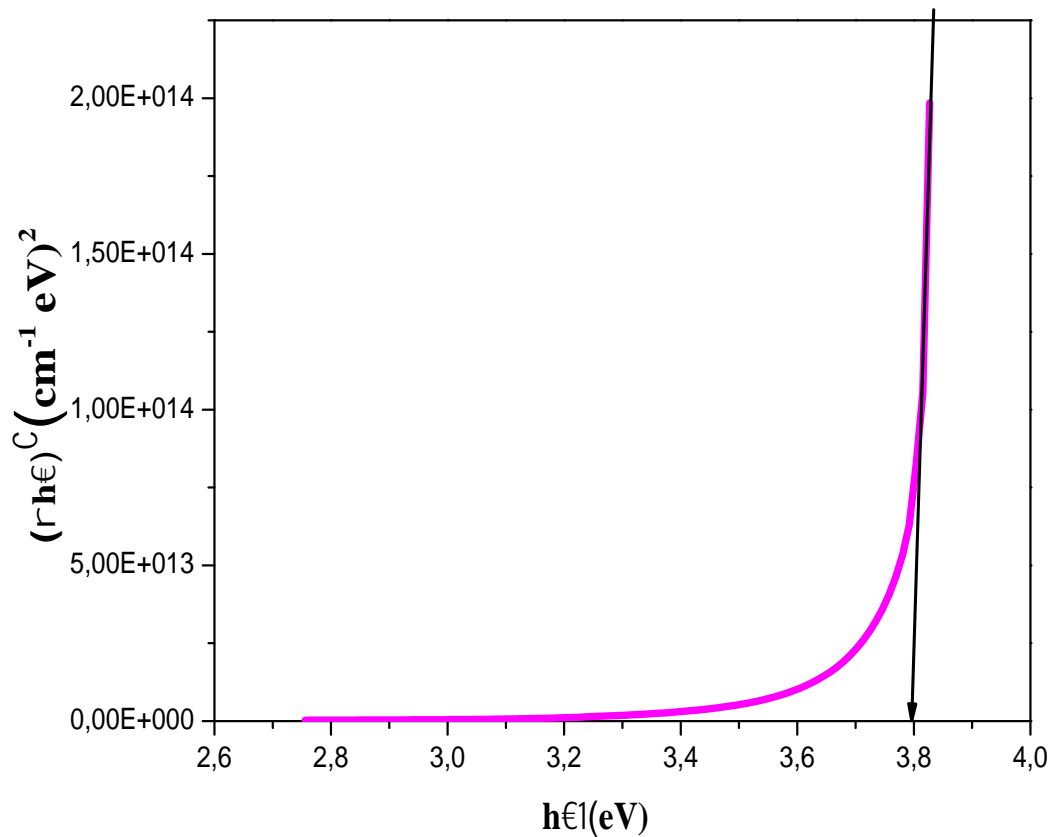


Figure II.11: determination of  $E_g$

### II.2.12. Disorder calculating:

$E_{00}$  is usually used to describe the width of the localized states in the bandgap (but not their positions). Pankove has shown that the value of  $E_u$  is related to the impurity concentration [49]. However, Redfield has shown that all defects (point, line, and planar defects) lead to local electric fields that cause band tailing. Thus, the Urbach energy can be considered a parameter that includes all possible defects [50]. According to the Urbach law of the expression of the absorption coefficient is as follow:

$$\alpha = \alpha_0 \exp \frac{h\nu}{E_{00}} \quad (\text{II. 9})$$

By drawing  $\ln(\alpha)$  versus  $h\nu$  we can determine  $E_u$  value as the reciprocal of the linear part slope [51] (figure II.12):

$$\ln \alpha = \ln \alpha_0 + \frac{h\nu}{E_{00}} \quad (\text{II. 10})$$

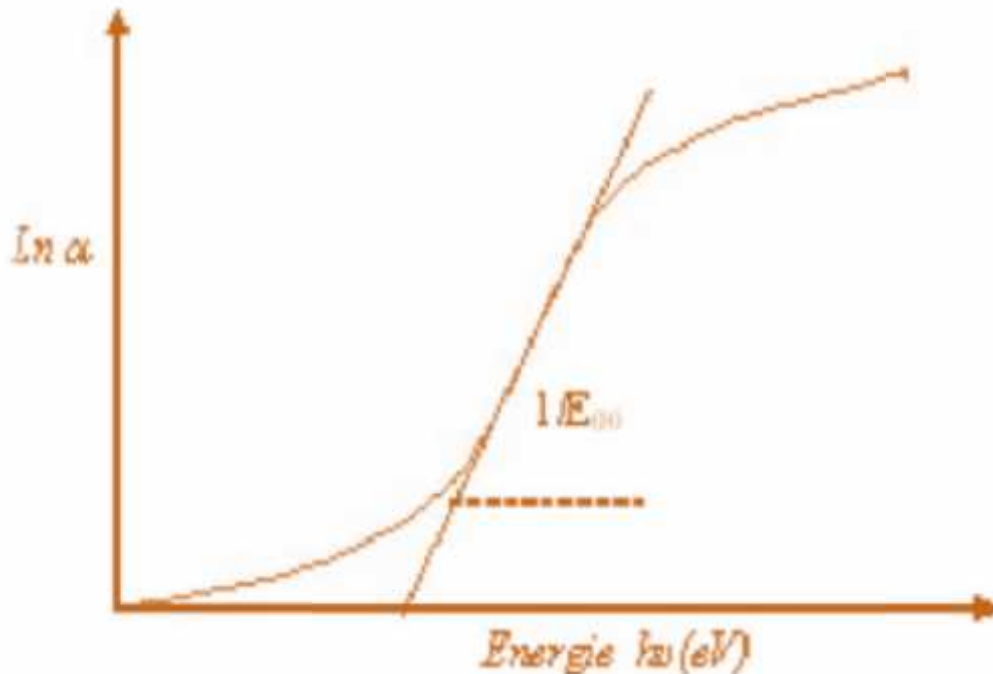


Figure II.12: Determination of the disorder

### II.2.13. Refractive index

The refractive indices ( $n$ , in the chapter IV) were determined from the reflectance ( $R$ ) data using [52.53]:

$$R = \frac{n - 1}{n + 1}^2 \quad (\text{II. 11})$$

### II.2.14. Four-point probe resistivity measurements

Four-point probe measurements are made using four identical probes, equally spaced along the surface of the sample. A current is forced through the outer two probes while measuring the voltage across the inner two probes. Using a high-impedance voltmeter or electrometer, very little current flows through the inner probes, minimizing the contact resistance associated with the voltage measurement. Using only two-point measurements, the voltage is measured with current-carrying probes. As such, the probe and contact resistances become non-trivial.

The more usual probe geometry configuration is when the four probes are placed in a line, as shown in Figure II.12. The voltage at probe 2,  $V_2$ , induced by the current flowing from probe 1 to probe 4 is given by:

$$V_2 = \frac{\rho l}{2\pi} \cdot \frac{1}{s_1} - \frac{1}{s_2+s_3} \quad (\text{II. 12})$$

The voltage at probe 3 is:

$$V_3 = \frac{\rho l}{2\pi} \cdot \frac{1}{s_1+s_2} - \frac{1}{s_3} \quad (\text{II. 13})$$

Then, by measuring  $V=V_2-V_3$ , the voltage drop between probes 2 and 3, and the current  $I$  through probes 1 and 4, the resistivity can be determined using (II.12) and (II.13) as:

$$\rho = \frac{2\pi V/I}{\frac{1}{s_1} + \frac{1}{s_2} - \frac{1}{s_2+s_3} - \frac{1}{s_1+s_2}} \quad (\text{II. 14})$$

Thus, a direct measurement of the resistivity can be made using a high-impedance voltmeter and a current source. When the probe spacings are equal ( $s_1= s_2= s_3= s$ ), which is the most practical case, then (II.14) becomes:

$$\rho = 2\pi s \cdot \frac{v}{I} \quad (II.15)$$

Equations (II.14) and (II.15) are valid only for semi-infinite samples; that is, when both the thickness  $t$  and the sample surface are very large ( ), and the probes' locations must be far from any boundary. Because these relations can be applied only to large ingots, then in many cases a correction factor  $f$  must be introduced in order to take into account the finite thickness and surface of the sample and its boundary effects. Further, for epitaxial layers,  $f$  must also consider the nature of the substrate – whether it is a conductor or an insulator. Thus, (II.15) becomes:

$$\rho = 2\pi s \cdot \frac{v}{I} \cdot f \quad (II.16)$$

For a thin semiconductor wafer or thin semiconducting layer deposited on an insulating substrate, and for the condition  $t < s/2$ , which represents most practical cases because the probe spacing  $s$  is usually on the order of a millimeter, then the correction factor due to the thickness is:

$$f = \frac{t/s}{2 \ln 2} \quad \text{So that:} \quad \rho = 4.532 t \cdot \frac{v}{I} \quad (II.17)$$

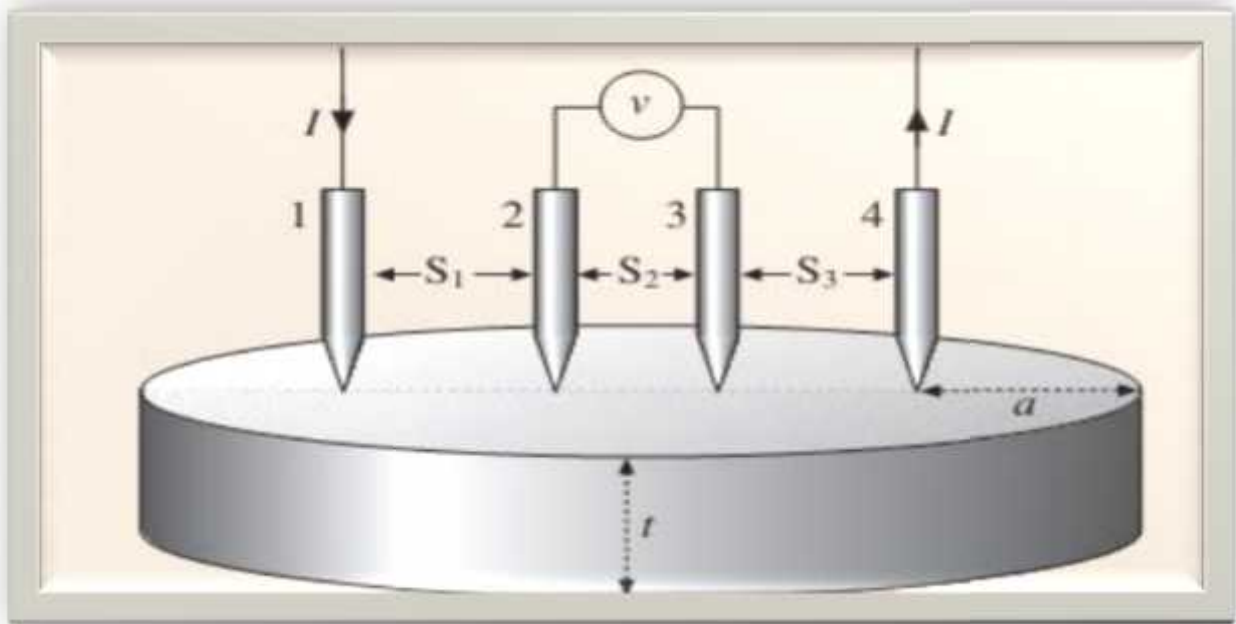


Figure II.13: Linear four-point probe configuration. The sample thickness is  $t$  and  $a$  is the Distance from the edge or boundary of the sample [54].

# Chapter III

Deposition times influence on  
indium oxide thin films  
properties

### III.1. Introduction

It is well recognized, that the properties of  $\text{In}_2\text{O}_3$  films obtained by ultrasonic spray process are close related by the deposition parameters of this technique. Therefore, deposition conditions have been widely studied in order to improve these properties of sprayed  $\text{In}_2\text{O}_3$  films. The most studied parameters are: substrate–nozzle distance (SND) [11] substrate temperature [12,13] and doping [14].

In this chapter, we will studied the influence of the deposition times on the crystalline structure, morphologic, optical, and electrical properties of sprayed  $\text{In}_2\text{O}_3$  thin films; and we evaluated the relationship between these properties in general.

### III.2. Growth rate

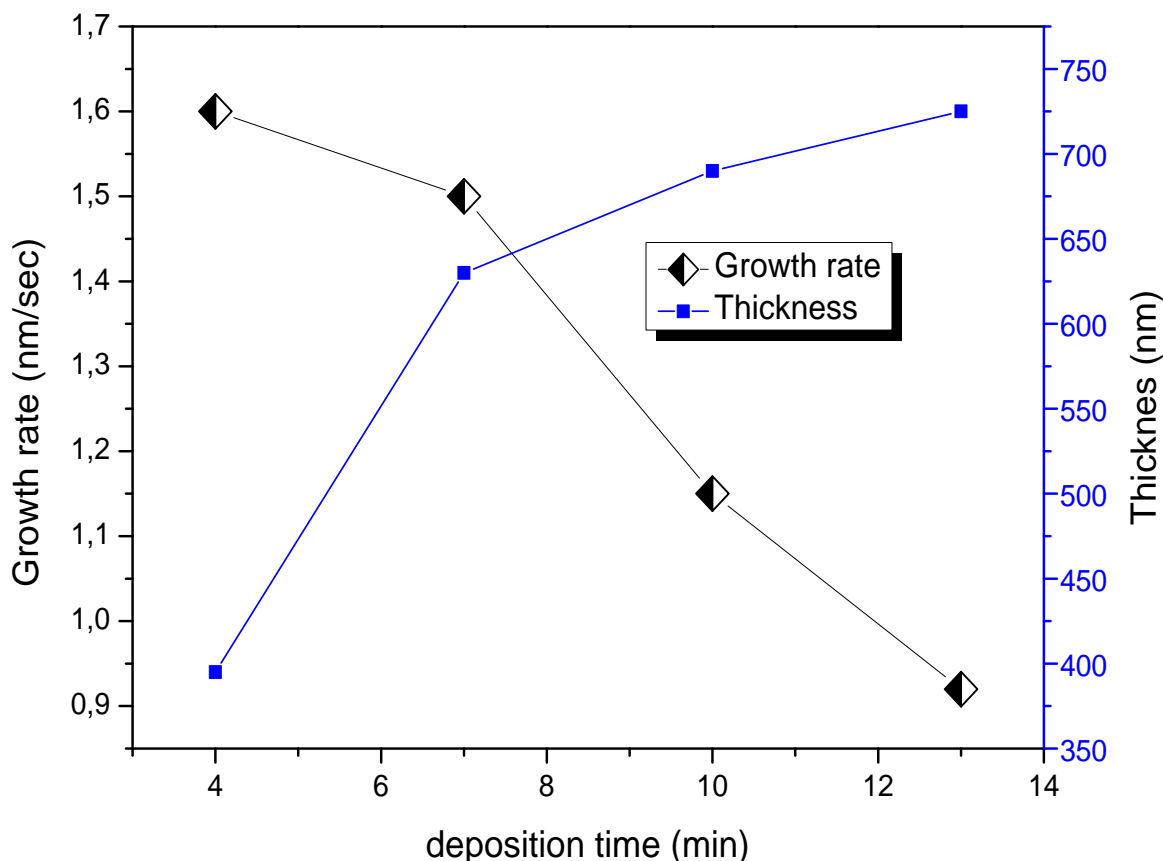


Figure. III.1. Variation of Thickness and deposition rate as a function of deposition time

Dependence of the thickness and growth rate of  $\text{In}_2\text{O}_3$  films on deposition time is plotted in Fig.III.1. The growth rate is estimated from the ratio of film thickness on the deposition time. As can Be seen, the growth rate decrease with the increasing of the deposition time although the amount of the

solution sprayed on the surface substrate augment, this can be accounted to the limited-increase of the films thickness. Saad Rahman found the similar observation for variation of the growth rate as a function of the deposition time [55].

### III.3. XRD analysis

The XRD patterns for  $\text{In}_2\text{O}_3$  thin films grown at various deposition times are shown in Fig. III.2.

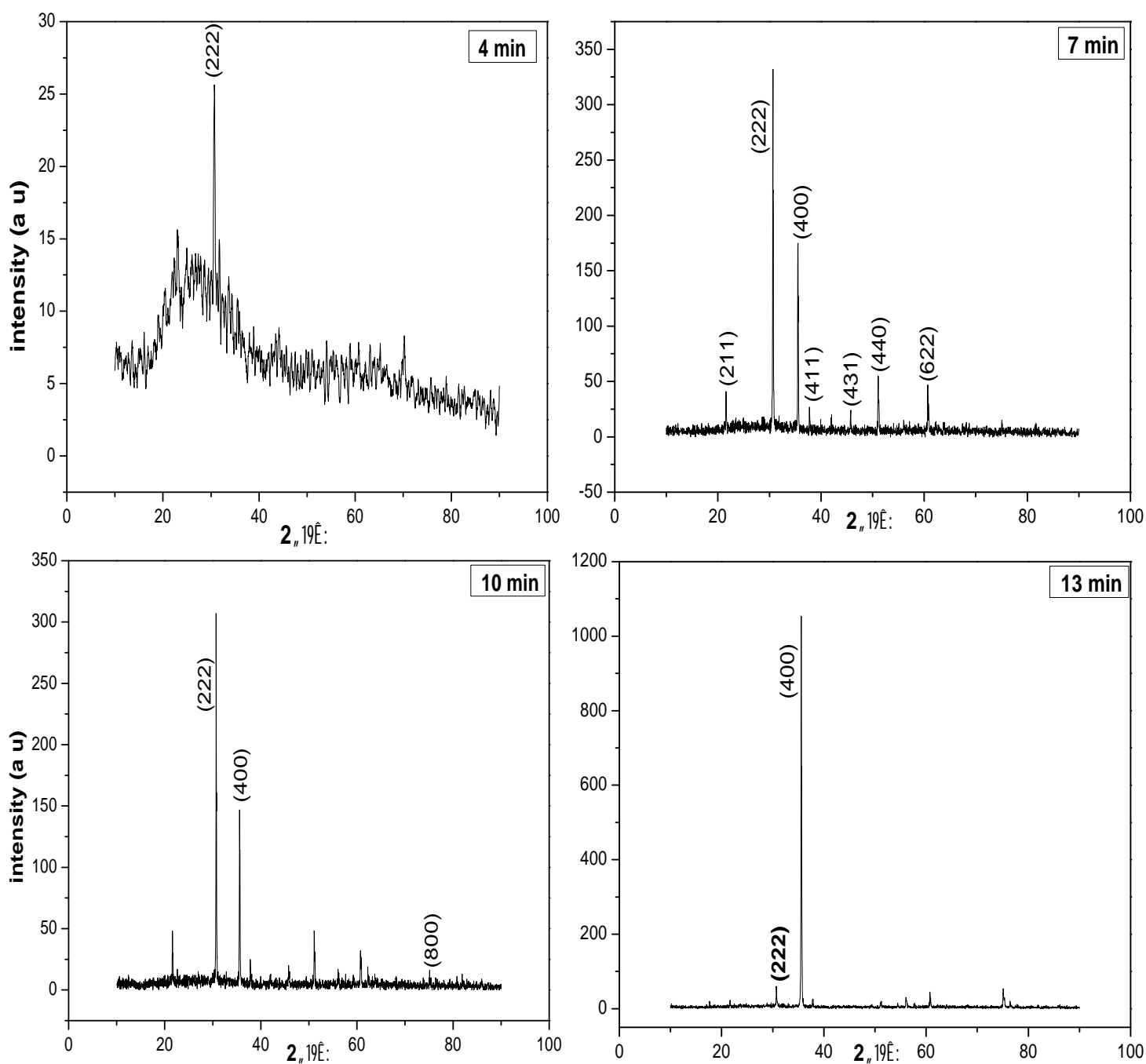
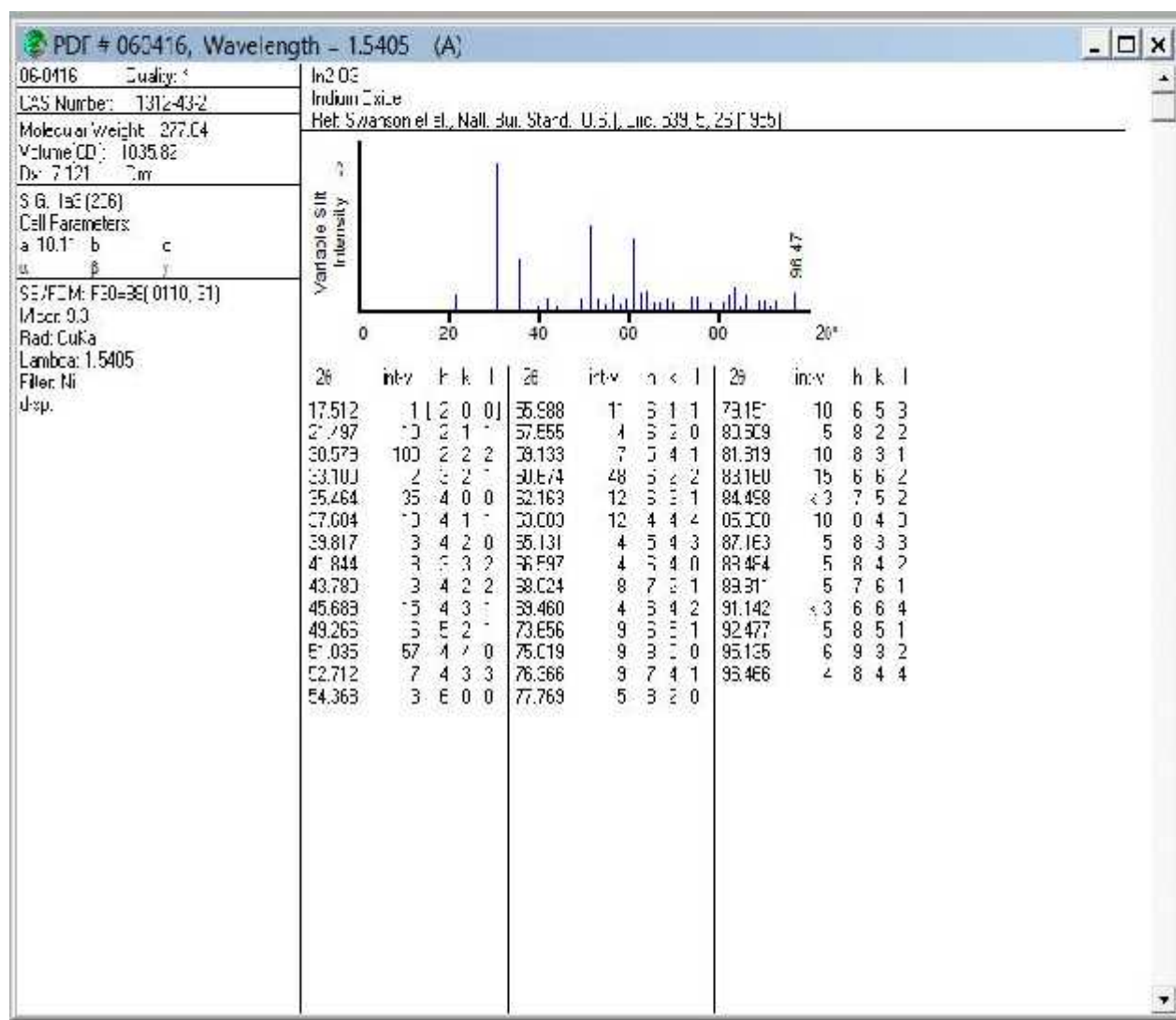


Figure. III.2. Evolution of the spectra of X-rays diffraction of  $\text{In}_2\text{O}_3$  thin films for all deposition

For the deposition time ( $t$ ) equals 4 min the XRD spectrum of this sample exhibits a preferential orientation peak located at  $2\theta = 30.69^\circ$ . However, we noticed the presence of a broad peak between  $20^\circ$  and  $25^\circ$ , indicating clearly the presence of an amorphous phase in the film network. This suggests that the structure of this film is heterogeneous, it is formed with a small grains embedded in an amorphous phase in the film network. With increasing of deposition time by more than 4 min, we notice that the broad peak has been disappeared completely in addition to the presence of two main peaks and weak peaks: two main peaks occur at  $2\theta = 30.69^\circ$  and  $35.58^\circ$ . These peaks correspond to the diffraction from the (222) and (400) planes of  $\text{In}_2\text{O}_3$ , respectively. The weak peaks centered at  $21.77^\circ$ ,  $37.80^\circ$ ,  $45.69^\circ$ ,  $51.23^\circ$ ,  $60.69^\circ$  and  $75.01^\circ$  peaks are identified as  $\text{In}_2\text{O}_3$  (211), (411), (431), (440) (622) and (800) planes, respectively.

Figure. III. 3. ASTM file of  $\text{In}_2\text{O}_3$

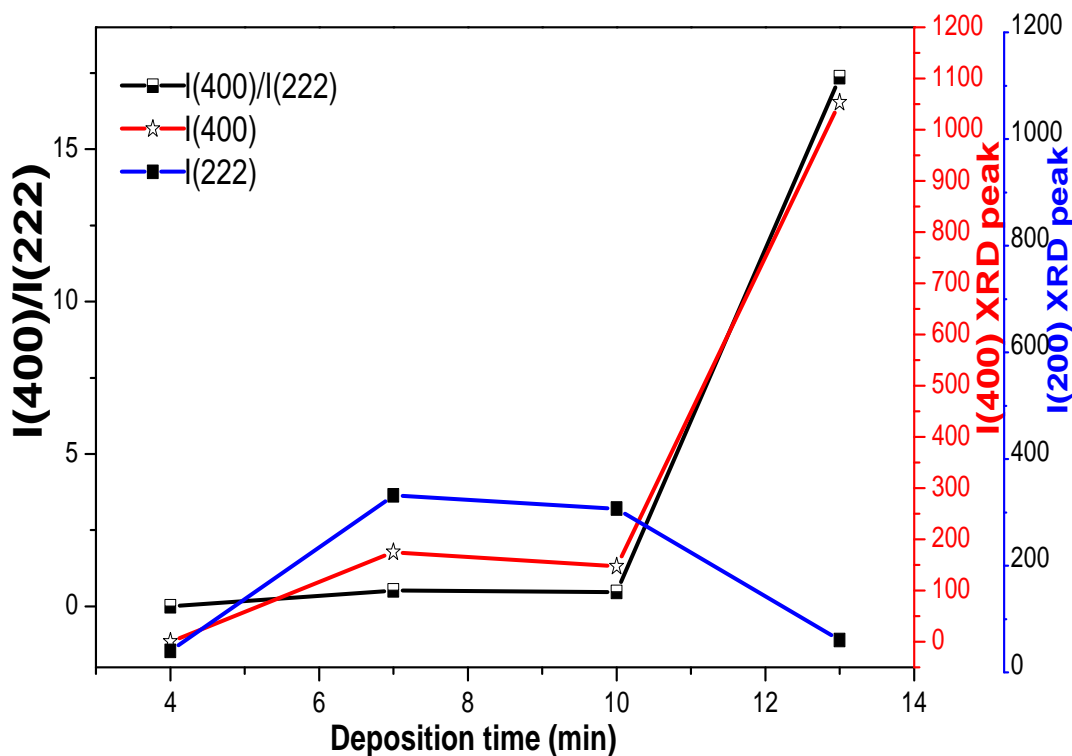


Fig. III.4. Deposition time effect on the film texture.

All peaks from XRD patterns coincide well with those given in the JCPDS data card (6-416) (see figure III.3). the preferred growth orientation of  $\text{In}_2\text{O}_3$  thin films depends on the deposition time. The intensity ratio of the (400) to (222) reflection is used to evaluate the deposition time effect on the film texture of the films, as shown in Figure. III.4. Depending on the results of the current study we found that the ratio  $I(400)/I(222)$  increase with the increasing of deposition time from 4 min to 7 min. Then decreases slightly as the deposition time was 10 min. finally it increases considerably for 13 min and the (400) orientation becomes predominant. Korotcenkov et al. presented that; the ratio  $I(400)/I(222)$  increase with the increase of spray pyrolysis temperature in sprayed  $\text{In}_2\text{O}_3$  [56] or the increase of film thickness [57]. They have also found that the peak intensity ratio of  $I(400)/I(222)$  increases with increasing film thickness [58]. The  $I(400)/I(222)$  ratio suggests that films deposited at 4, 7 and 10 min possess a strong crystallographic texture along the [1 1 1] direction and when the deposition time increase to 13 min, the texture is changed to [10 0] direction. The preferential orientation development of crystalline grains mainly depends on the initial orientations during the nucleation process. For the deposition time equals 4 min the (222) nucleation is a primary nucleation due to the surface free energy of formation of the main planes of the  $\text{In}_2\text{O}_3$  bixbyite

phase, the (111) texture is expected since the high atomic density (111) plane of the bixbyite presents a lower surface free energy plane, as it has been previously discussed [59], and this accounts for the presence of one diffraction peak for  $t = 4$  min. However, with increasing of deposition time more than 4 min, the growth of nuclei takes place due to surface diffusion of impinging solution sprayed. Then the (400) nucleation can be formed competitively with the (222) nucleation. In the same regard, Jin-Hong Lee et al has found that the nuclei number increase with the increase of deposition time and it will grow as well [60]. Finally the (400) nucleation is preferred for 13 min, and a strict improvement in preferred growth is observed, although the (111) texture presents a lower surface free energy plane. This can be attributed to the increase of the film thickness which suppresses the intensity of the (222) plane and stimulate the (400) orientation of the  $\text{In}_2\text{O}_3$  films. This goes in harmony with the XRD analysis which indicates that with increasing of deposition time the intensity of the plane (222) decreases (see figure.III. 2), Qiao Z et al was mentioned that the growth of the (222)-grains is suppressed with increasing thickness [61]. On the other hand, the change in the strongest orientation of the XRD peak is correlated with the change in grain shapes as observed by SEM analysis (explained later). This probably indicates that the deposition time influences the evolution of microstructures and thereby reflects on the strongest orientation observed by XRD studies.

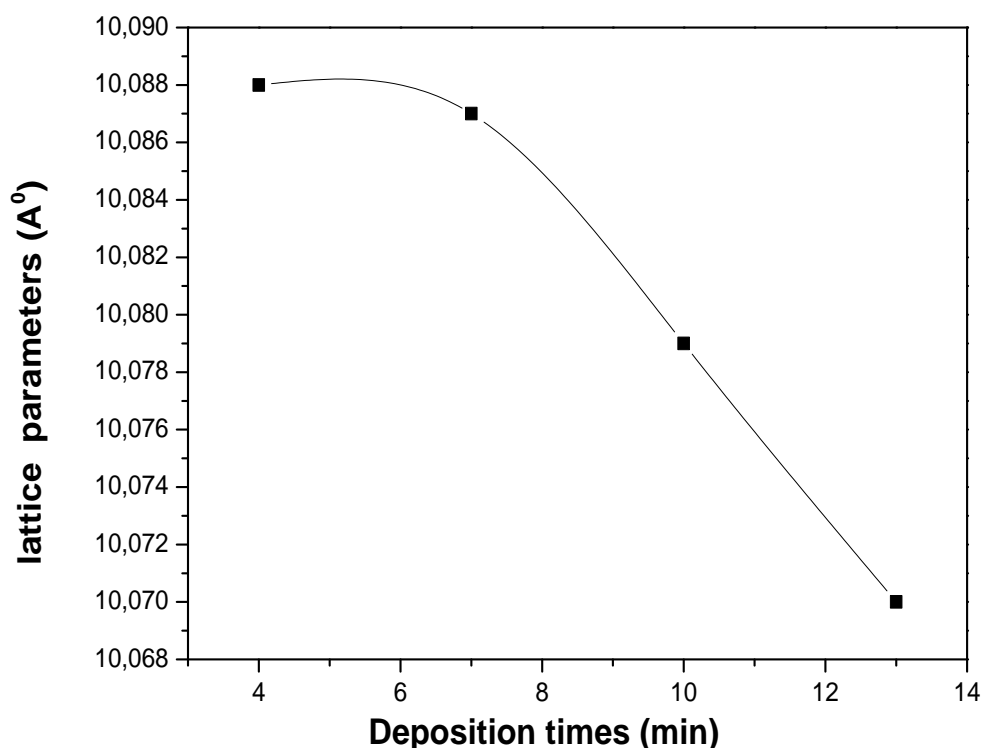


Figure. III.5. The lattice parameters ( $a = b = c$ ) of the  $\text{In}_2\text{O}_3$  films

The lattice parameters ( $a = b = c$ ) of the  $\text{In}_2\text{O}_3$  films are shown in figure III.5. it is clear that the lattice parameters is slightly smaller than the reported value of  $10.11 \text{ \AA}$  for pure indium oxide (see Figure. III. 3). This change in the value of lattice parameter may be attributed to the strain effect arising from thermal expansion [62].

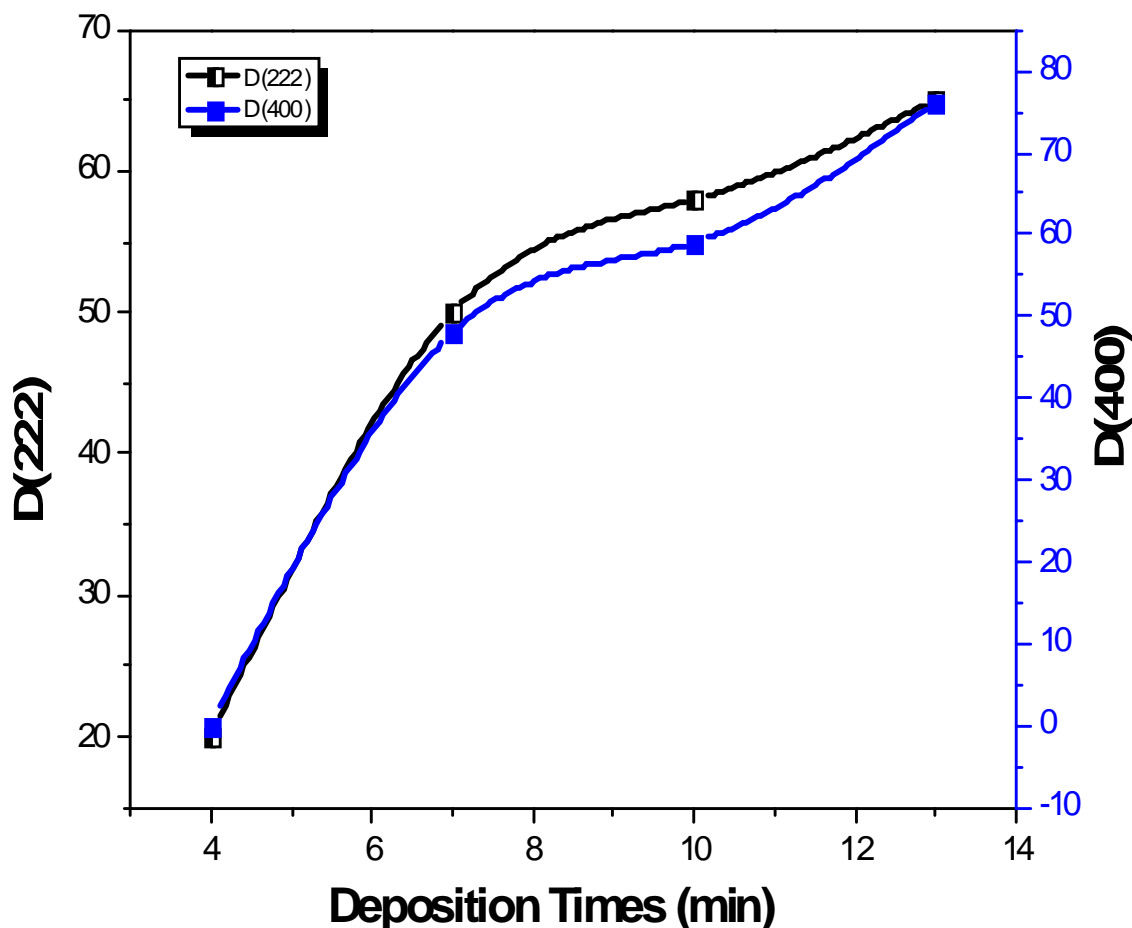


Figure III.6. Average grain size of  $\text{In}_2\text{O}_3$  thin film as a function of deposition time.

Figure III.6. Presents variation of grain size as a function of deposition time, the results show that average grain size increases from 20 to 76 nm with increasing of deposition time. The increase of the crystallite size with the increase of deposition time can be explained as follows. As the deposition time increases, the amount of solute reaching on the surface of the substrate increases to form film and therefore the electrostatic interaction between solute atoms becomes larger, there by increases the probability of more solute to be gathered together to form a crystallite [63]. However, it is interesting to note that the average grain size increases slightly when the deposition time change from 7 min to 13 min. this can be attributed to that cohesive growth with the lower grains

does not go on forever, and new grains are nucleated on top of the old ones above this deposition time; the grain size cannot be increased indefinitely because of the limitation on the surface mobility of the adsorbed species [64] and the SEM surface (side view. Figure III.7) of the film deposited at 13 min confirm this explanation. Such behavior of  $\text{In}_2\text{O}_3$  grains were observed in several studies [65, 57].

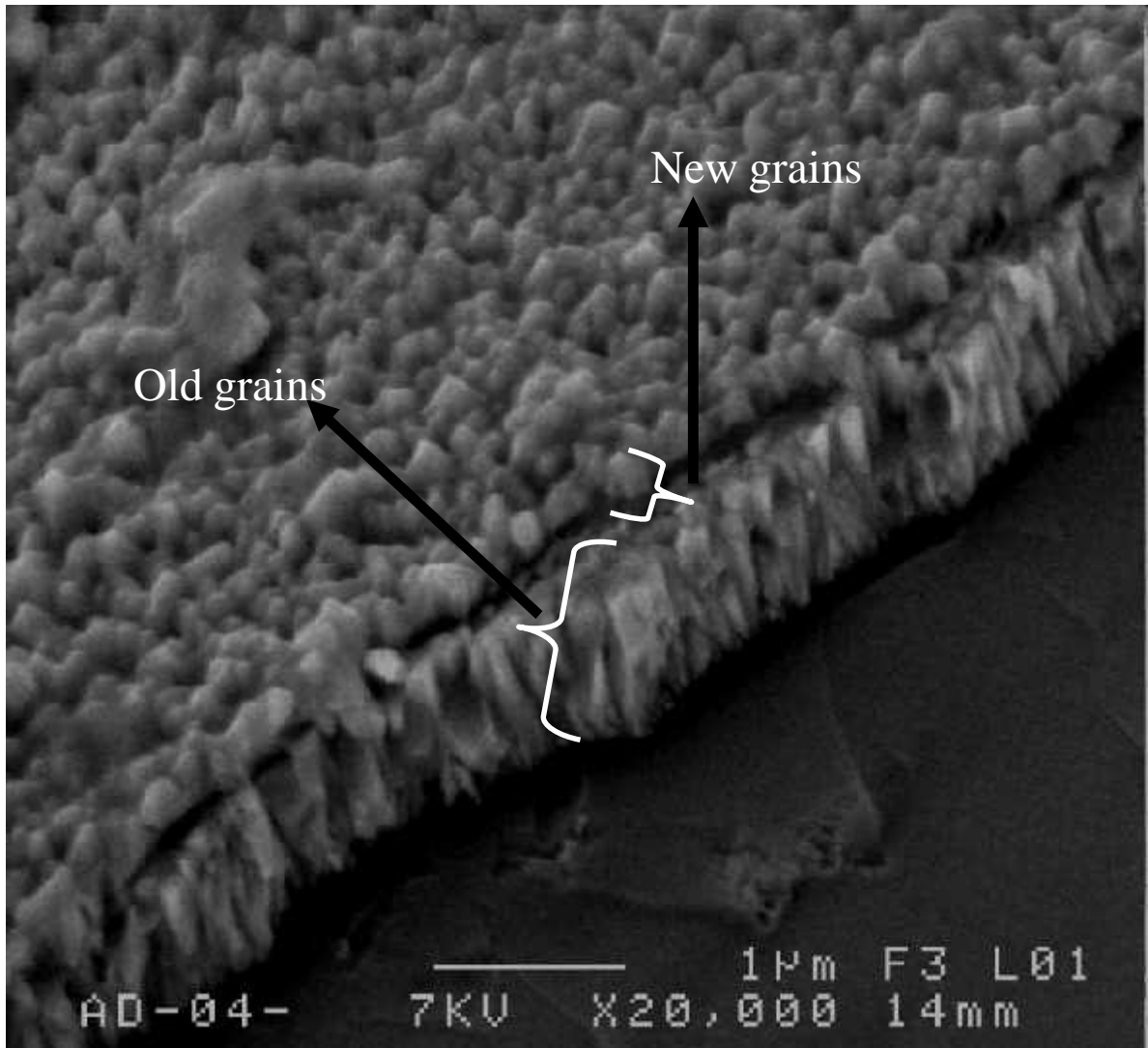


Figure III.7. SEM surface Image of  $\text{In}_2\text{O}_3$  thin film deposited at 13 min (side view)

The dislocation density ( ) and the strain ( ) of (222) plane are shown in figure III.8. The dislocation density and strain show a decreasing trend with increasing in deposition time. This is due to the Improvement of crystalin quality of the films with the increase of the deposition time. M. Jothibas et al found that the crystal defect show a decreasing trend with the improvement in crystalin state of the indium oxide thin films [66].

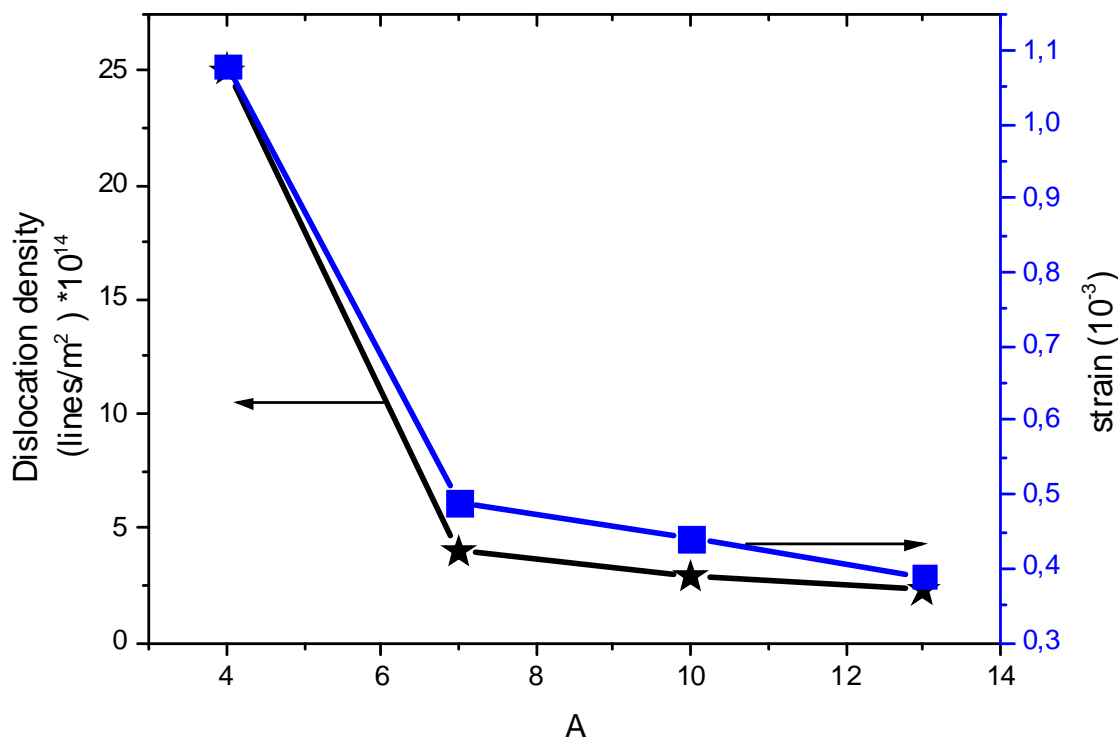


Figure III.8. The dislocation density ( ) of the films as a function of deposition time

### III.4. Morphological properties

Figure III.9. Shows the SEM surface images of the  $\text{In}_2\text{O}_3$  thin films deposited at different deposition times. As the deposition time increases, changes in the morphology of the films are observed. It is interesting to note that, in the case of the films deposited at 4 min (Fig. III.9 (a)) and 7 min (Fig. III.9 (b)), grains with pyramidal-shape are formed. While for the film deposited at 10 min (Fig. III.9 (c)), in addition to the pyramid-shaped grains, we notice emergence another grains are granular in shape. The sample deposited at 13 min (Fig. III.9 (d)) shows that the grains are granular in shape but seen to be densely packed. The difference in grain shapes probably suggests difference in growth orientations and corroborates the XRD studies. The fact that the mean crystallite size obtained using Scherer's formula is in all cases substantially smaller than the dimension of the grain observed by the SEM images, indicating that these grains are probably aggregates of many crystallites of  $\text{In}_2\text{O}_3$ . The Gibbs free energy of the surface of nano crystals is usually high, and the grains have the tendency toward aggregate formation, thereby reducing the Gibbs free energy [67]. The forgoing discussion, leads to the conclusion that the grains shape can be changed by varying

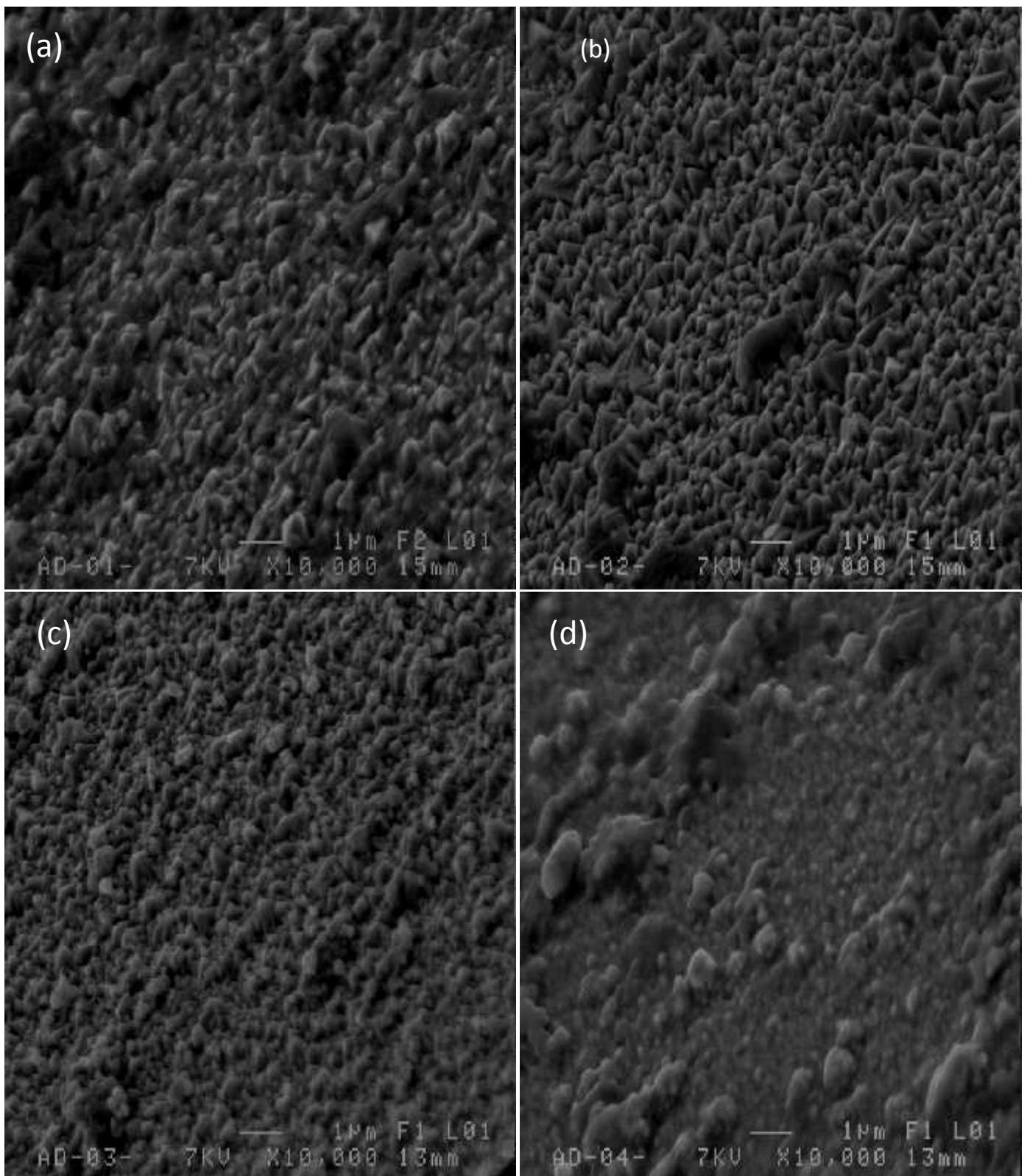


Figure III.9. SEM surface images of the  $\text{In}_2\text{O}_3$  thin films deposited at various deposition time of: (a) 4min, (b) 7min, (c) 10 min and (d) 13min.

deposition time, these results are consistent with the fact the grain shape depends on the growth conditions [68]. Also the SEM surface Images shows that the film deposited at 13 min is less Roughness than the other films. The less roughness surface is probably due to the most preferential growth in the [100] direction over the entire surface. It was recently reported that the preferential growth induces flat surfaces of ITO films by Kim et al. [69]. However, we believe that the surface morphology of the films deposited at 4, 7 and 10 min are more suitable for utilization as transparent oxide front layer in solar cells application than the film deposited at 13 mi because this surface morphology enhances the light trapping in silicon absorber layer [70] and The optical properties confirm this hypothesis (explained later; in the optical properties).

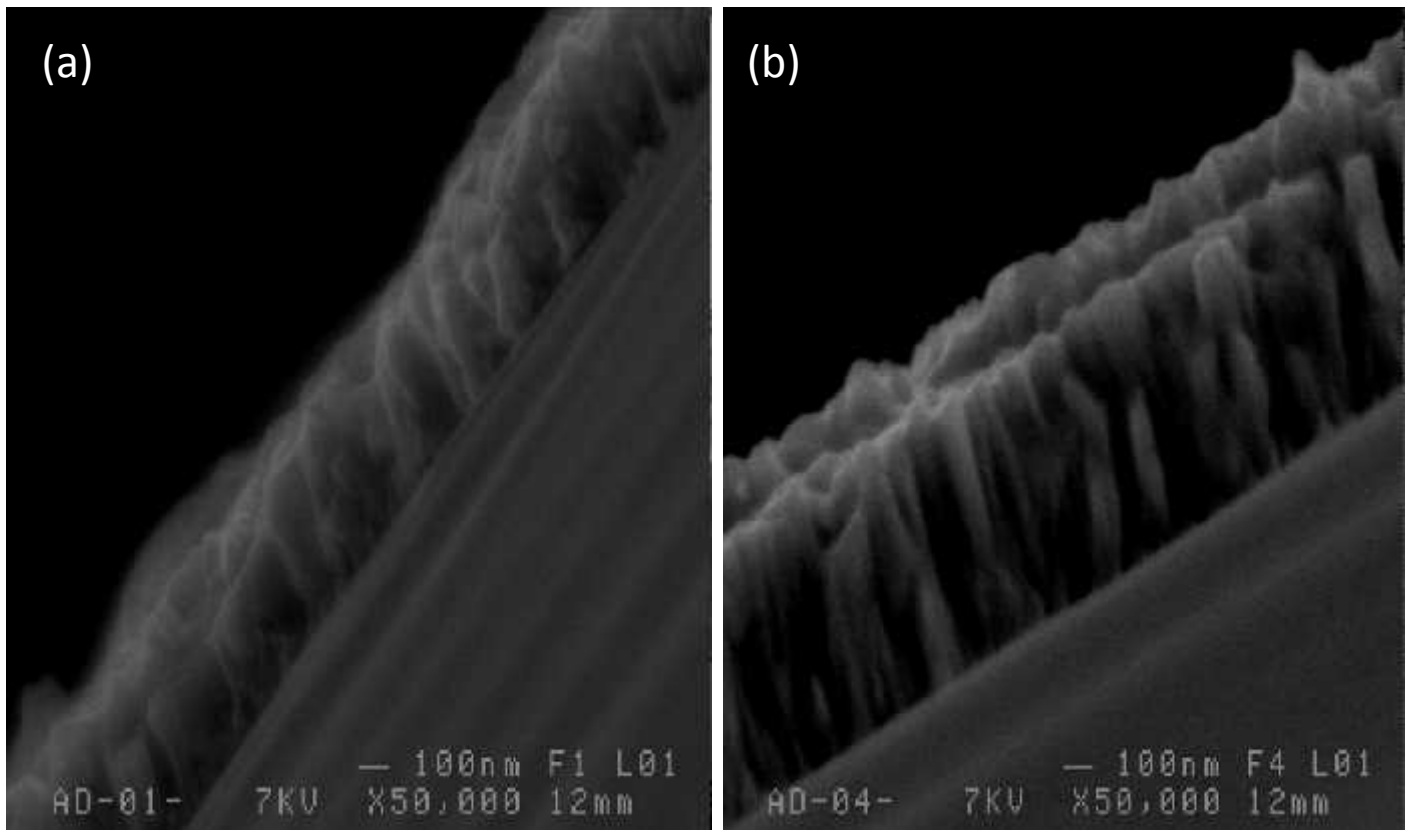


Fig. III.10. Cross-sectional images of the  $\text{In}_2\text{O}_3$  thin films deposited at various deposition time of: (a) 4 min and (b) 13 min.

Figure III.10. Confirms that microstructure is greatly influenced by the deposition time, From Fig. III.10. (a) it is observed that some grains grew in the through-thickness direction, but others did not. It can be seen also in Fig. III.10. (b) that there is a very clear columnar structure. Furthermore,

it is Clear that the thicker film consists of two layers. Z. Qiao et al reported the similar results [61]. The good cohesion between the  $\text{In}_2\text{O}_3$  thin film and the glass substrate is obviously observed.

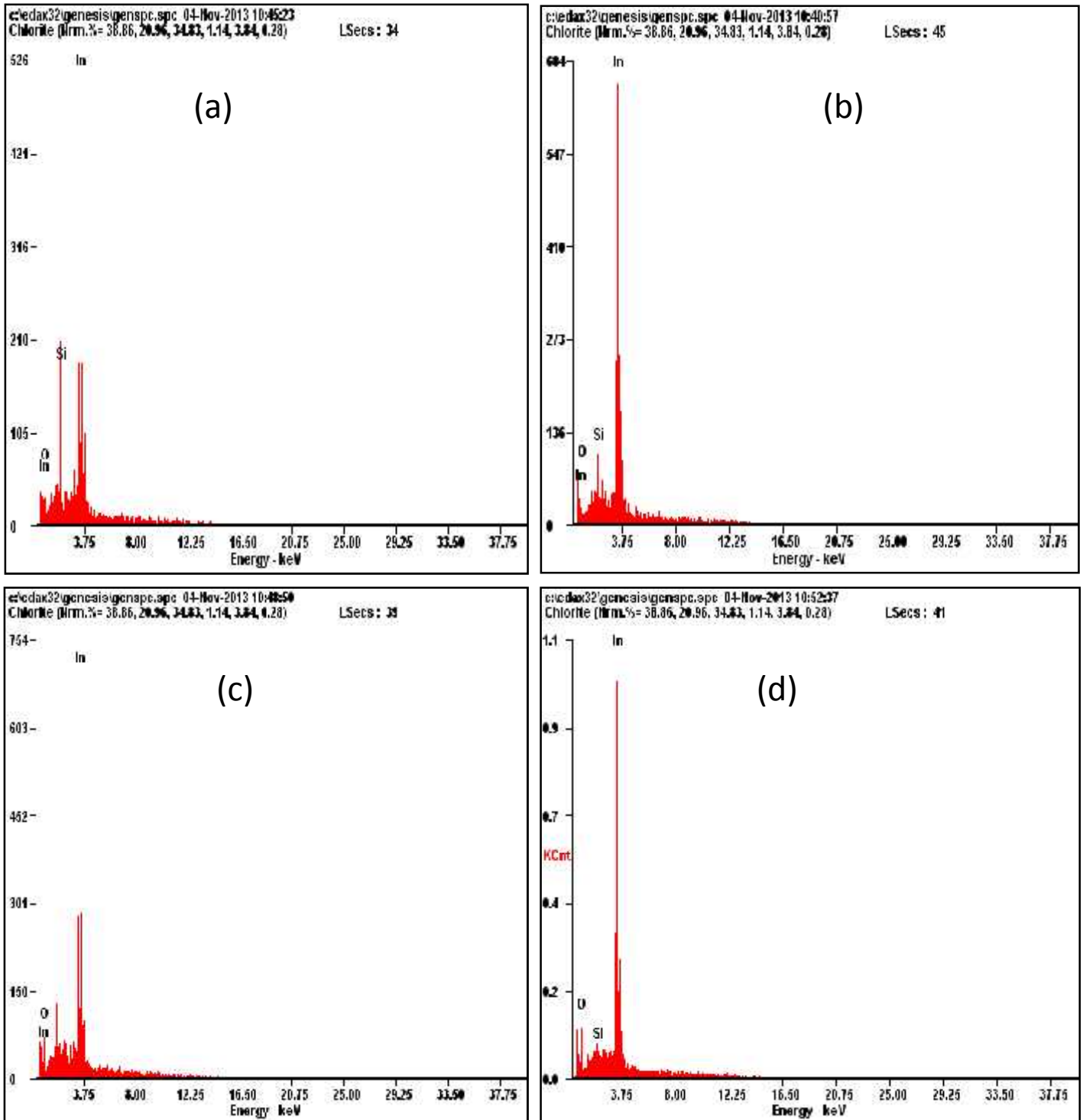


Figure III.11. EDS analysis of the  $\text{In}_2\text{O}_3$  thin films deposited at various deposition time of: (a) 4min, (b) 7min, (c) 10 min and (d) 13min.

Energy dispersive analyses of X-rays (EDAX) generated by the incident electron beam were carried out to investigate the composition of indium oxide films formed (see figure III.11.). All of the  $\text{In}_2\text{O}_3$  films are composited from O and In atoms in addition to Si which come from the substrate.

### III.5. optical properties

The optical transmittance measured as a function of the wavelength is depicted in Figure III.12.

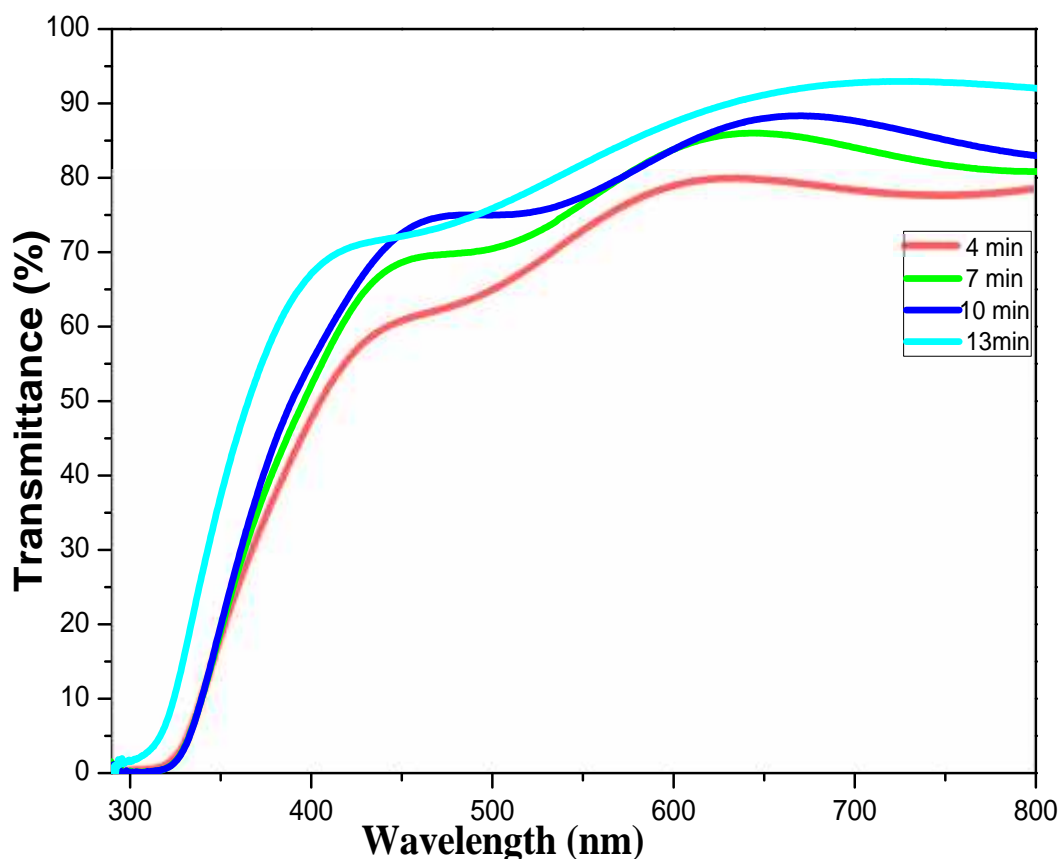


Fig. III.12. Optical transmittance spectra of  $\text{In}_2\text{O}_3$  thin films as a function of the wavelength

As the deposition time change in the optical transmittance observed (see figure III.13). A maximum visible transmittance (VT) of 93% is observed at 709 nm for the films prepared at 13 min (thickness of this film = 725 nm), whereas the smallest optical transmittance (VT) of 79% is Observed at 628 nm for the film prepared at 4 min (thickness of this film = 395 nm) despite that this film is thinner than the other films. Similar observation has been found by other researcher [71].

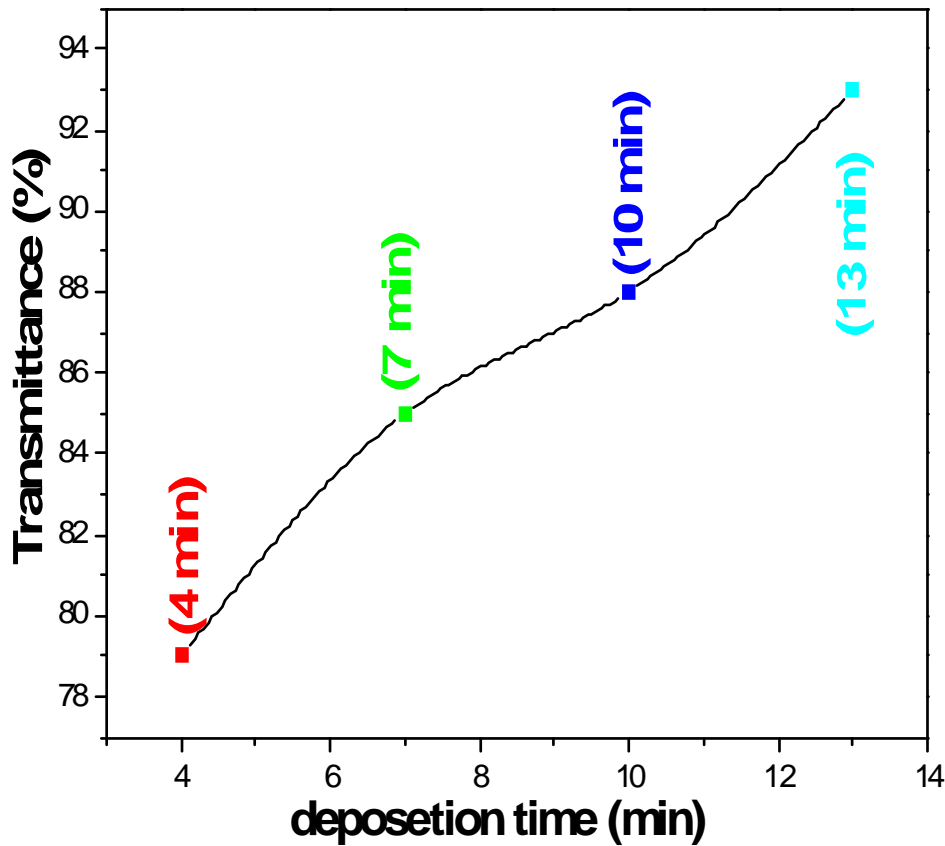


Figure. III.13. Optical transmittance of  $\text{In}_2\text{O}_3$  thin films as a function of deposition time

The higher transmittance observed in the films is attributed to decline of scattering effects, structural homogeneity and better crystallinity, whereas low transmittance observed in the layer might be due to the less crystallinity leading to more light scattering [72]. On the other hand, the high transmittance of the film deposited at 13 min is due to the less roughness of this film. It is well known that rough surface causes the light scattering resulting in transmittance reduction [73]. In conclusion, the maximum visible transmittance value of films is the result of the combination of several effects: structural homogeneity, better crystallinity and the smooth surface.

The values of the optical band gap are obtained by extrapolating the tangential line of the data to the abscissa axis in the plot of  $\alpha \nu^2$  as a function of  $h\nu$  as shown in Figure IV.13. Film deposited at 4 min has low band gap 3.46 eV, this is due to the presence of an amorphous phase in this film network as deduced from the XRD. Amorphous phase is generally accompanied by a disorder in the film network. For film highly disordered, the band tail width (Urbach tail) is large; consequently the optical band gap is narrowed. This situation is reported in amorphous silicon thin

films a-Si:H [74] and silicon nitride thin films a-Si:N [75]. They have also found the optical band gap shift towards the lower energies induced by a disorder in the film network [76, 77]. Moreover,

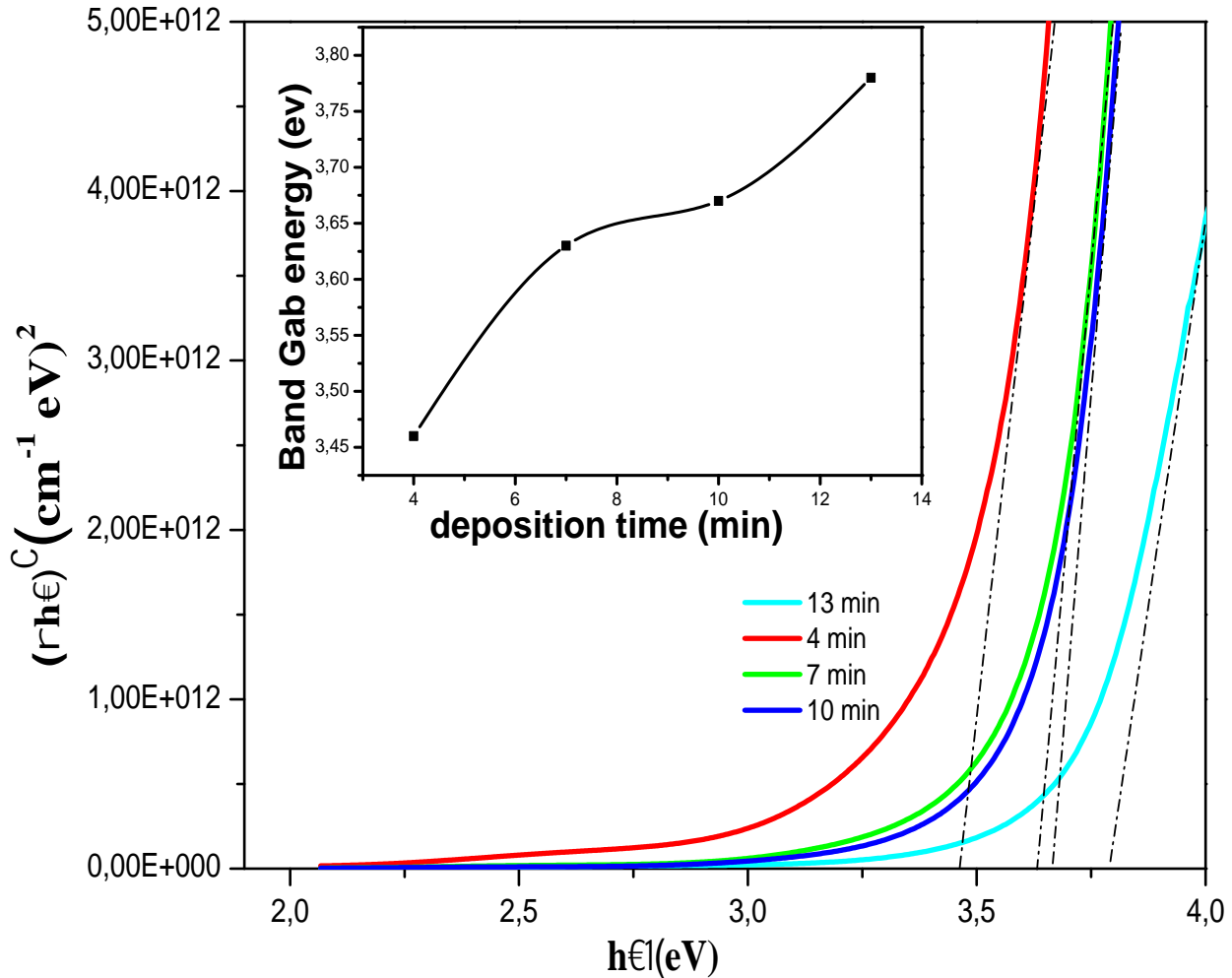
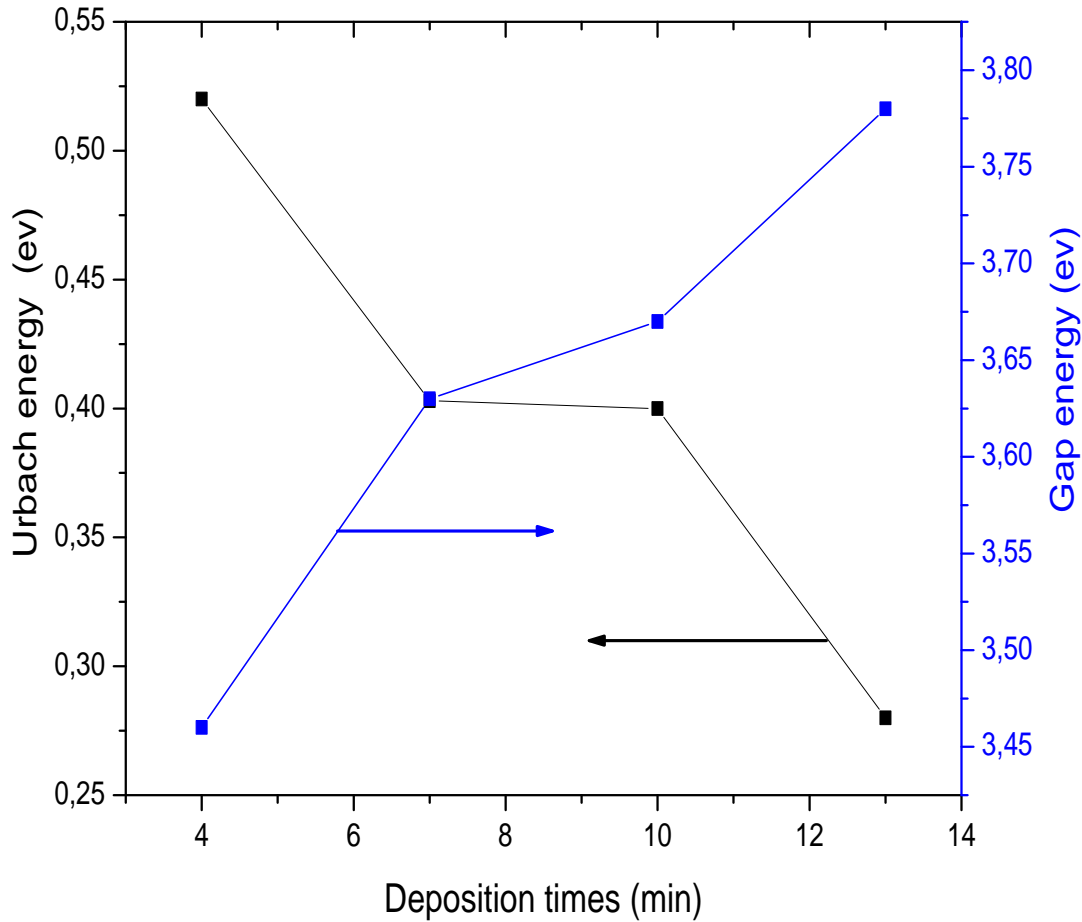


Figure III.13. Optical band gap energy for the  $\text{In}_2\text{O}_3$  thin films deposited at various deposition times.

The value of the Urbach tail energy for the film deposited at 4 min confirms this hypothesis (see figure III.14.). The optical gap of films which deposited at 7, 10, and 13 min is close to its value for  $\text{In}_2\text{O}_3$  bulk material. This is due to the good crystallinity of these films [73]. Similar values of optical band gap have been found by other researchers [78, 64].

Figure III.14. Shows variation of optical band gap energy and Urbach energy with deposition times. It is clear that Urbach energy decreases with increasing of deposition times. This is due to the enhancement crystallinity of the films.



III.14. Variation of Optical band gap energy and urbach energy for the  $\text{In}_2\text{O}_3$  thin films deposited at various deposition time.

### III.1.6. Electrical properties

Figure III.15. Shows the dependence of electrical resistivity ( $\rho$ ) and figure of merit on deposition time. Resistivity decreases continuously with increase in the deposition time. They have also observed decrease in the resistivity of  $\text{In}_2\text{O}_3$  thin films with increasing of deposition time [60]. The high values of the electrical resistivity observed in films deposited at 4, 7 and 10 min are mainly attributed to the increasing number of scattering centres and trapping centres in these films. The SEM surface images of these films show distinct grain boundaries and surfaces roughnesses (see figure III.9.a, b and c). In contrast, the film deposited at 13 min consists of a dense array of grains without discernible boundaries (see figure III.9.c.). The grain boundaries act as scattering centres and hence reduce the effective electron mobility of the film, while the adsorption of oxygen in the grain boundaries leads to trapping centres that decrease the free-electron concentration; as the origin for the formation of potential barriers at the grain boundaries is the existence of defect States

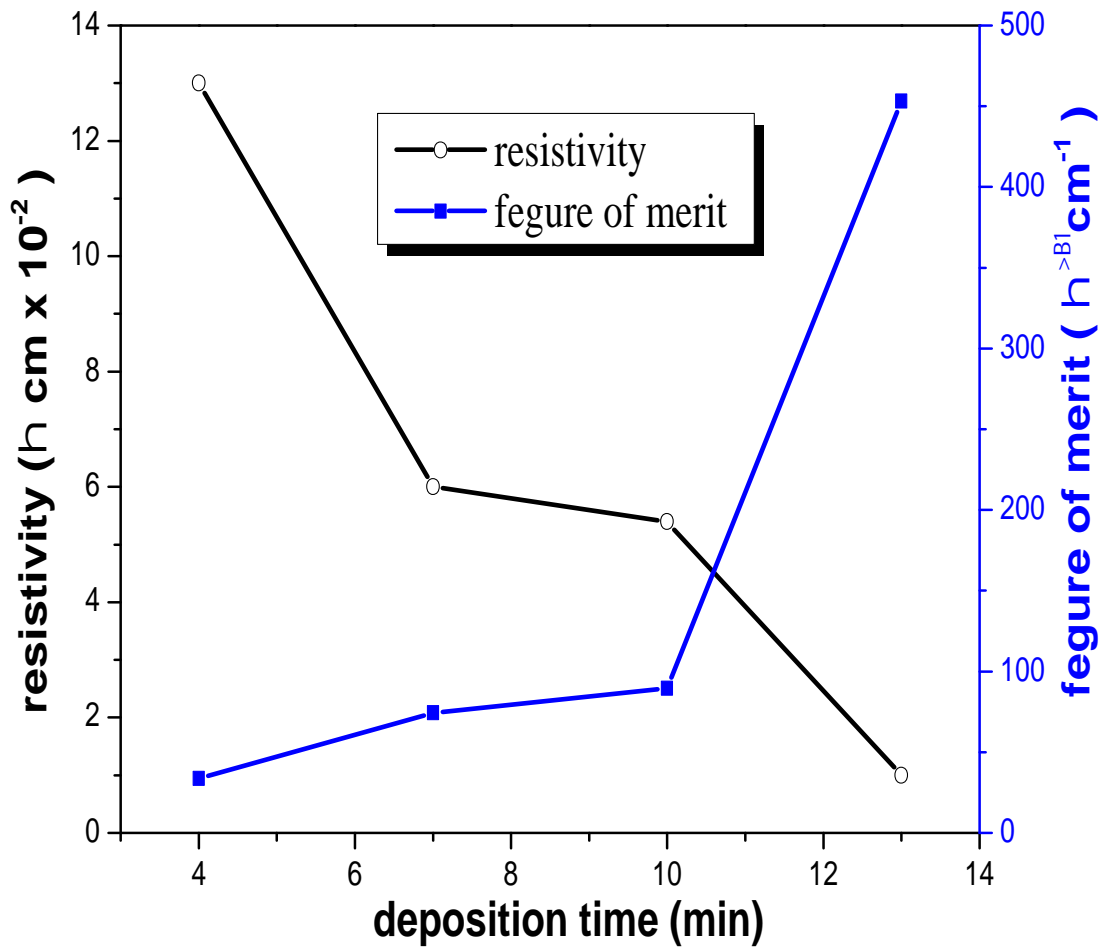


Figure III.15. Electrical resistivity and figure of merit of  $\text{In}_2\text{O}_3$  thin film deposited at various deposition times

In the boundary region, it is expected that any increase in the density of these defect states will cause an increase in the barrier height [79]. The effect of oxygen on the grain boundaries has been experimentally confirmed for polycrystalline indium-tin oxide (ITO) films by temperature dependence of Hall mobility measurements carried out by Morris et al. [80]. From this discussion we can say that the grain boundaries in polycrystalline semiconducting films behave like “sponges” absorbing oxygen and passing it on the grains and this process is associated with the complex nature of the conduction mechanism involved in polycrystalline films.

The figure of merit is known to be an index for evaluating the performance of transparent conducting films, and it is given by the equation  $F = (-\ln T)^{-1}$ , where  $F$  is the electrical resistivity and  $T$  is the average transmittance in the wavelength range of 400 – 800 nm [81]. The figure of merit for the  $\text{In}_2\text{O}_3$  thin film deposited at 4 min was estimated at  $33.61 \text{ cm}^{-1}$ . As the deposition time increases to 13 min, the figure of merit increases to  $453 \text{ cm}^{-1}$  (see figure IV.13.).

The increase in the figure of merit results from the decrease in the electrical resistivity with increasing deposition time. The experimental data suggest that a deposition time of 13 min is the best condition for depositing high-quality  $\text{In}_2\text{O}_3$  films.

### III.7. Conclusion

The effect of the deposition time on the crystalline state, surface morphology, optical, and electrical properties of  $\text{In}_2\text{O}_3$  films was investigated. X-ray diffraction reveals a polycrystalline nature for all films with a preferred grain orientation along to (222) plane when the deposition time changes from 4 to 10 min, but when the deposition time equals 13 min we found that the majority of grains preferred the plane (400). SEM images show that the films are rough surface and the shape of grains changes with the change of the preferential growth orientation.

The optical characterization showed that our films are transparent and The transmittance improvement of  $\text{In}_2\text{O}_3$  films was closely related to the good crystalline quality of the films. We have found also that the optical gap is varied between 3.46 eV and 3.79 eV, and the values found of resistivity are between  $13 \times 10^{-2}$  cm and  $10^{-2}$  cm. Finally, we conclude that deposition time is interesting factor for control the quality of the thin films deposited by ultrasonic spray technique.

# Chapter IV

Solution flow rate influence on  
properties of indium oxide thin  
films

In this chapter, we have studied the influence of solution flow rate on the crystalline structure, morphological, optical and electrical properties of sprayed  $\text{In}_2\text{O}_3$  thin films; and we evaluated the relationship between these properties in general.

### IV.1. Growth rate

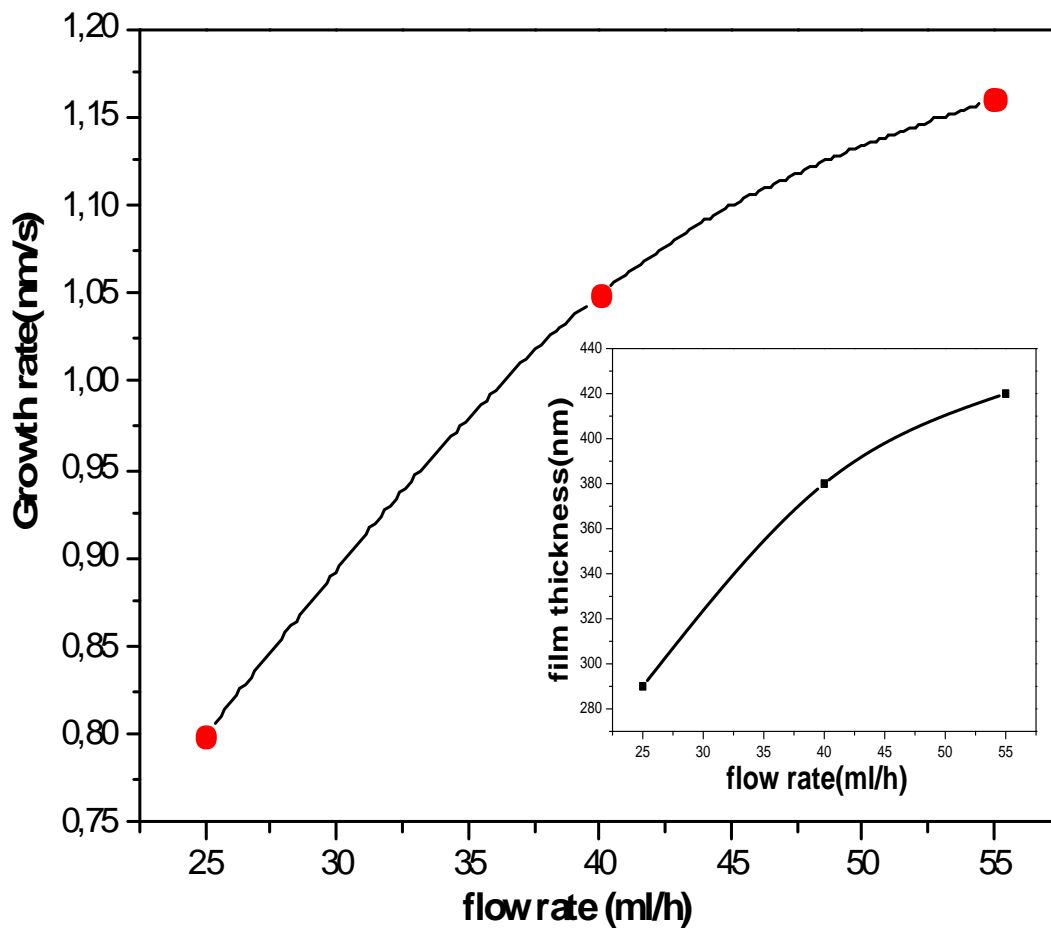


Figure.IV.1. Deposition rate dependence on solution flow rate, inset shows Variation of film thickness as a function of solution flow rate.

Figure IV. 1. Shows variation in growth rate (nm/s) with solution flow rate. The growth rate increase with the increase of the solution flow rate due to the increase of film thickness (see figure IV.1.) as result of increase in spray volume flux over substrate surface.

## IV.2. Structural properties

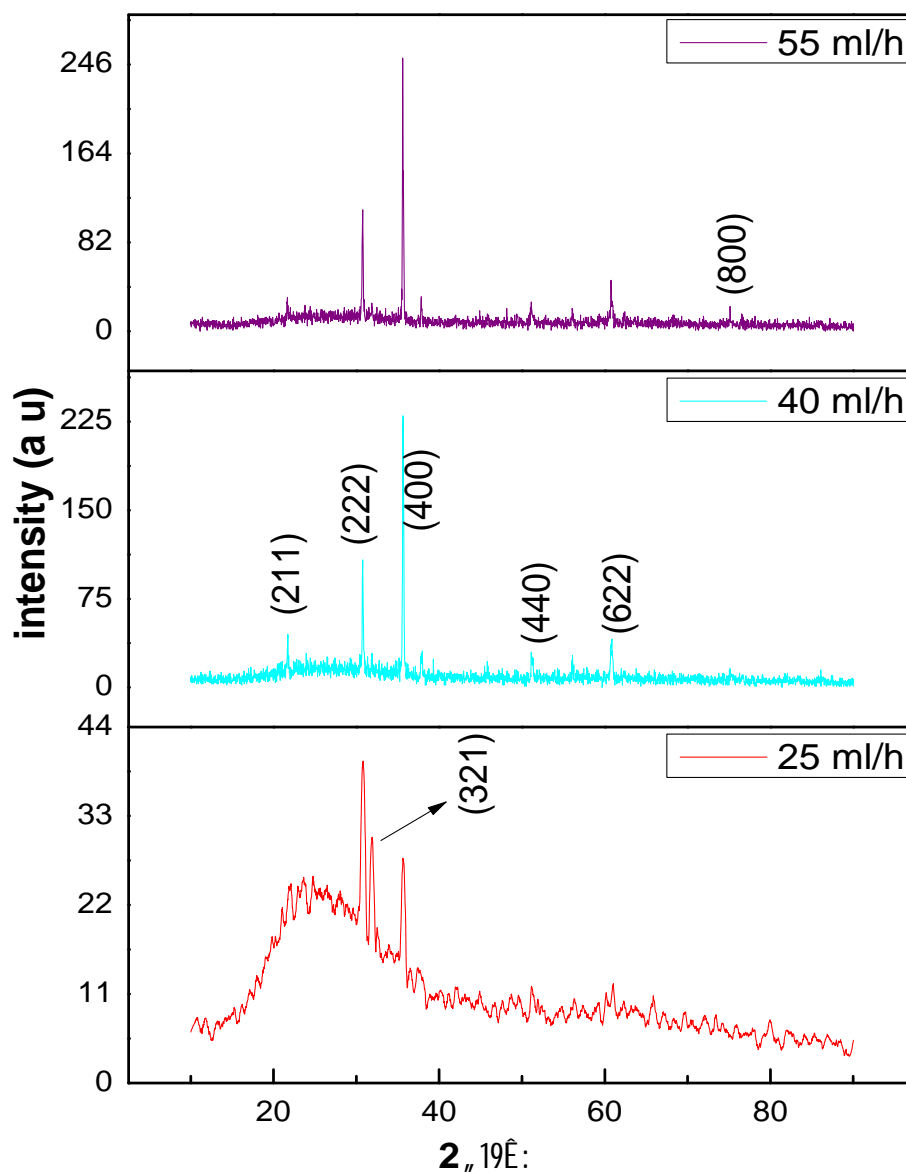


Figure IV.2. XRD diffraction pattern of  $\text{In}_2\text{O}_3$  thin films prepared with different spray rates.

The XRD patterns for  $\text{In}_2\text{O}_3$  thin films grown at different spray rate are shown in figure IV. 2. It is obvious that the  $\text{In}_2\text{O}_3$  thin films reveal polycrystalline structure with differently orientated crystalline planes such as (211), (222), (321), (400), (411), (440) and (622). All peaks from XRD patterns coincide well with those given in the JCPDS card (no 06-0416) (see figure III.3.). It is interesting to note that with the increasing of spray rates from 25 ml/h to 50 ml/h there is

preferential growing competition between (222) and (400) planes, this indicates that the spray rate has significant effect on the crystal grain orientation of  $\text{In}_2\text{O}_3$  thin films. The intensity ratio of the (400) to (222) reflection is used to evaluate the spray rate effect on the film texture of the films is shown in IV. 3.

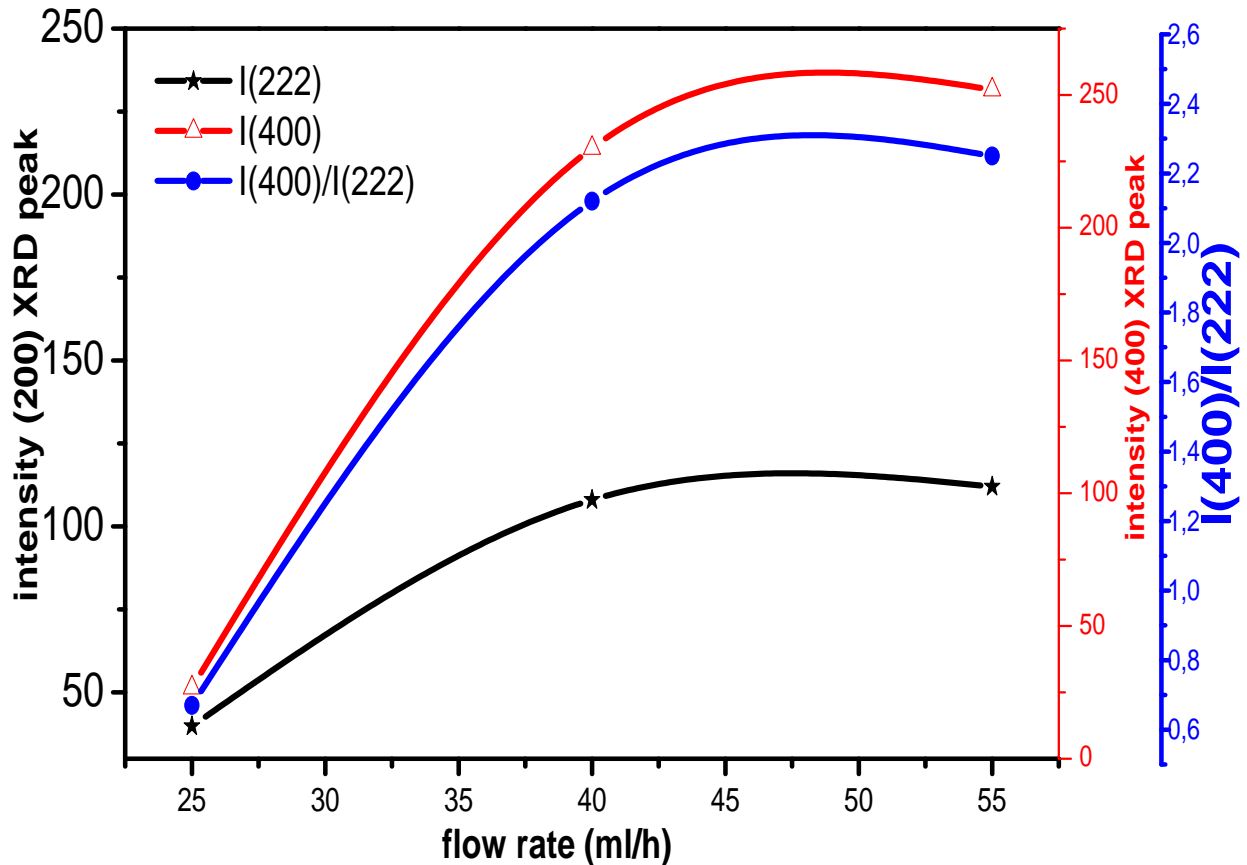


Figure V.3. Flow rate effect on the film

Depending on the results of the current study we found that the ratio  $I(400)/I(222)$  increase with the increasing of spray rate from 25 ml/h to 55 ml/h. The  $I(400)/I(222)$  ratio suggests that the films deposited at 25 ml/h possess a preferred growth orientation along the [1 1 1] direction and when the spray rate increase to 55ml/h, the preferred growth orientation is changed to [100] direction. We believe that the preferred growth development of crystalline grains mainly depends on the initial orientations during the nucleation process and the growth process. For the spray rate equals 25ml/h The (222) nucleation is a primary nucleation due to the surface free energy of formation of the planes of the  $\text{In}_2\text{O}_3$  cubic structure, the (111) texture presents a lower surface free energy plane due to the high atomic density of this plane [59], However, with increasing of spray rate rates more than 25ml/h, the (400) nucleation is preferred, and a strict improvement in preferred growth is observed. The presence of the strong crystallographic texture along the [100] is a priori unforeseen according

To the surface energy of the  $\text{In}_2\text{O}_3$  cubic structure. This discrepancy can be explained as follows: with the increasing of the spray rate the films thickness increases which suppresses the intensity of the (222) plane and stimulate the (400) orientation of the  $\text{In}_2\text{O}_3$  films [61]. Moreover, the promotion of (400) plane texturing has also been associated with improvement in crystallinity in these cases. Similar effect has been observed by Saxena et al [82]. In their study of thickness dependence on the structural properties of  $\text{In}_2\text{O}_3:\text{Sn}$  films prepared by spray pyrolysis. Also, P. Thilakan et al found that ITO films with (400) crystallographic orientation have larger grain size than the (222) textured films [83]. On the other hand, it is interesting to note that the number of the diffraction peaks increase with the increasing of the spray rates due to formation of new nuclei on the growing surface; with the rise of the solute atoms, formation of new nuclei may occur on areas freshly exposed as a consequence of coalescence. Furthermore, we found that the preferred growth orientation connected with the grain shapes as observed by SEM analysis (explained later). This goes in harmony with the result of the deposition time effect on the structural and morphological properties (chapter III).

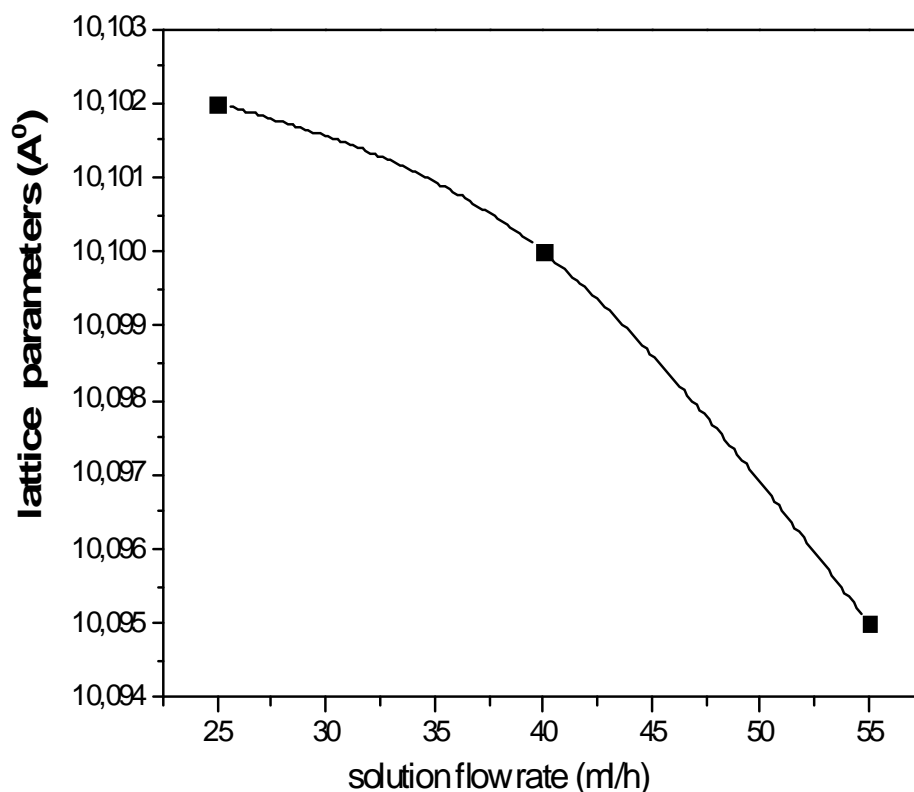


Figure. IV.4. the lattice parameters ( $a = b = c$ ) of the  $\text{In}_2\text{O}_3$  films as a function of the solution flow rate.

The lattice parameters ( $a = b = c$ ) of the  $\text{In}_2\text{O}_3$  films are shown in figure IV.4. A characteristic shift towards higher angle compared to reflexes of ideal crystals is always observed for all peaks. This indicates that the lattice parameters is slightly smaller than the reported value of  $10.11 \text{ \AA}$  for pure indium oxide which is my be due to strain effect arising from thermal expansion [62].

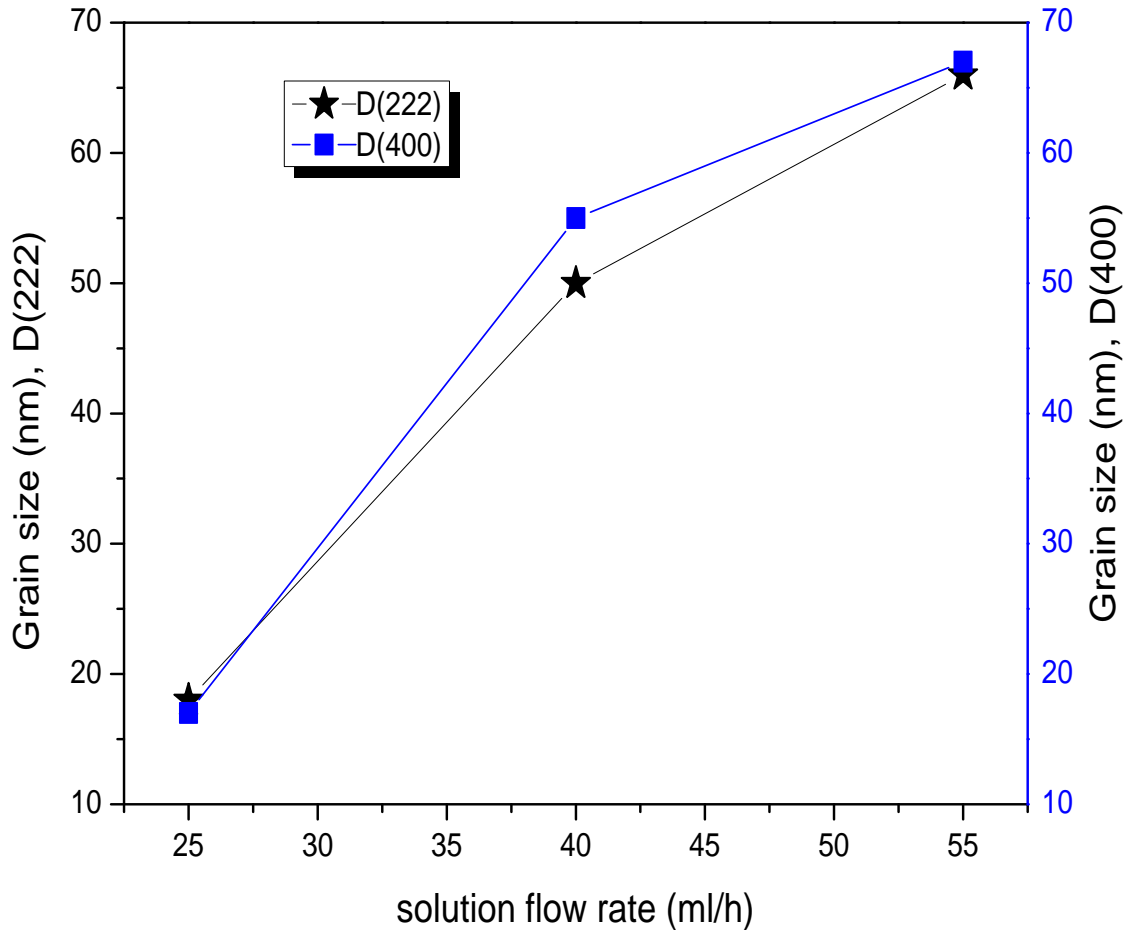


Figure IV.5. Average grain size of  $\text{In}_2\text{O}_3$  thin film as a function the solution flow rate

Figure IV.5. Presents variation of grain size as a function of solution flow rate. The results show that average grain size increases from 17 to 67 nm with increasing of the solution flow rate. This is probably due to the increased nucleation numbers which cluster together to form larger grains. The raise in the nucleus numbers due to an increase of the solute atoms arriving to substrate. G. Korotcenkov et al found that the grain size increase with increase of the solution flow rate [57].

The dislocation density ( ) and the strain ( ) are shown in figure IV.6. The crystal defect shows a decreasing trend with increasing in solution flow rate. This is due to the Improvement of crystalin quality of the films with the increase of the solution flow rate [66].

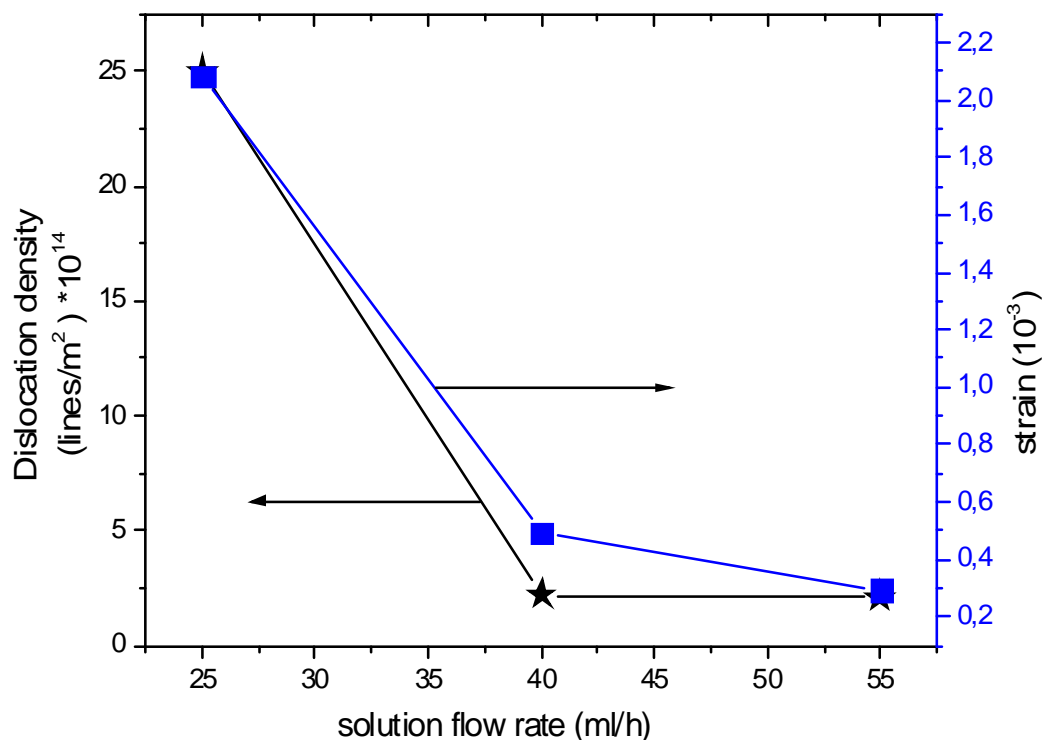


Figure IV.6. The dislocation density ( ) of the films as a function of deposition time

### IV.3. Morphological properties

The scanning electron microscope (SEM) pictures in figure.IV.7 show the typical surface morphology of differently prepared  $\text{In}_2\text{O}_3$  films as a function of solution flow rate. It is clear that the solution flow rate has significant impact on the morphological properties of these films. For the film deposited at 25 ml/h (figure IV.7.a.), a large number of quasi- pyramidal shaped crystallites have developed on top of glass substrate. Also, the SEM surface image of this film show distinct grain boundaries. On the other hand, the samples deposited at 40 ml/h (Fig. IV.7. (b)) and 55 ml/h (Fig. IV.7. (c)) show that the grains are granular in shape but seen to be densely packed (without discernible boundaries) and a relatively smooth surface whit a porous. This porous may be due to the increase of the solution sprayed. Based on the results of the XRD analysis we can say that: there is a relation chip between the structural and morphological properties. The chap of the crystallites changes with the change of the preferred growth orientation. This indicates that the difference in grain shapes suggests difference in preferred growth orientation. This goes in harmony with the result of the deposition time effect on the structural and morphological properties of  $\text{In}_2\text{O}_3$  (chapter III).

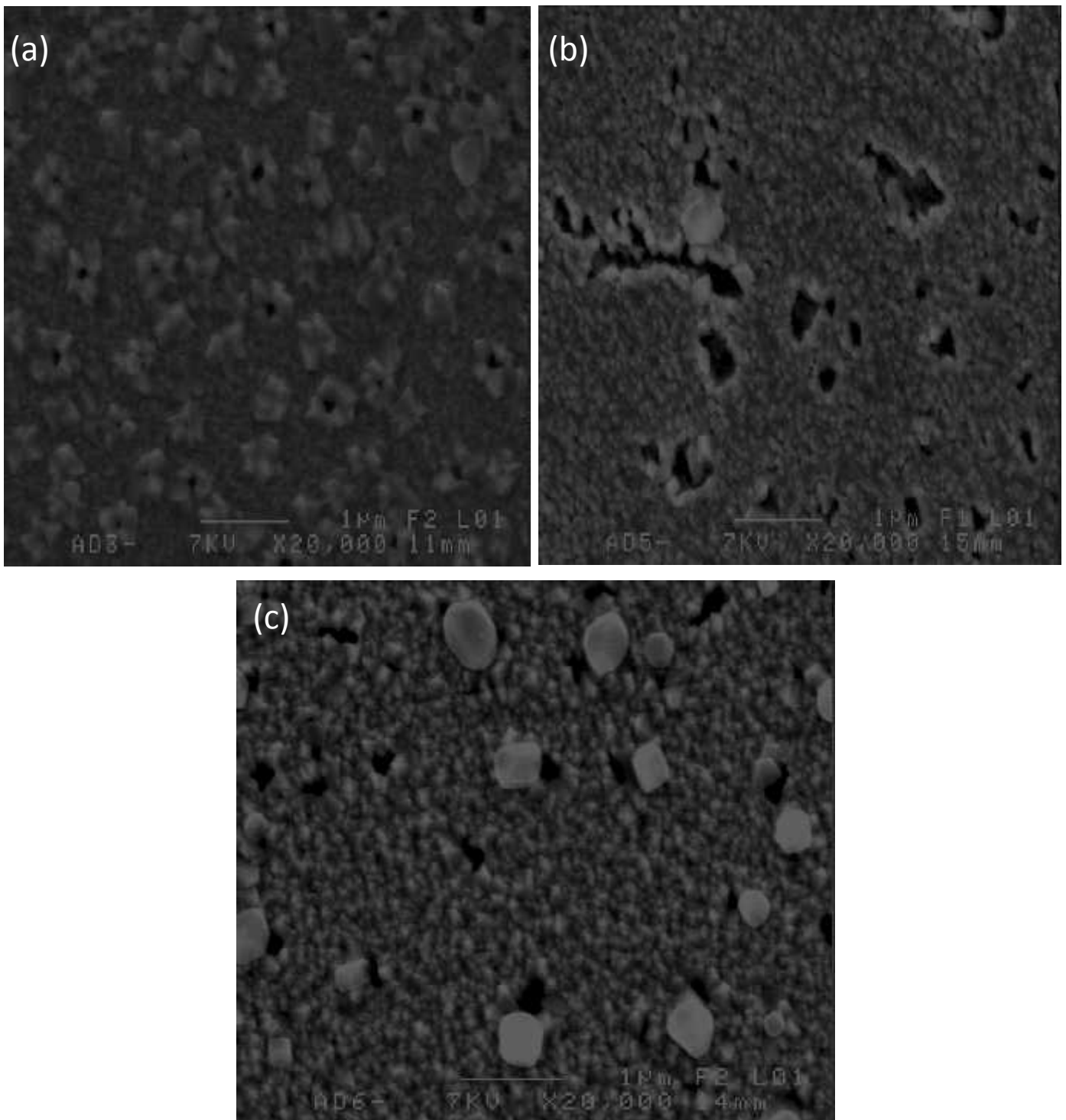


Figure IV.7. SEM surface images of the  $\text{In}_2\text{O}_3$  thin films deposited at various flow rate of: (a) 25 ml/h, (b) 40 ml/h and (c) and 55 ml/h.

The Cross-sectional images confirm that microstructure is greatly influenced by the spray rates, From Fig. IV.7 (a), it is observed that this film contains only one layer. Besides, some grains grew the direction perpendicular to the substrate, but others did not. However, from Figure. IV.7 (b) it is

Observed that this film contains two layers. Furthermore, it is clear that the lower layer has a columnar structure. Y. Shigesato et al found that columnar structure is consistent with the trend toward increasing (100) texture with increasing thickness of  $\text{In}_2\text{O}_3$  thin films [58].

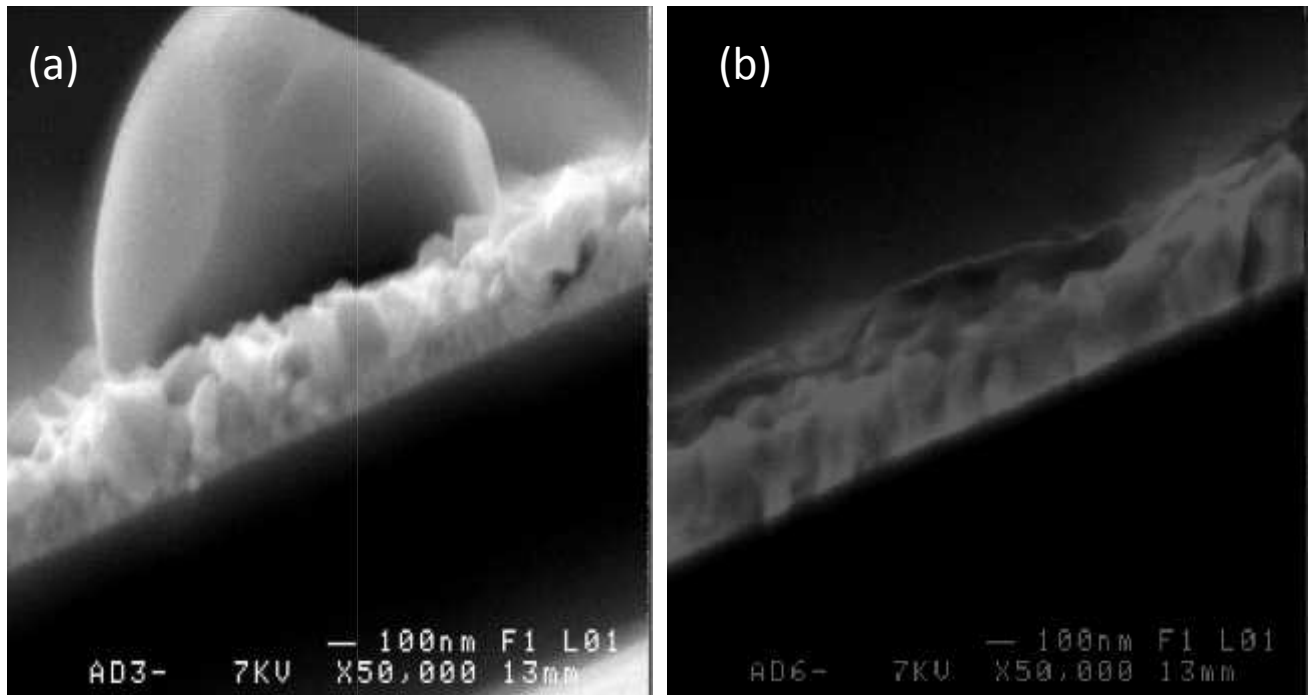
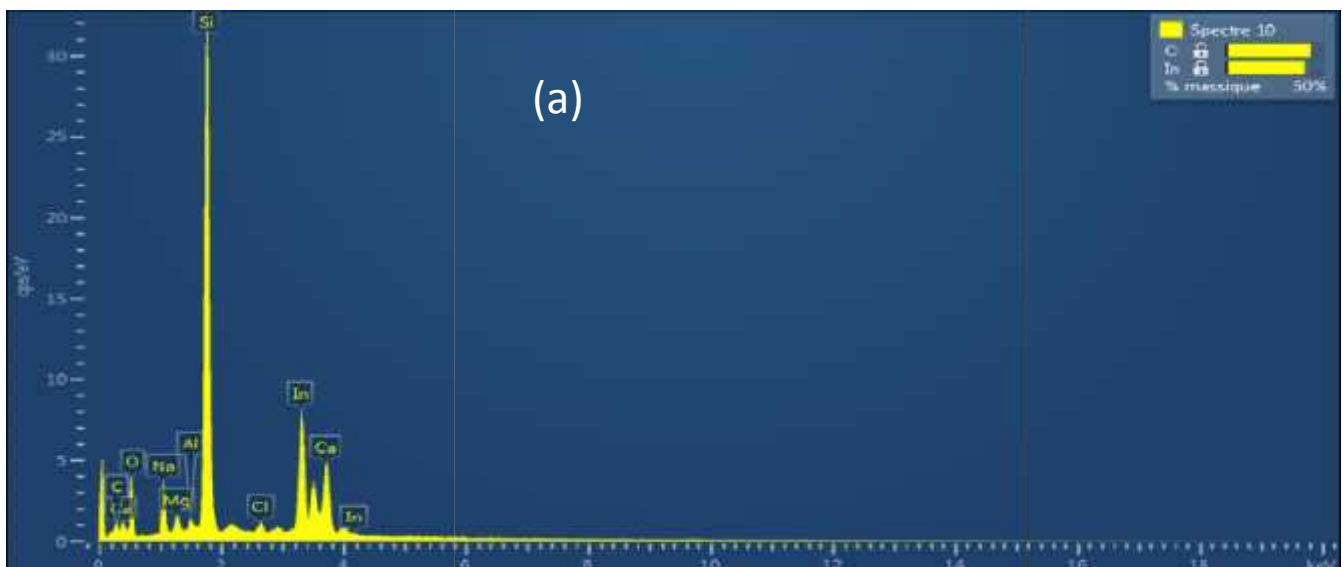


Fig. IV.8. Cross-sectional images of the  $\text{In}_2\text{O}_3$  thin films deposited at various solution flow rate of: (a) 25 ml/h and (b) 55 ml/h.

Figure. IV.9. Show that all of the  $\text{In}_2\text{O}_3$  films are composited from O and In atoms. The presence of the calcium and silicon peak in the spectrum is due to the glass substrate, but the presence of others elements such as carbon may be due to the contamination.



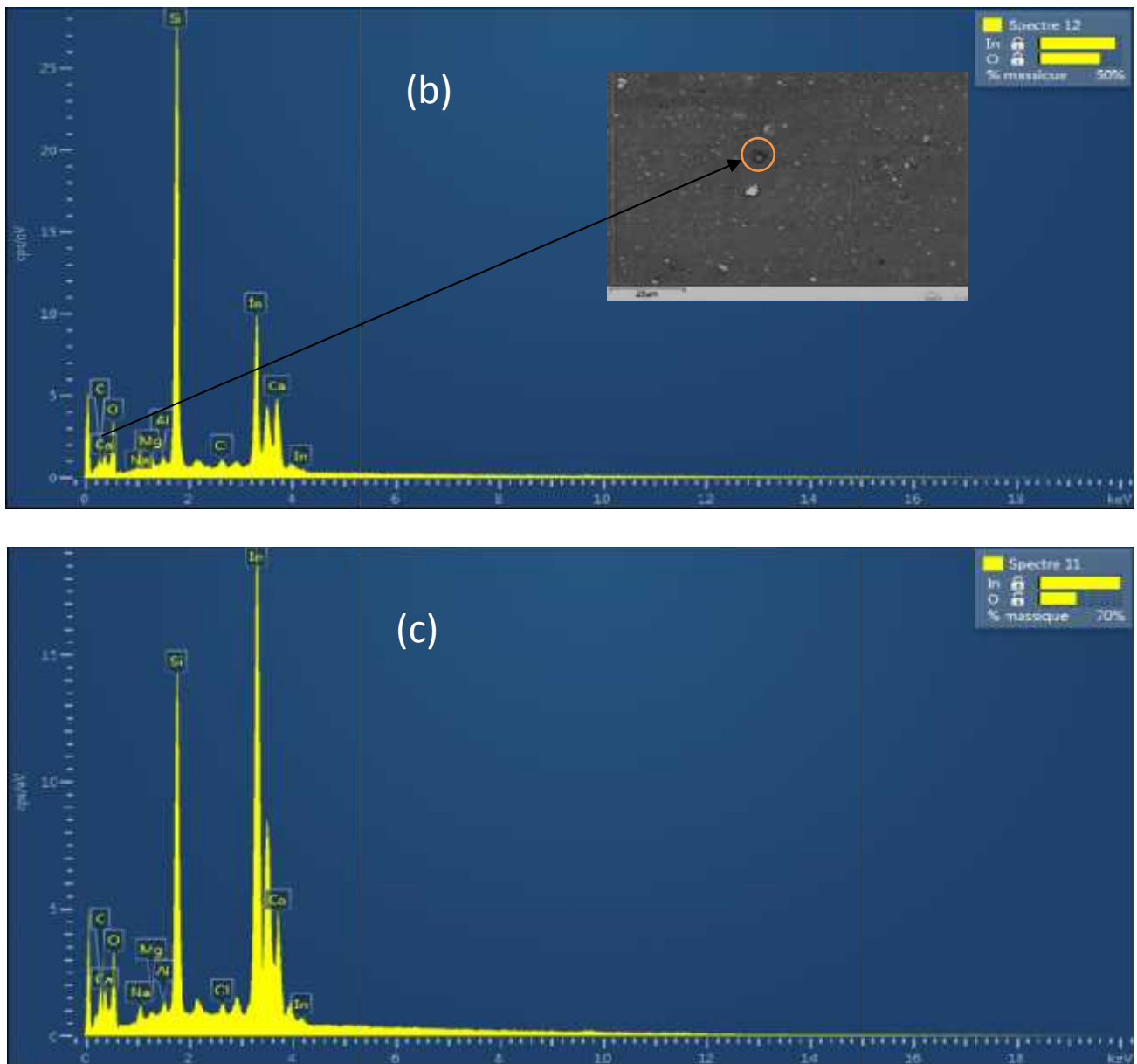


Figure IV.9. EDS analysis of the  $\text{In}_2\text{O}_3$  thin films deposited at various solution flow rate of: (a) 25 ml/h, (b) 40 ml/h and (c) 55 ml/h.

#### IV.4. optical properties

Analysis of optical (transmission/absorption) spectra is one of the most useful techniques for the understanding of the band structure and energy gap of both crystalline and amorphous materials. Figure IV.10. Shows the dependence of the optical transmission and spectra of the investigated thin films in the wavelength region 290–900 nm as a function of solution flow rate. The films deposited at solution flow rate 25 and 55 ml/h show almost identical transmittance in 400–900 wavelength, whereas the films deposited at solution flow rate 40 ml/h show high optical transmittance (91%).

In general the transmittance of the film decreases due to the following factors: (i) presence of mixed phases, (ii) increase in thickness, (iii) presence of defects and oxygen vacancies, (iv) large rms surface roughness, (v) grain boundary scattering, etc. in the present case The low transmittance observed in the film deposited at 25 ml/h (thinner layer) might be due to the presence of mixed phases (the broad peak in the XRD spectra), less crystallinity and roughness surface of this film leading to more light scattering. On the other hand, the high transmittance of the film deposited at 40 ml/h is due to the Improvement of crystalline quality of this film and the less roughness of this film as shown in SEM images. Furthermore, it is clear that the interference fringes absence in the spectrum of films deposited at 25 ml/h and 55 ml/h. This can be attributed to the roughness of the interface air/film; incident light is diffused instead of reflected in one direction. Moreover, the beginning of its presence in the transmission spectrum of the film deposited at 40 ml/h indicates that the film surface is less roughness. This is supported by the SEM surface images which indicate that the film deposited at 40 ml/h is less roughness.

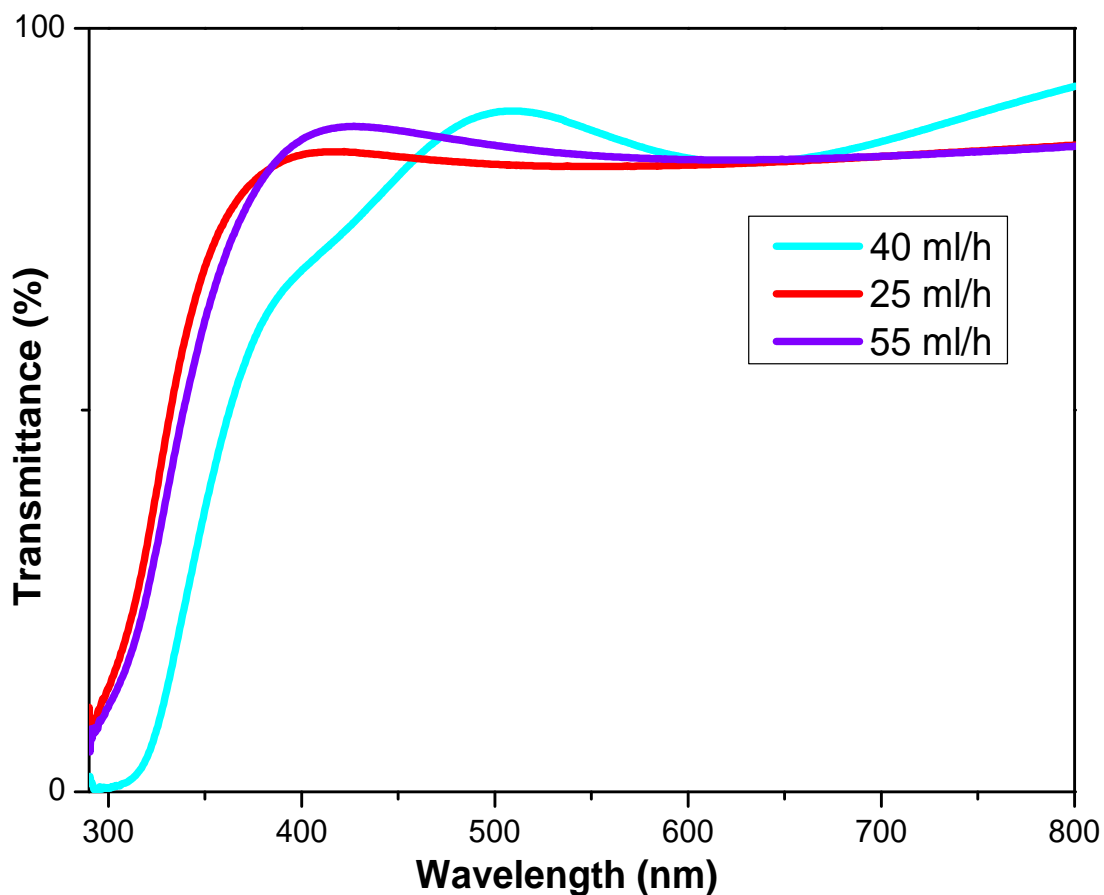


Fig. IV.10. Optical transmittance spectra of In<sub>2</sub>O<sub>3</sub> thin films as a function of solution flow rate

The values of the optical band gap are obtained by extrapolating the tangential line of the data to the abscissa axis in the plot of  $\alpha \nu^2$  as a function of  $h\nu$  as shown in Fig IV.11. Film deposited at 25 ml/h has higher band gap 3.93eV, this due to the quantum confinement effect due to the small grain size [84]. It is well known that the energy band gap of semiconductor nanoparticles increases with decreasing the grain size, which leads to a blue shift of the optical absorption edge and have been observed in many semiconductor nanoparticles system [85]. The optical gap of films which deposited at 55 ml/h ( $E_g = 3.79$  eV) somehow big which is not due to the quantum size confinement, but probably due to the reduction of disorder in film network due to the improvement in crystalline quality of this layer. The values of optical gap are same with those obtained by precedent studies [84, 85].

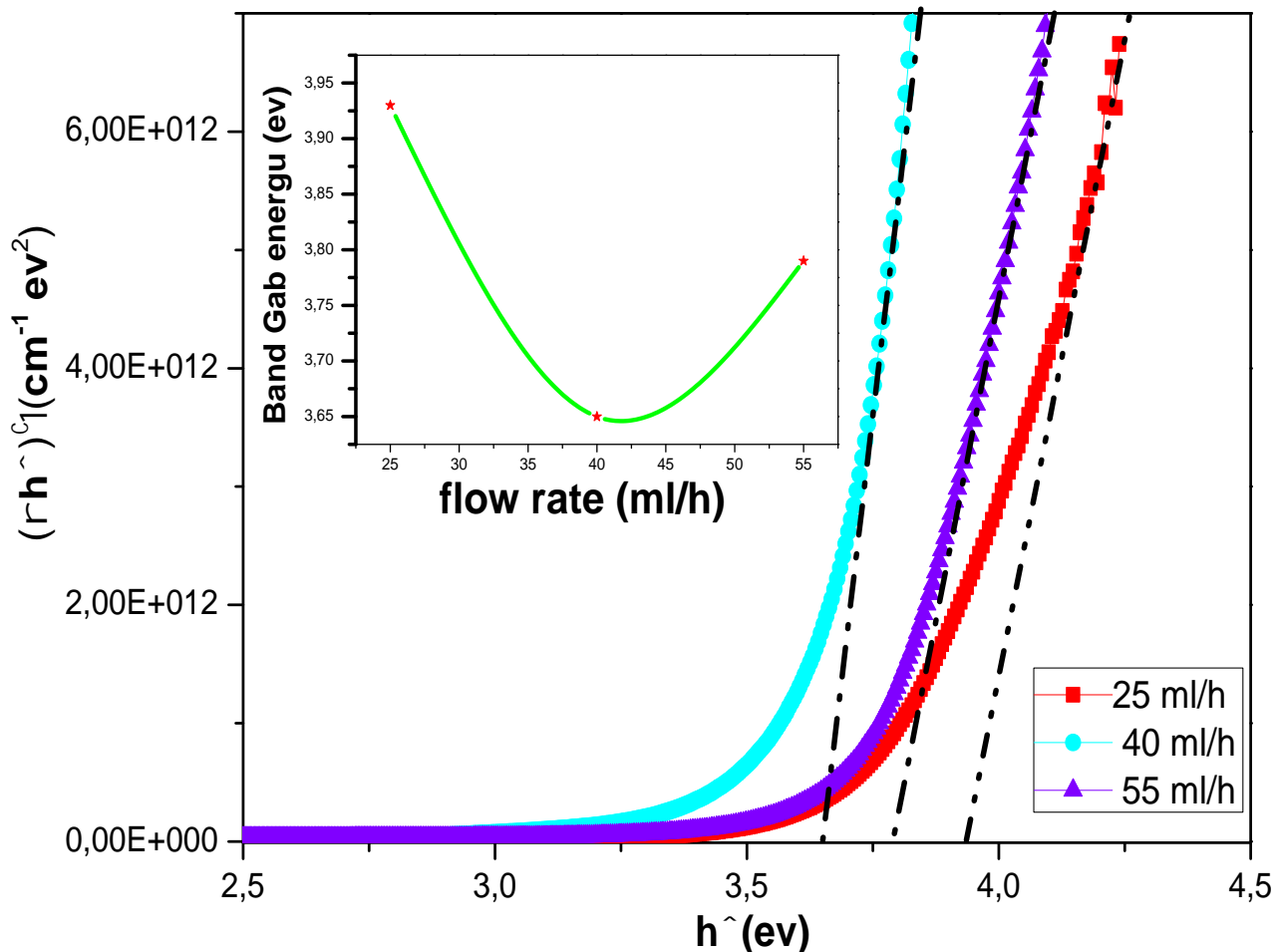


Fig IV.11. Optical band gap energy for the  $\text{In}_2\text{O}_3$  thin films deposited at various solution flow rate.

Figure IV.12. Shows variation of Urbach energy with solution flow rate. It is clear that Urbach energy decrease with increasing of deposition times. This is due to the enhancement crystallinity of the films. Melsheimer and Ziegler [86] suggest that the Urbach tail parameter  $E_0$ , could be a function of structural disorder ( $E_0$  decreases with the increase of structural order). This hypothesis is verified in our results.

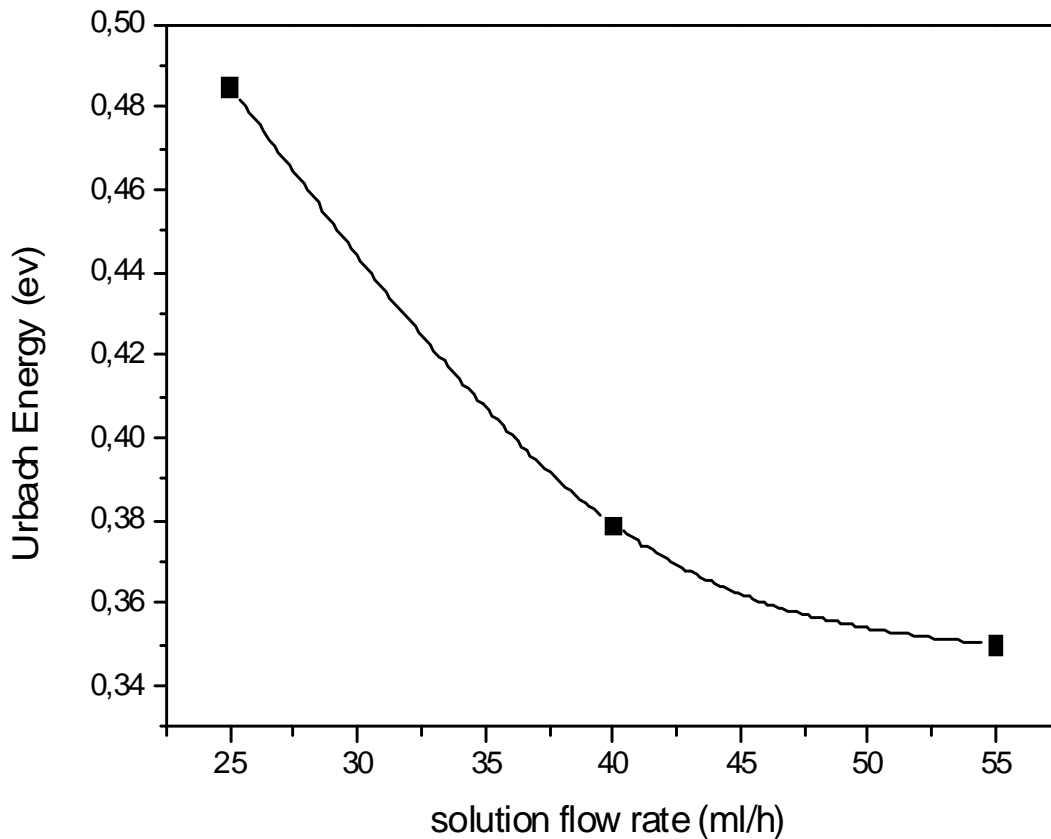


Figure. IV.12. Variation of Urbach energy for the  $\text{In}_2\text{O}_3$  thin films deposited at various solution flow rate.

Figure. IV.13. Shows Variation of reflectance as function of wavelength for  $\text{In}_2\text{O}_3$  films prepared at 25, 40 and 55 ml/h. It is clear that the film deposited at 25 ml/h shows a low reflection by comparison with other films. This can be attributed to the roughness surface of this film. C. Eberspacher et al, found that a roughness with 500 nm r.m.s. or less is sufficient to reduce optical reflection for sprayed ZnO thin film [87]. Also, A. Mosbah et al found that the film with a roughness surface exhibits a low reflection [70].

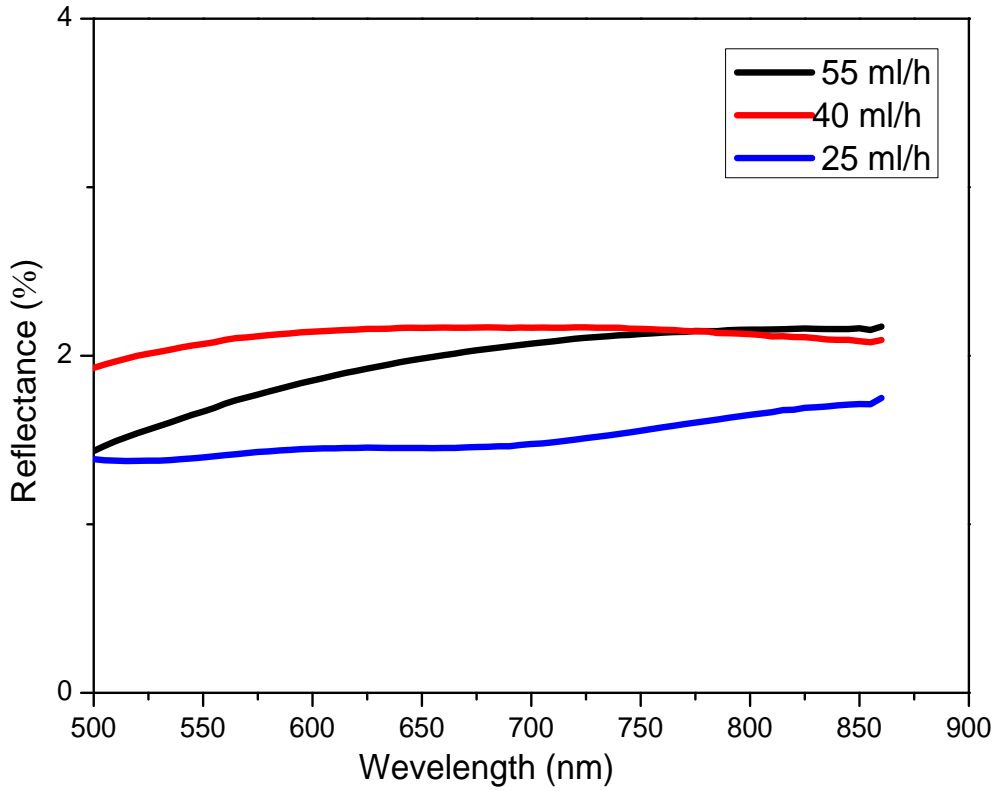
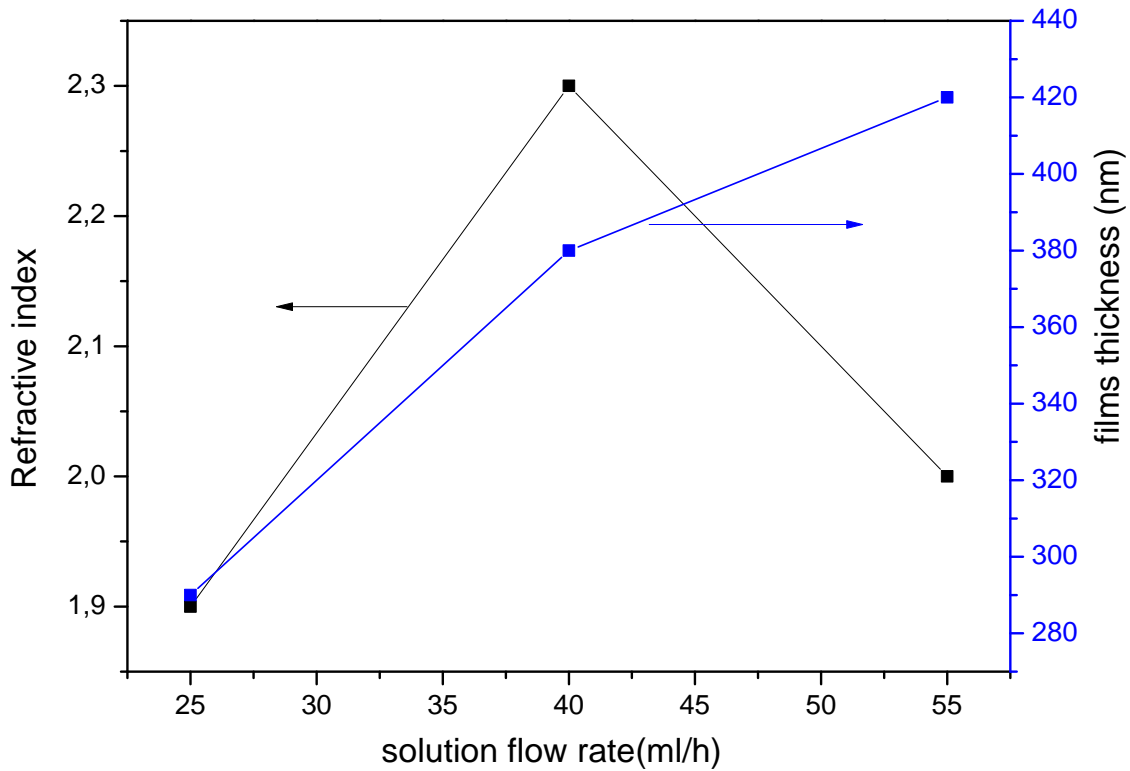


Figure. IV.13. Variation of reflectance for the In<sub>2</sub>O<sub>3</sub> thin films deposited at various solution flow rate.



IV.14. Variation of refractive indices and films thickness for the In<sub>2</sub>O<sub>3</sub> thin films deposited at various solution flow rate.

Fig IV.14. Shows Variation of refractive indices for the  $\text{In}_2\text{O}_3$  films deposited at different solution flow rate. Generally refractive indices of the films increase with the increase of the film thickness. This can be attributed to the rise of average density of the film due to the augment of the solute atoms arriving at the substrate. M. Kaid et al found that the refractive indices decrease from 3.75 to 1 when the films thicknesses take values from 500 nm to 200 nm [88]. however, refractive indices of the film deposited at 55 ml/h ( $d=420$  nm) is less than the film deposited at 380 ( $d=380$  nm). This can be account to the increased porosity of the film deposited at 55 ml/h. D. Beena et al found that the lower values of refractive indices exhibited by the  $\text{In}_2\text{O}_3$  films which are more porous in nature [89].

#### IV.5. Electrical properties

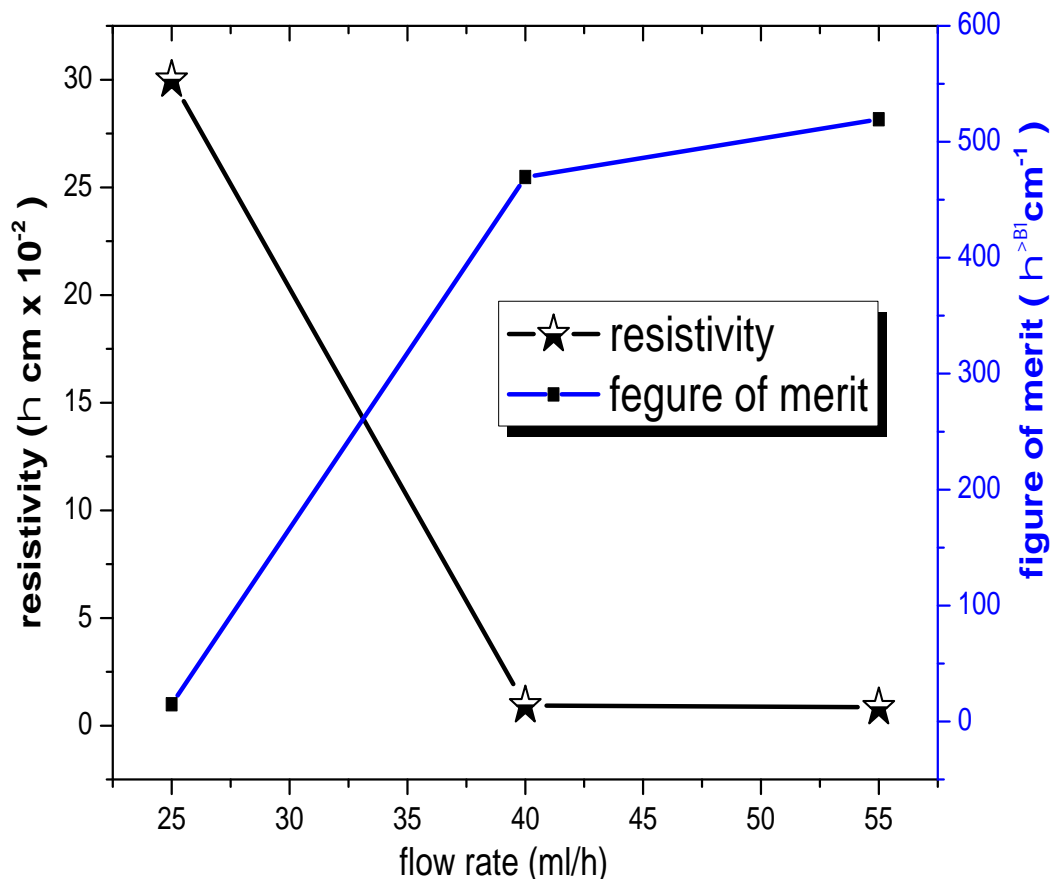


Figure IV.15. Electrical resistivity and figure of merit of  $\text{In}_2\text{O}_3$  thin film deposited at various solution flow rate

Figure IV.25. Shows the dependence of electrical resistivity ( ) and figure of merit on deposition time. We find that the Resistivity decreases continuously with increase in the flow rate, which is believed to be due to improvement in the film crystallinity. This is supported by X-ray diffraction analysis which indicates that the crystallinity increases with increase in solution flow rate. an increase in grain size leads to reduced grain boundary scattering and thus a decrease in electrical resistivity [90]. On the other hand, we believe that the surface morphology has significant impact on the electrical properties. With the increase of the solution flow rate the films show denced and packed grains which leads to the decreasing of number of scattering centres and trapping centres. The high dense and packed grains cause an increase of carrier mobility and electron Concentration [91].

The figure of merit for the  $\text{In}_2\text{O}_3$  thin film deposited at 25 ml/h was estimated at  $14.71 \text{ }^{-1}\text{cm}^{-1}$ . As the flow rate increases to 55 ml/h, the figure of merit increases to  $519.35 \text{ }^{-1}\text{cm}^{-1}$ .

## IV.6. Conclusion

The effect of the flow rate on the crystalline state, surface morphology, optical, and electrical properties of  $\text{In}_2\text{O}_3$  films was investigated. X-ray diffraction reveals a polycrystalline nature for all films with a preferred grain orientation along to (222) plane when the flow rate equals 25 ml/h, but when the flow rate increases we found that the majority of grains preferred the plane (400). Depending on the results of the current study we found that the preferential orientation development of crystalline grains mainly depends on the initial orientations during the nucleation process and the growth process. SEM images show that the films are rough surface and the shape of grains changes with the change of the preferential growth orientation.

The optical characterization showed that our films are transparent. And the transmittance improvement of  $\text{In}_2\text{O}_3$  films was closely related to the good crystalline quality of the films. We have found also that the optical gap is varied between 3.65 eV and 3.93 eV, and the values found of resistivity are between  $30 \cdot 10^{-2} \text{ cm}$  and  $8.5 \cdot 10^{-3} \text{ cm}$ . Finally, we conclude that solution flow rate is interesting factor for control the quality of the thin films deposited by ultrasonic spray technique.

# Chapter V

Influence of the Surface  
Substrate and annealing  
temperature on indium oxide thin  
films properties

### V.I.1. Introduction

It is well known, that the electrical properties of  $\text{In}_2\text{O}_3$  films obtained by ultrasonic spray process are close related by the deposition parameters of this technique. Therefore, deposition parameters has been widely studied in order to improve the electrical properties of sprayed  $\text{In}_2\text{O}_3$  films. The most studied parameters are: substrate–nozzle distance (SND) [11] substrate temperature [60, 13] deposition time [92] and doping [14]. However, only a few studies have been devoted to the influence of surface substrate in ultrasonic spray technique.

The electrical conductivity of  $\text{In}_2\text{O}_3$  films is due to a transport of electrons. The high n-type conductivity observed in  $\text{In}_2\text{O}_3$  films results from their anion deficiency, which usually appears in the Form of oxygen vacancies in the crystal lattice. However, when  $\text{In}_2\text{O}_3$  film is completely stoichiometric it can only be an ionic conductor. Such materials are of no interest as transparent conductors because of the high activation energy required for ionic conductivity. Real  $\text{In}_2\text{O}_3$  films used for transparent conductors are hardly completely stoichiometric. The above explanation reveals a way to improve the electrical properties of the  $\text{In}_2\text{O}_3$  films, i.e. to prevent more oxygen incorporating into the films at the beginning of the film growth. However, this way is very complicated for the films deposited by ultrasonic spray process due to the presence of  $\text{O}_2$  molecular cannot be avoided.

In order to improve the electrical properties of the  $\text{In}_2\text{O}_3$  films deposited by ultrasonic spray process, we have deposited  $\text{In}_2\text{O}_3$  films on KCl single crystal Substrate which is voracious to the  $\text{O}_2$  molecular. Moreover,  $\text{In}_2\text{O}_3$  thin films were deposited on glass and single crystalline Si (400) wafer Substrates. The Surface Substrate effects and annealing temperature on growth mechanism, optical and electrical properties of  $\text{In}_2\text{O}_3$  thin films were observed and highlighted.

### V.I.2 Surface Substrate affects on indium oxide thin films properties

#### V.I.2.1. Growth rate

Figure V.I.1. Shows the growth rate (nm/s) for  $\text{In}_2\text{O}_3$  thin films grown on the glass (glass/  $\text{In}_2\text{O}_3$ ), single crystalline Si (400) wafer (Si/  $\text{In}_2\text{O}_3$ ) and KCl single crystal (KCl/  $\text{In}_2\text{O}_3$ ) Substrates. It is clear that the values of the growth rate are very small. This is physically reasonable because the rate of lateral growth at the beginning formation of the thin layers is much higher than the perpendicular growth [64]. However, it is interesting to note that the growth rate increase slightly for Si/  $\text{In}_2\text{O}_3$  and KCl/  $\text{In}_2\text{O}_3$ . This indicates that the rate of lateral growth in this case is faster than the film deposited on glass substrate due to the Improve the nucleation process. Surface substrate influence on the nucleation process is very clear in the XRD analysis (explained later).

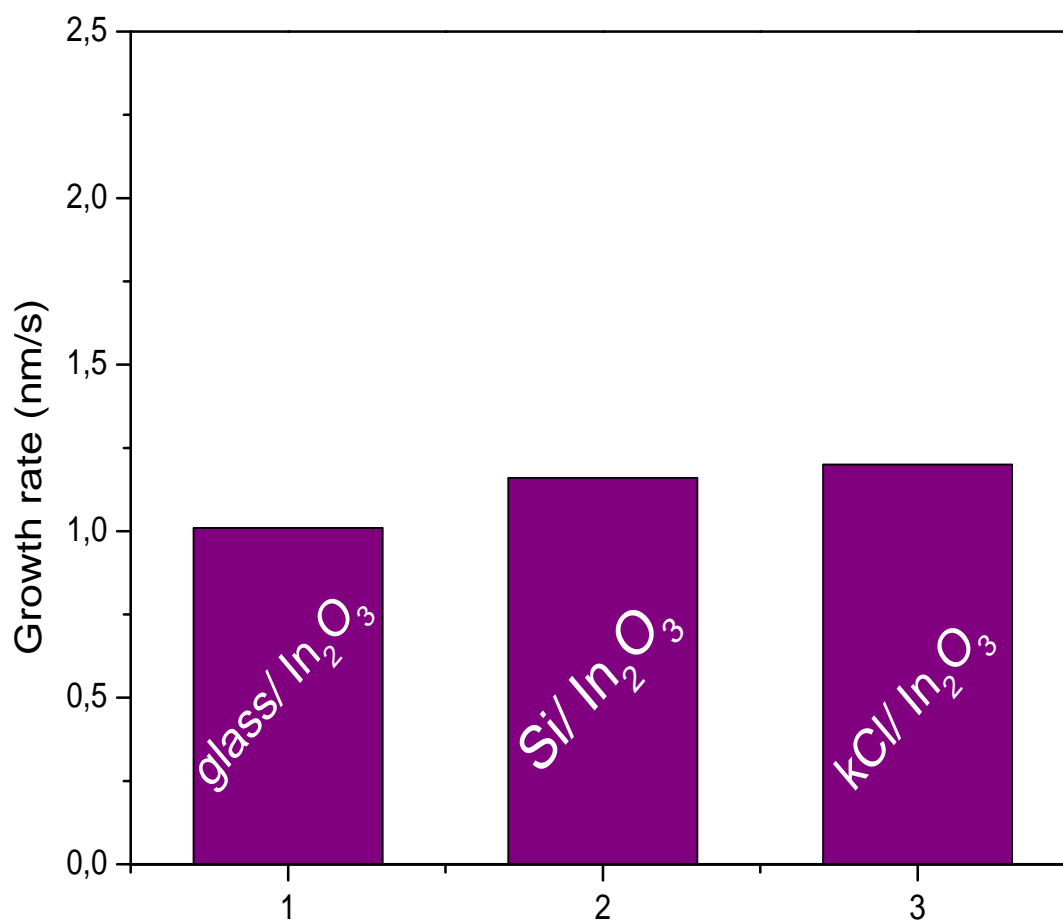


Figure.V.I.1. Deposition rate dependence on surface substrate.

### V.I.2.2. Structural properties

The XRD patterns for In<sub>2</sub>O<sub>3</sub> thin films grown on the glass (glass/ In<sub>2</sub>O<sub>3</sub>), single crystalline Si (4 0 0) and KCl single crystal (KCl/ In<sub>2</sub>O<sub>3</sub>) Substrates are shown in figure V.I.2. For the glass/ In<sub>2</sub>O<sub>3</sub> film the XRD spectrum of this sample exhibits a preferential orientation peak of low intensity located at  $2\theta = 30.76^\circ$  representing (222) orientation. However, the Si/ In<sub>2</sub>O<sub>3</sub> film exhibits several peaks at  $29.61^\circ$ ,  $30.76^\circ$ ,  $33.06^\circ$ ,  $35.76^\circ$ , and  $51.31^\circ$ , corresponding to the (211), (222), (321), (400) and (440) planes respectively, with a specific orientation along the [1 1 1] direction. In addition, we observed a Si single crystal peaks at  $69.54^\circ$  corresponding to the (400) plane (JCPDS 27-1402 file). But in the case of KCl/ In<sub>2</sub>O<sub>3</sub> film, we notice the presence of two main peaks and weak peaks: the two main peaks occur at  $2\theta = 30,69^\circ$  and  $35, 55^\circ$ . These peaks correspond to the diffraction from the (222) and (400) planes of In<sub>2</sub>O<sub>3</sub>, respectively. The weak peaks centered at  $63,74^\circ$  and  $75,11^\circ$  are identified as In<sub>2</sub>O<sub>3</sub> (444) and (800) planes, respectively. moreover, we observed a KCl peaks at  $2\theta = 28,42^\circ$  and  $2\theta = 58,74^\circ$  corresponding to the plan (200) and its harmonics (400) respectively (JCPDS 41-1476 file), beside the peaks related to the In<sub>2</sub>O<sub>3</sub> phase and to the substrate KCl single crystal, a

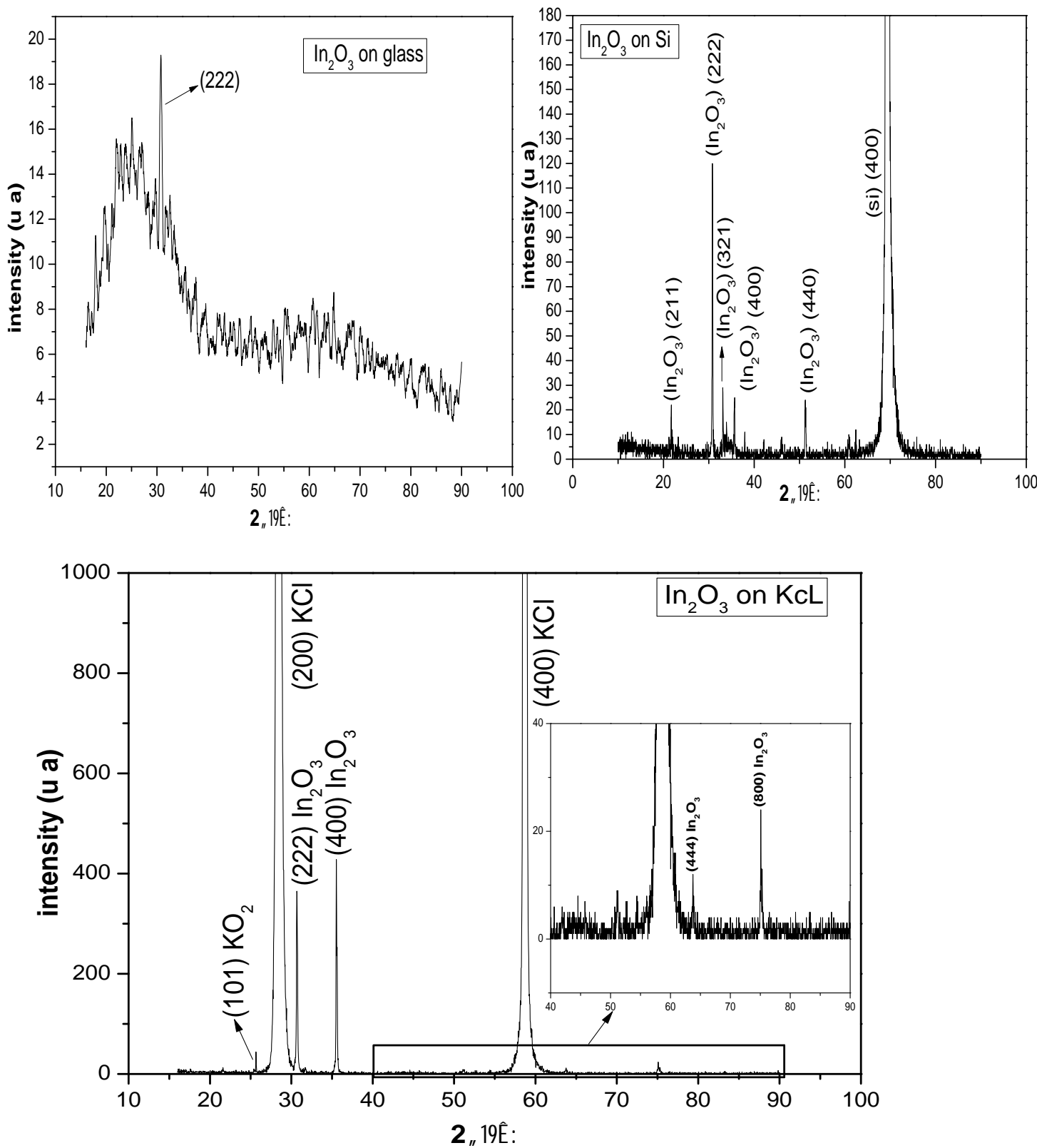


Figure. V.I.2: XRD diffraction pattern of  $\text{In}_2\text{O}_3$  thin films deposited on glass, single crystalline Si (4 0 0) and KCl single crystal Substrates

KO<sub>2</sub> peak at  $2\theta = 25,65^\circ$  corresponding to the plan (101) (JCPDS 39-0697 file, see figure V.3) is also present; a KO<sub>2</sub> phase originates from the reaction between the O<sub>2</sub> molecular and the substrate because the O<sub>2</sub> molecular has a high degree of solubility in the KCl single crystal substrate heated at 550 °C [93]. In order to explore the dependence of structural properties on surface substrate, we investigated changes in intensity of the main diffraction peak ((222), (400)) by means of XRD (see figure. V.I.4).

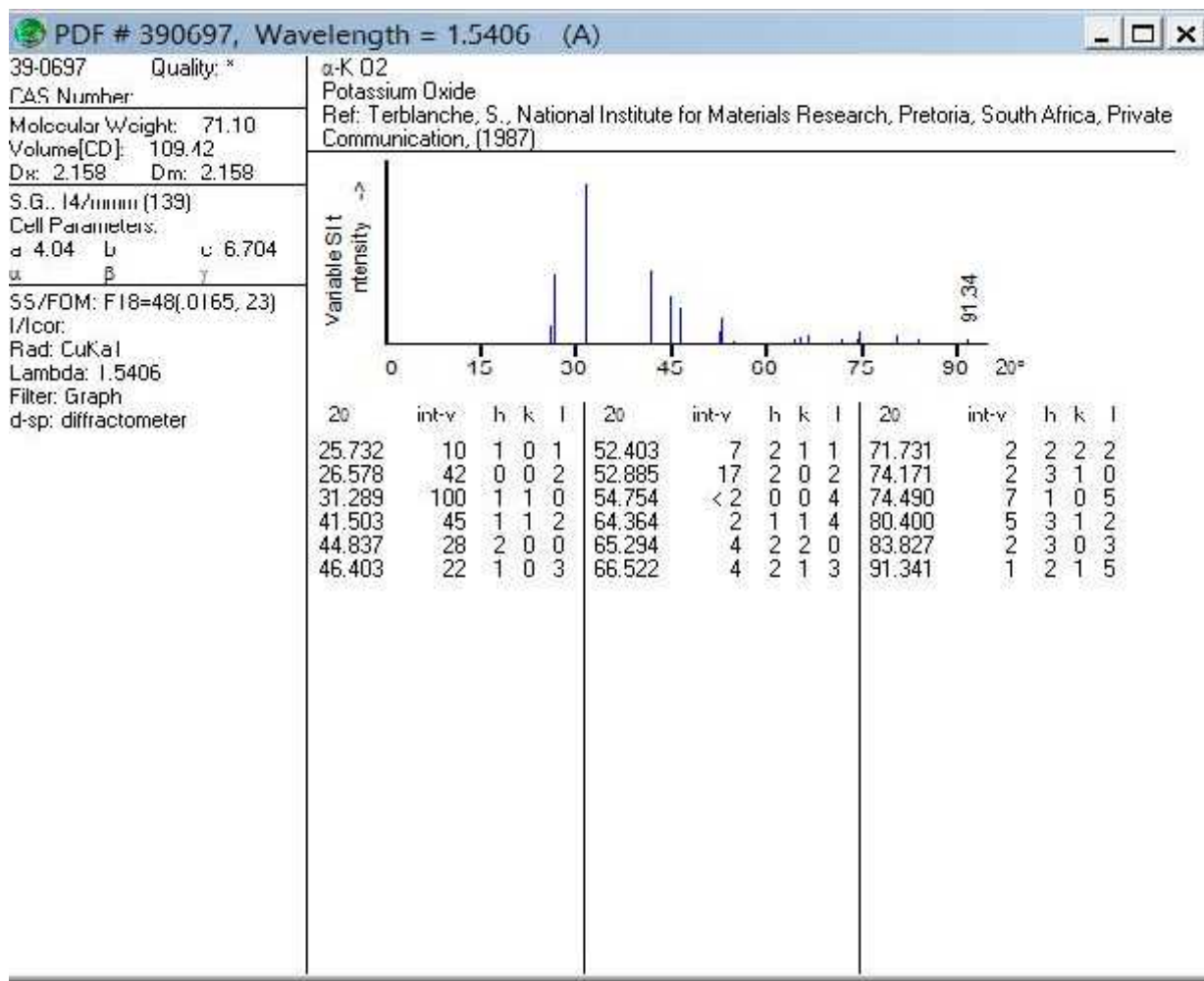


Figure. V.I. 3. ASTM file of KO<sub>2</sub>

The increase in intensity of diffraction peak for the Si/ In<sub>2</sub>O<sub>3</sub> film and KCl/ In<sub>2</sub>O<sub>3</sub> film reveals the enhancement crystallinity of these films. This is due to the high crystalline quality of these substrates which is enhanced the nucleation of condensed In<sub>2</sub>O<sub>3</sub> atoms [94]. However, it is interesting to note that the increase in intensity of diffraction peak for KCl/ In<sub>2</sub>O<sub>3</sub> film is more than Si/ In<sub>2</sub>O<sub>3</sub> film. This can be attributed to the topography of KCl single crystal Substrate which

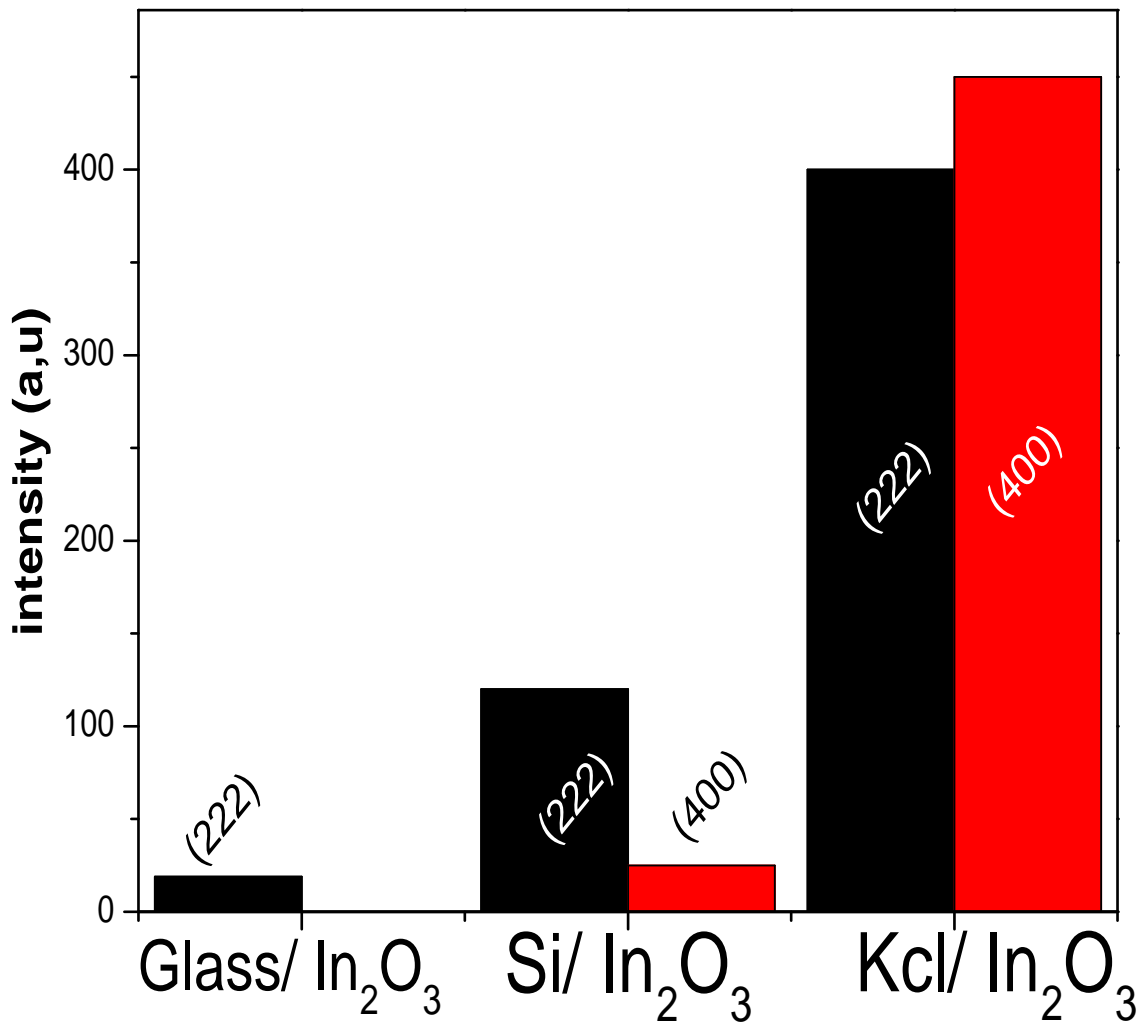


Figure. V.I. 4. Surface substrate effect on the film texture

Supports the nucleation process. It well know that the nucleation density and the average nucleus size depend on a number of parameters such as the rate of impingement, temperature, topography, and chemical nature of the substrate [64].

The most importing feature in the XRD analysis is the change in the preferred growth orientation with the change of the used substrate. For the KCl/  $\text{In}_2\text{O}_3$  film the texture changes from the [1 1 1] direction to [100] direction. The presence of the preferred growth of (400) grains is a priori unforeseen according to the surface energy of the  $\text{In}_2\text{O}_3$  cubic structure because the (111) texture presents a lower surface free energy plane [59] and/or the low thickness of this film (based on the above explanation; effect of the deposition time and solution flow rate). This can be attributed to the low oxygen concentration in the film structure; the  $\text{O}_2$  molecular has a high degree of solubility in the KCl single crystal substrate heated at  $550^\circ\text{C}$  [93] which lead to prevent the incorporation of oxygen in the structure, and this will permit to presence the preferred growth of (400) grains [95].

In general, the intensity of the plane changes with the change of oxygen concentrations in the films. Several studies revealed that decrease of the oxygen concentrations in the  $\text{In}_2\text{O}_3$  films suppresses the intensity of the (222) plane and stimulate the (400) orientation of the  $\text{In}_2\text{O}_3$  films [96,97]. On the other hand, the presence of the preferred growth of the (400) grains probably due to other parameter which is possible epitaxy of the (400) plane on the KCl single crystal [98]. However, we believe that solubility of  $\text{O}_2$  molecular in KCl single crystal substrate is more important.

**Tabl1** Evaluated data of  $\text{In}_2\text{O}_3$  films deposited on different substrates

Substrates	Preferred orientation	intensity (u a)	Crystallite size (nm)	Resistivity ( cm)	Eg (ev)	Film thickness (nm)	Strain ( ) * $10^{-3}$	Dislocation density ( ) * $10^{14}$ lines/m <sup>2</sup>	lattice constant (A°)
glass	(222)	19.27	18	33	3.72	255	2.85	26	10.087
KCl single Crystal	(400)	426.7	70	$0.8 \cdot 10^{-3}$	3.94	290	0.42	2.04	10.161
<b>Si single Crystal</b>	(222)	119.4	62.5	/	/	280	0.64	2.56	10.083

The average grains size  $D$  of  $\text{In}_2\text{O}_3$  is estimated using Scherer's formula are reported in Table 1. We found that the KCl/  $\text{In}_2\text{O}_3$  film and Si/  $\text{In}_2\text{O}_3$  film showed a higher value of average grain size than the film grown on the glass substrate. This increase in grain size probably due to an increase of the nucleus number which cluster together to form larger grains. The raise in the nucleus numbers Due to the high crystalline quality of KCl single crystal and Si single crystal substrate which supported the nucleation process. Also, the strain and dislocation density decrease for the KCl/  $\text{In}_2\text{O}_3$  film and Si/  $\text{In}_2\text{O}_3$  film. This can be attributed to the improve of crystalline quality of these films. However the calculated value of lattice constant  $a= 10.161 \text{ A}^\circ$  for the KCl/  $\text{In}_2\text{O}_3$  film is slightly greater than the reported value  $10.118 \text{ A}^\circ$  for pure indium oxide. This increase in the value of lattice parameter may be related to oxygen deficiency [62] due to solubility of the  $\text{O}_2$  molecular in the KCl substrate.

The FT-IR spectral analysis of KCl/  $\text{In}_2\text{O}_3$  film and Si/  $\text{In}_2\text{O}_3$  film is shown in Fig.V.I. 5. the FT-IR spectral analysis of KCl/  $\text{In}_2\text{O}_3$  film shows several peaks located, respectively, at 420, 471, 594, 612, 672 and  $874 \text{ Cm}^{-1}$ , these peaks correspond the In-O and In-In vibration modes. Similar results have been found by other researchers [99.56]. The In-O stretching mode is found at 420, 594, 612 and  $672 \text{ Cm}^{-1}$ . The observed band at  $471 \text{ Cm}^{-1}$  attributed to the In-In stretching mode. Whereas, the bands at  $874 \text{ cm}^{-1}$  are the characteristic absorption of In-O bending vibrations. However, in the case

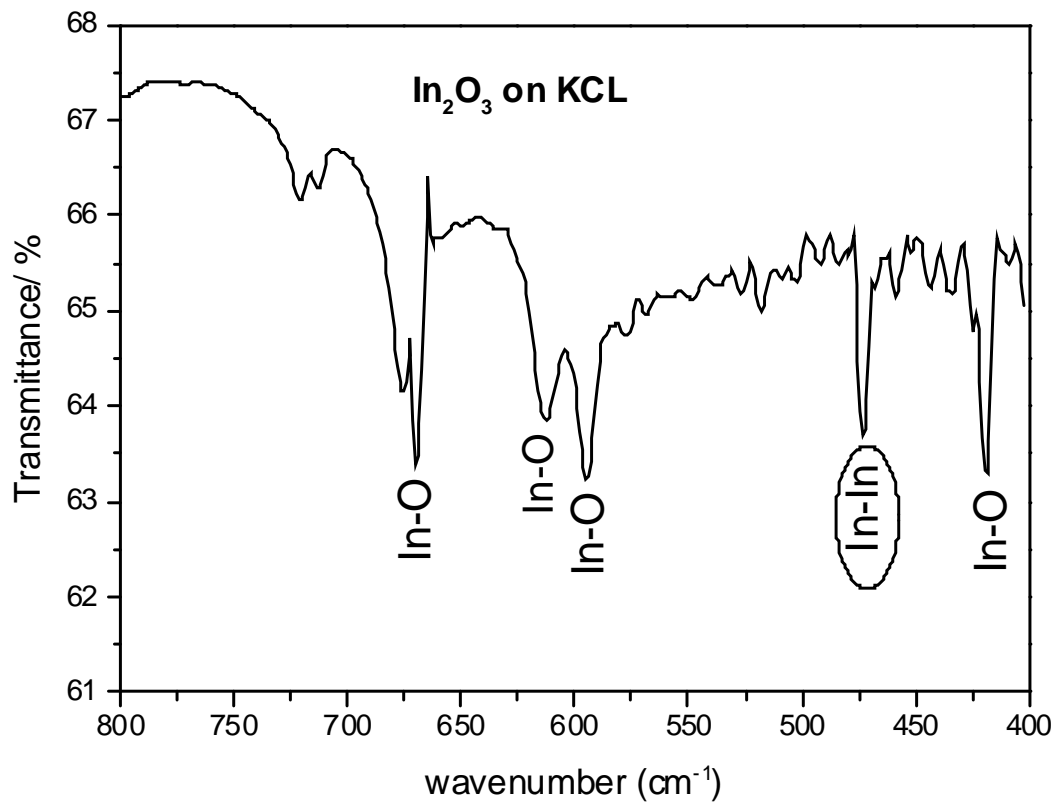


Figure. V.I. 5. FT-IR spectra of KCl/  $\text{In}_2\text{O}_3$  film and Si/  $\text{In}_2\text{O}_3$  film.

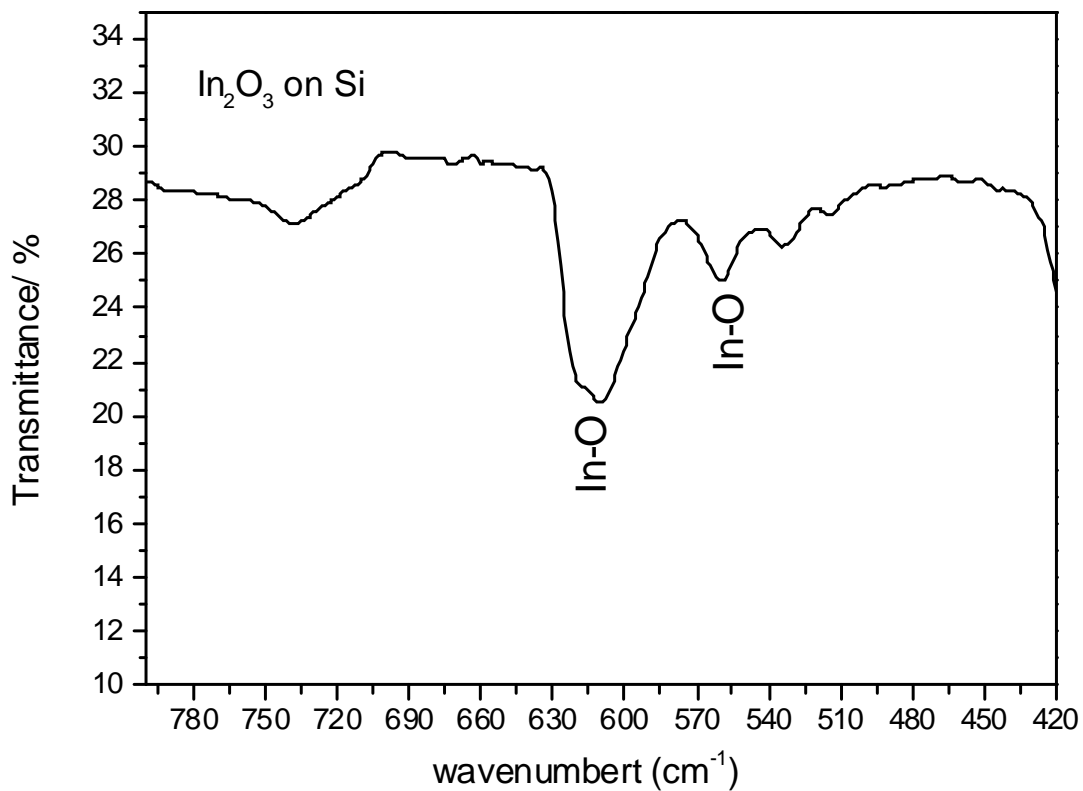


Figure. V.I. 5. FT-IR spectra of Si/  $\text{In}_2\text{O}_3$  film and Si/  $\text{In}_2\text{O}_3$  film.

Of Si/In<sub>2</sub>O<sub>3</sub> film we observe peaks located at 558 and 610 Cm<sup>-1</sup>. These peaks correspond, In-O stretching mode. The presence of the In-In vibration mode in the case of KCl/ In<sub>2</sub>O<sub>3</sub> film attributed To the oxygen deficiency in the film structure. This result consistent with the result of the XRD characterization.

### V.I.2.3. Morphological properties

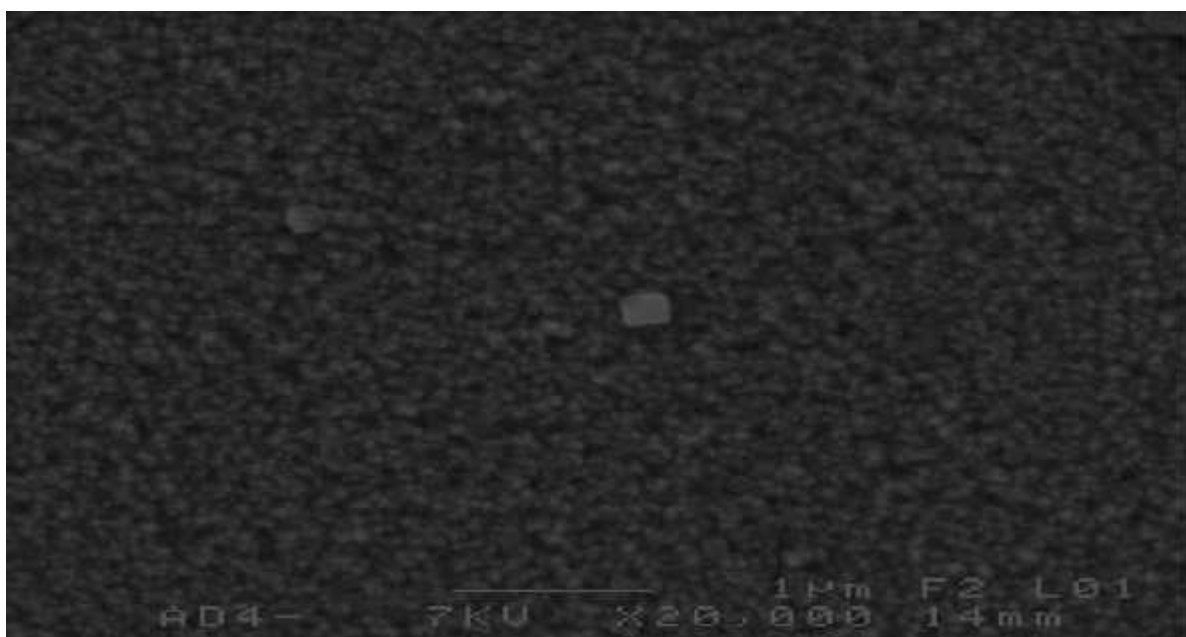


Figure.V.I.6. SEM surface image of glass/In<sub>2</sub>O<sub>3</sub>

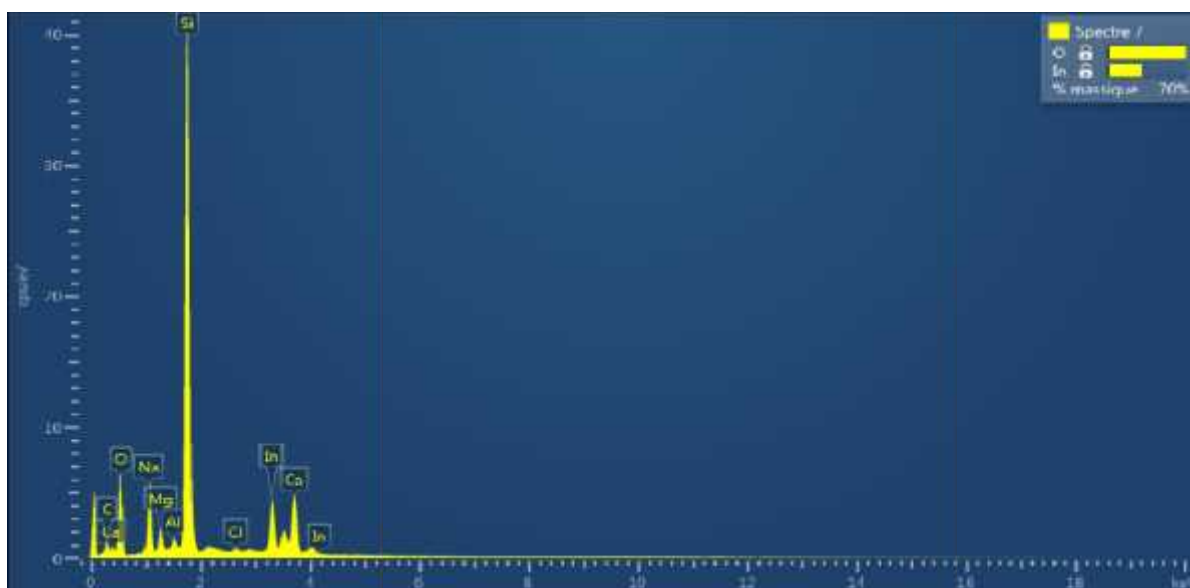


Figure. V.I.7. EDS analysis of glass/In<sub>2</sub>O<sub>3</sub>

Fig.V.I.6 shows SEM micrograph of glass/  $\text{In}_2\text{O}_3$  nanostructured thin film. The film exhibits a smooth surface and the quasi-spherical crystalline particle size is approximately 80 nm. The smooth surface of this film may be due to the preferential growth in the [111] direction over the entire surface. Figure. V.I.7. Show that the glass/ $\text{In}_2\text{O}_3$  is composited from O and In atoms. The presence of the calcium and silicon peak in the spectrum is due to the glass substrate, but the presence of others elements such as carbon may be due to the contamination.

#### V.I.2.4. optical properties

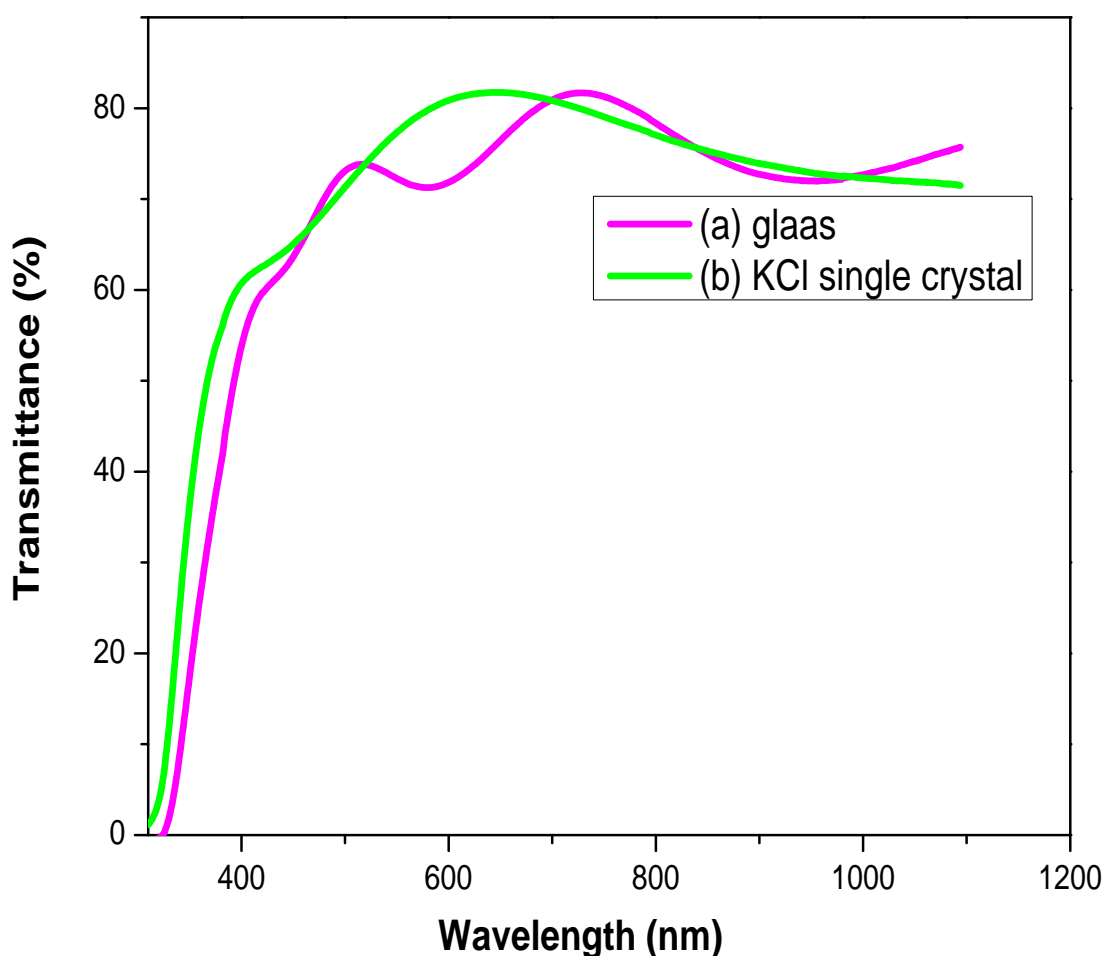


Figure. V.I. 8. Optical transmittance spectra of  $\text{In}_2\text{O}_3$  thin films deposited on (a) glass and (b) KCl single crystal substrate.

The optical transmittance measured as a function of the wavelength is depicted in Fig.V.I.8. The films glass/ $\text{In}_2\text{O}_3$  and Kcl/ $\text{In}_2\text{O}_3$  show almost identical transmittance in 400–900 nm wavelengths

regions, although the KCl/ In<sub>2</sub>O<sub>3</sub> film is thicker than the glass/In<sub>2</sub>O<sub>3</sub> film and the transmittance of the bare glass substrate is higher than the bare KCl substrate [69]. This is attributed to the important crystalline quality of this layer [72]. However, it is interesting to note that, the glass/ In<sub>2</sub>O<sub>3</sub> film exhibits interference fringe in the transmittance spectrum. This is due to the smooth surface of this film.

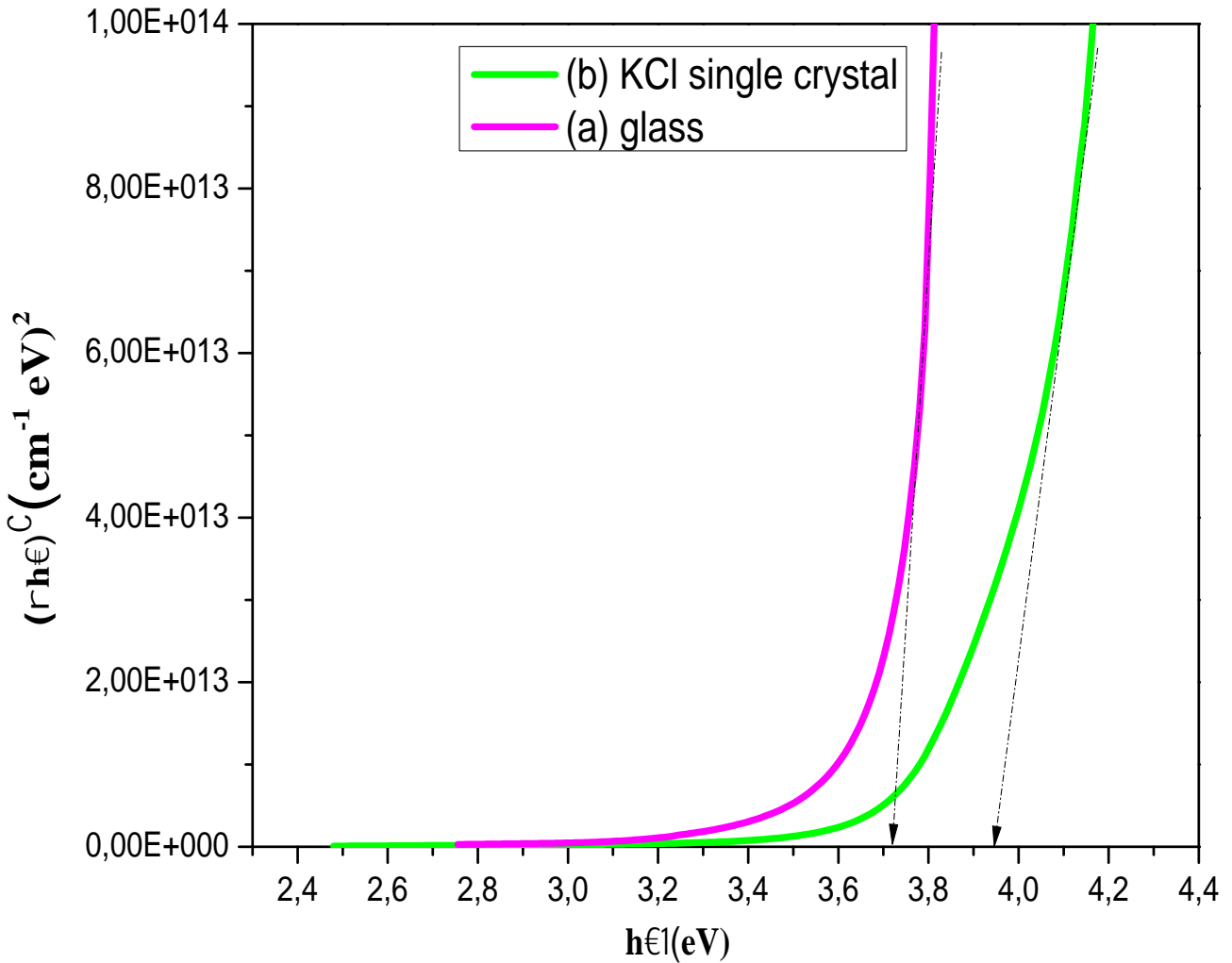


Figure. V.I. 9. Optical band gap energy for the In<sub>2</sub>O<sub>3</sub> thin films deposited on (a) glass and (b) KCl single crystal substrate.

The values of optical band gap are obtained by extrapolating the tangential line of the data to the abscissa axis in the plot of  $\alpha^2 \nu^2$  as a function of  $h\nu$  as shown in V. 9. KCl/ In<sub>2</sub>O<sub>3</sub> film has higher band gap 3.93eV, this can be attributed to the reduction of disorder in the film network due to the improvement in crystalline quality of this layer [92]. On the other hand, the oxygen concentrations

in the  $\text{In}_2\text{O}_3$  films may play a main role in increasing optical band gap. For KCl/  $\text{In}_2\text{O}_3$  film the amount of oxygen was Low due to the high degree of solubility of  $\text{O}_2$  molecular in the KCl Substrate, this means the increase of oxygen vacancies. The latter causes augment in the optical band gap due to the raise of carrier concentrations in the  $\text{In}_2\text{O}_3$  film (Burstein–Moss effect; an enhancement in the electron concentration leads to a rise in the Fermi level within the conduction band, causing the increase in the value of the band gap for this sample [100]). The glass/  $\text{In}_2\text{O}_3$  film has lower band gap 3.72 ev. Although the low grains size of this film (  $D= 18$  nm). Therefore, the theoretical optical gap of a glass/  $\text{In}_2\text{O}_3$  film in our case can be estimated by the effective mass theory [101] using relation:

$$E_g \text{ nano} = E_g \text{ bulk} + \frac{\hbar^2}{8R^2} \left( \frac{1}{m_e^*} + \frac{1}{m_h^*} \right) - \frac{1.8e^2}{4\pi\epsilon\epsilon_0 R} \quad (1)$$

Where  $E_g$  (nano) is the energy band gap of nanoparticles,  $E_g$  (bulk) in the energy band gap of bulk sample.  $R$  is the average radius of particles,  $m_e^*$  and  $m_h^*$  are the effective mass of an electron and a hole respectively and  $\epsilon$  stand for the relative dielectric constant. For  $\text{In}_2\text{O}_3$  crystal,  $m_e^* = 0.3 m_0$ ,  $m_h^* = 0.6 m_0$  ( $m_0$  is the free electron mass) and  $\epsilon = 9$  [102]. So the theoretical optical gap can be about 3.95 ev, which is larger than the experimental optical gap 3.72 eV. This deference between the two values is due to the film disorder due to the low crystalline state of this film (see XRD analysis). Based on these findings, we infer that optical gap shift towards the higher energies induced by the quantum confinement effect and the shift towards the lower energies induced by the large band tail width due to the film disorder.

The glass/  $\text{In}_2\text{O}_3$  film has higher band tail width 0.523 eV. This is due to the low crystalline state of this film. Also, KCl/  $\text{In}_2\text{O}_3$  film has a high band tail width 0.497 ev despite the high crystalline quality of this film. This can be attributed to the non-stoichiometric of this film; increase the interstitial indium atoms due to the oxygen deficiency.

### V.I.2.5 Electrical properties

The KCl/  $\text{In}_2\text{O}_3$  film showed lower value of electrical resistivity ( ) than the glass/  $\text{In}_2\text{O}_3$  film (see table 1.). This is owing to combination of two factors: (i) the large grain size of KCl/  $\text{In}_2\text{O}_3$  film and (ii) The formation of oxygen vacancies in the structure of this film due to solubility of  $\text{O}_2$  molecular in the KCl substrate. The increase in the grain size leads to reduced grain boundary scattering. Thus

increasing the mobility [103], while the formation of oxygen vacancies in the structure leads to the increase of carrier concentration. Both of them reduce the resistivity of the KCl/ In<sub>2</sub>O<sub>3</sub> film.

### V.I.2.6. Conclusions

The effect of the substrates surface on the crystalline state, optical, and electrical properties of In<sub>2</sub>O<sub>3</sub> films were investigated. X-ray diffraction reveals a polycrystalline nature for all films with a preferred grain orientation along to (222) for the film deposited on glass and Si single crystal Substrates, but in the case of the KCl single crystal Substrate we found that the majority of grains preferred the plane (400). Depending on the results of the current study we found that the preferential orientation development depends on the oxygen concentrations in the films. On the other hand we found that The KCl/ In<sub>2</sub>O<sub>3</sub> film showed a higher value of average grain size than the film grown on the glass substrate.

The optical characterization showed that our films are transparent. We have found also that the optical gap is 3.94eV for the KCl/ In<sub>2</sub>O<sub>3</sub> film and 3.72 for the glass/ In<sub>2</sub>O<sub>3</sub> film. The KCl/ In<sub>2</sub>O<sub>3</sub> film showed lower value of electrical resistivity ( ) than the glass/ In<sub>2</sub>O<sub>3</sub> film. To sum up, the substrates surface is an interesting factor for control the quality of the thin films deposited by ultrasonic spray technique.

## V.II. Effects of annealing temperature on indium oxide thin films properties

### V.II.1. Structural properties

The typical XRD patterns for the as-deposited  $\text{In}_2\text{O}_3$  thin films and for the  $\text{In}_2\text{O}_3$  films annealed at two different temperatures are shown in figure.V.I.1.

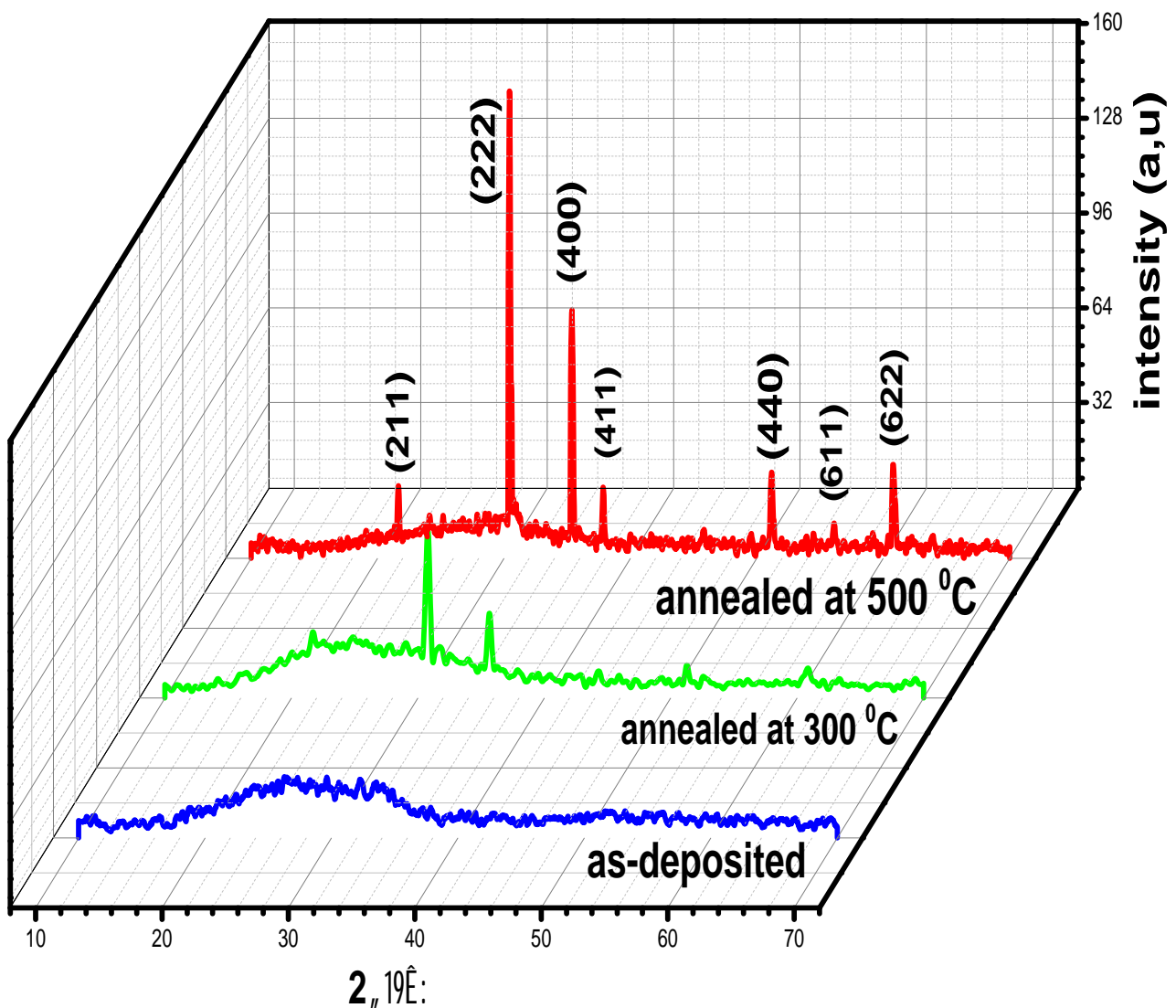


Figure V.II.1. XRD diffraction pattern for the as-deposited  $\text{In}_2\text{O}_3$  thin films and for the  $\text{In}_2\text{O}_3$  films annealed at two different temperatures.

The XRD pattern of the as-deposited  $\text{In}_2\text{O}_3$  thin film does not show any clear diffraction peak except a broad diffraction pattern for  $2\theta$  the range of  $25\text{--}35^\circ$ . This indicates to the poor crystalline quality of this film and very small grain sizes in the as-deposited film. However, The XRD pattern obtained for the film annealed at  $300^\circ\text{C}$  shows reflection peaks at  $30.80^\circ$  and  $35.66^\circ$  corresponding to the (222) and (400) suggesting that film is polycrystalline in nature. However, as the annealing temperature increases to  $500^\circ\text{C}$ , intensity of the (222) and (400) diffraction peaks increases. This reveals the enhancement of crystallinity due to having a sufficient amount of kinetic energy and mobility of the grains [104]. It was also observed that intensity of the diffraction peaks increased with increasing annealing temperature [104,105]. On the other hand, it is interesting to note that the number of the diffraction peaks increase in this film which is probably due to the increased nucleation centers. Also the XRD spectra of the film annealed at  $500^\circ\text{C}$  shows a characteristic shift towards lower angle for the main peaks (see figure.V.II.2). This indicates a systematic lattice expansion. This phenomenon has also been reported by many other authors [106].

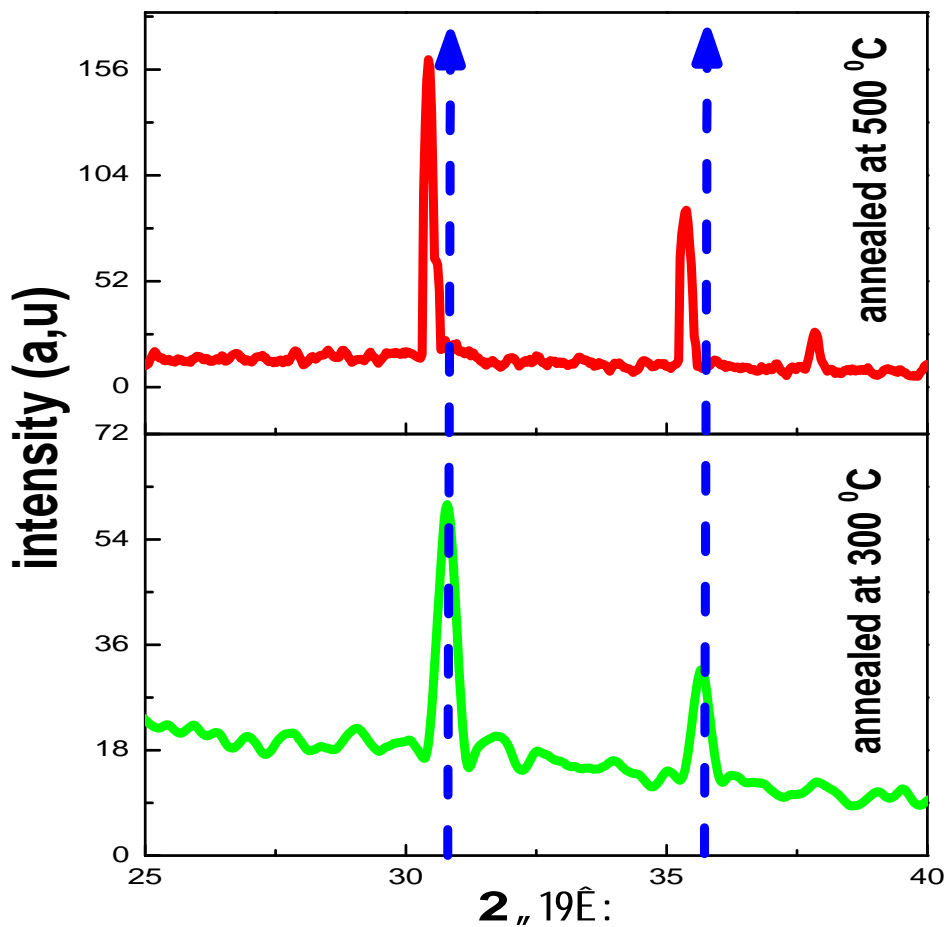


Figure V.II.2. Larger image for XRD diffraction pattern for the  $\text{In}_2\text{O}_3$  films annealed at two different temperatures.

Figure IV.3. Shows the values of FWHM for the films annealed at 350°C and 550°C. It is clear that the values of the FWHM decrease with the increase of the annealing temperature. The decreasing trend of FWHM values implied that the grain size increases. It was also observed that average grain size increased with increasing annealing temperature [104,107]. This can be attributed to coalescence of small grains by grain boundary diffusion which caused major grain growth.

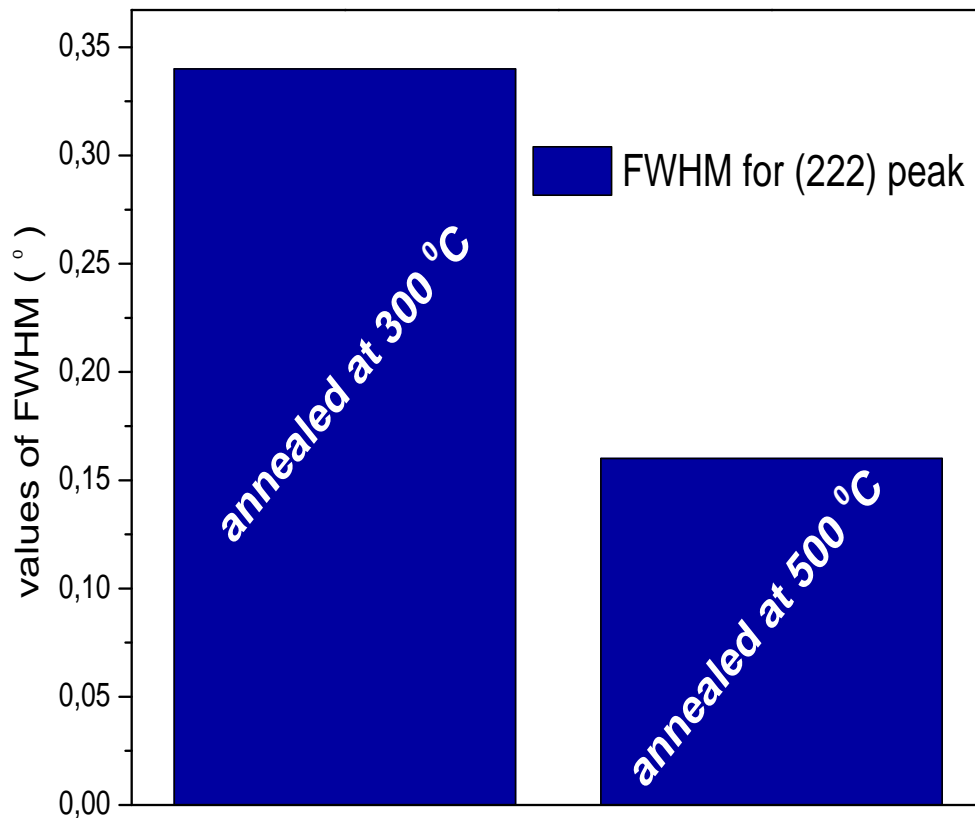


Figure V.II.3. FWHM for (222) peak.

The other structural parameters like lattice constant, dislocation density ( ) and strain ( ) calculated for the (2 2 2) prominent reflection are shown in table V.II.1. The calculated value of lattice constant  $a = 10.145 \text{ \AA}$  (cubic phase) for the film annealed at 500°C is slightly greater than the reported value  $10.118 \text{ \AA}$  for pure indium oxide (JCPDS Card No. 06-0416). This can be attributed to the oxygen deficiency [62] because the  $\text{In}_2\text{O}_3$  thin films tend toward reduction when they were annealed at high temperature [107,108]. On the other hand, the dislocation density ( ) and strain ( ) show a decreasing trend with increasing annealing temperature. This can be attributed to the recrystallization process in the polycrystalline films at high annealing temperature [109].

**TabL.II. 1** structural parameters of  $\text{In}_2\text{O}_3$  films at different annealing temperature

$\text{In}_2\text{O}_3$ thin film annealed at :	Lattice constant ( $\text{\AA}$ )	Dislocation density ( ) * $10^{14}$ lines/ $\text{m}^2$	strain ( ) * $10^{-3}$	Film thickness (nm)
300 °C	10.088	15	1.43	320
500 °C	10.145	3.01	0.6	280

## V.II.2. Optical properties

Figure II.4. Shows the dependence of the optical transmission spectra of the investigated thin films in the wavelength region 290–900 nm as a function of annealing temperature.

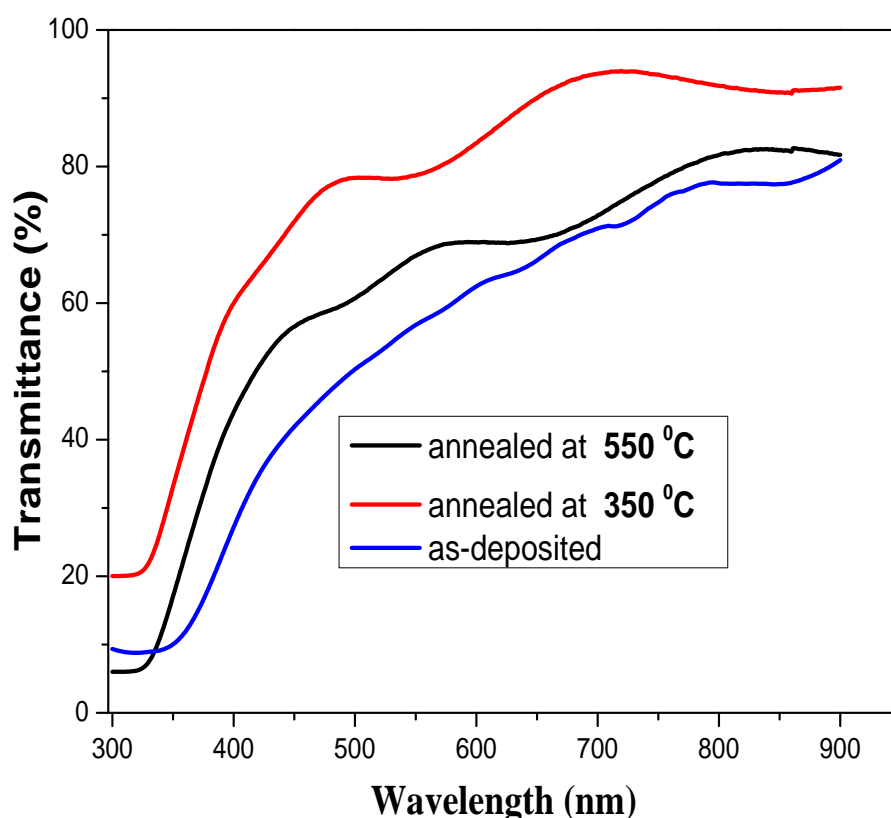


Figure V.II.4. Optical transmission spectra for the as-deposited  $\text{In}_2\text{O}_3$  thin films and for the  $\text{In}_2\text{O}_3$  films annealed at two different temperatures.

The as-deposited  $\text{In}_2\text{O}_3$  thin film shows low transmittance. This is owing to poor crystalline quality of this film and/or non-stoichiometric ; excess indium atoms due to the low deposition temperature. But in the case of the films annealed at 300 °C and 500 °C, we found that the optical transmittance increased due to enhancement the crystalline quality of the films [92]. However, the film annealed at 300 °C shows the high optical transmittance despite that the film annealed at 500 °C has a high crystalline quality than the film annealed at 300 °C. This can be attributed to the oxygen deficiency in the film structure due to the high annealing temperature [107.108]. It is well know that the oxygen deficiency in the film contributes to the blackening of the films [110.111].

The values of optical band gap are obtained by extrapolating the tangential line of the data to the abscissa axis in the plot of  $\alpha^2 \nu^2$  as a function of  $h\nu$  as shown in Figure. V.II.5.

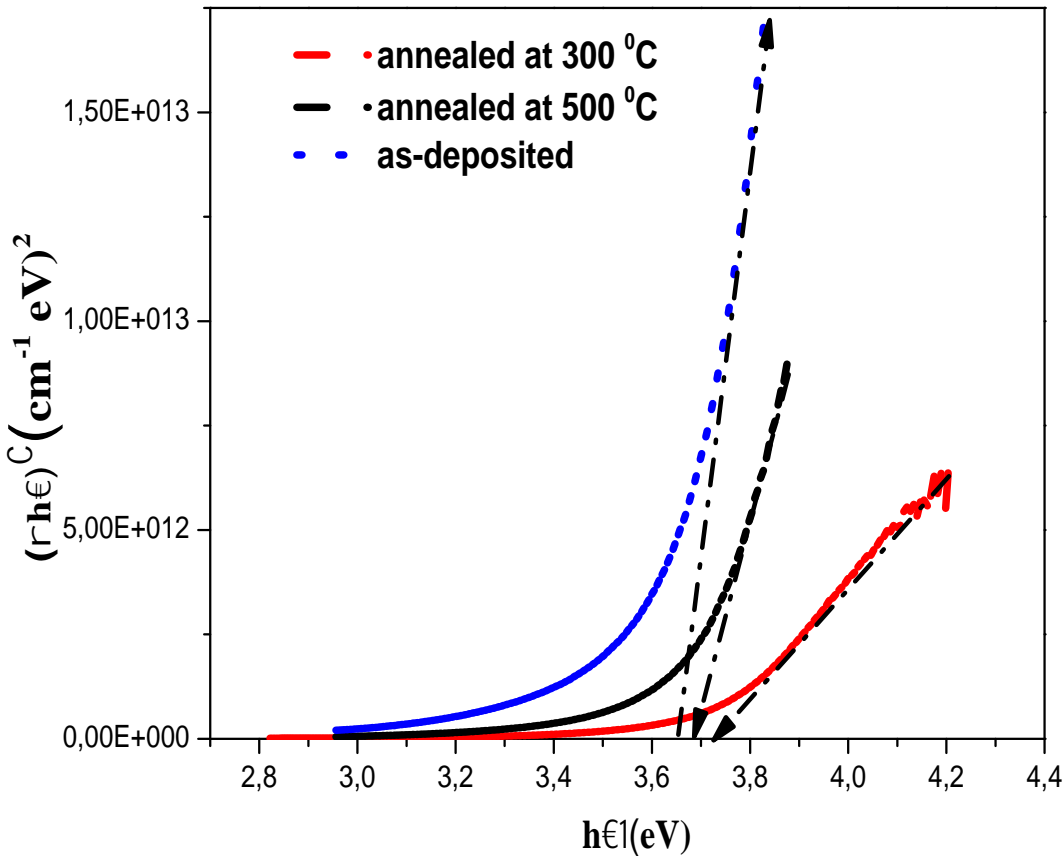


Figure V.II.5. Optical band gap energy for the as-deposited  $\text{In}_2\text{O}_3$  thin films and for the  $\text{In}_2\text{O}_3$  films annealed at two different temperatures.

It is clear that the value of the optical band gap increases for the  $\text{In}_2\text{O}_3$  films which annealed at  $300^\circ\text{C}$  and  $500^\circ\text{C}$ . This is due to the reduction of disorder in the film network due to the improvement in crystalline quality of this layer [92], and the band tail width values of these films confirm this hypothesis (The band tail width for the films annealed at 300 and 500 is 0.380 eV and 0.377 eV, respectively). The low value of the optical band gap obtained for the as-deposited film ( $E_g = 3.64$  eV) may be due to the poor crystalline quality of this film. The band tail width of the as-deposited films equals 0.480 eV.

### **V.II.3. Electrical properties**

The as-deposited film shows high electrical resistivity  $100 \text{ } \Omega\text{-cm}$ . This is due to the poor crystalline quality of this film. Also, the film annealed at  $300^\circ\text{C}$  shows high electrical resistivity  $80 \text{ } \Omega\text{-cm}$  although the improvement in the crystalline state of this film. This can be attributed to the excess oxygen in the film; Excess oxidation of this film for this annealing temperature [107]. The film annealed at  $500^\circ\text{C}$  shows the low electrical resistivity  $9.8 \times 10^{-3} \text{ } \Omega\text{-cm}$ . This is owing to the increase of grain size; an increase in grain size leads to reduced grain boundary scattering and thus a decrease in electrical resistivity [90]. On the other hand, we believe that the oxygen deficiency in film due to the high annealing temperature [107,108] play a Role in the decrease of the electrical resistivity.

### **V.II.4. Conclusions**

The effect of the annealing temperature on the crystalline state, optical, and electrical properties of  $\text{In}_2\text{O}_3$  films were investigated. X-ray diffraction reveals a polycrystalline nature for all films with a preferred grain orientation along to (222).the crystalline quality of the film increase with the increase of the annealing.

The optical characterization showed that our films are transparent. We have found also that the optical gap is 3.73eV for the film annealed at  $300^\circ\text{C}$  and 3.69 for the film annealed at  $500^\circ\text{C}$ . The film annealed at  $500^\circ\text{C}$  showed lower value of electrical resistivity ( ).

## General conclusion and perspectives

Indium oxide ( $\text{In}_2\text{O}_3$ ) thin films have been successfully prepared by ultrasonic spray technique using Indium chloride as precursor solution. The influence of various parameters on the structural, morphological, optical and electrical properties has been carried out to give good quality films. The optimized process parameters for our preparation of device-quality  $\text{In}_2\text{O}_3$  films are: deposition time, solution flow rate, surface substrate and annealing temperature.

The XRD results reveal a polycrystalline nature for all films except the film deposited at 150 °C. Also, the preferred growth orientation change from the (222) plane to (400) plane with the increase of the film thickness or decrease of the oxygen concentration in the film. On the other hand, the change in the strongest orientation of XRD peak is correlated with the change in grain shapes as observed by SEM analysis. Moreover, the promotion of (400) plane texturing has also been associated with improvement in crystallinity of the  $\text{In}_2\text{O}_3$  thin films. However, for the fourth parameter; annealing temperature, we found that the (222) plane is the predominant. The grain size of the  $\text{In}_2\text{O}_3$  films depend on a number of parameters which are: the amount of the solution sprayed. Surface substrate and annealing temperature and the higher value of the grain size obtained in this study was 76 nm. SEM images show that the films are rough surface and the shape of grains changes with the change of the preferential growth orientation; in the case of the (111) texture, grains with pyramidal-shape is formed. While for the (100) texture, the grains are granular in shape.

The optical characterization showed that our films are transparent with a value between 76% to 93%. Also, the transmittance improvement of  $\text{In}_2\text{O}_3$  films was closely related to the good crystalline quality of the films, the roughness of the surface and the oxygen concentration in the film. We have found also that the optical gap is varied between 3.64 eV and 3.93 eV. The optical gap shifts towards the higher energies induced by the quantum confinement effect and the shift towards the lower energies induced by the large band tail width due to the film disorder. The electrical characterization of our films shows a low electrical Resistivity about  $0.8 \times 10^{-3}$  cm.

Depending on the results of the current study, we found that the  $\text{In}_2\text{O}_3$  thin films deposited at low deposition time and solution flow rate on glass substrate are more suitable for utilization as a transparent oxide front layer in solar cells application. However, the films deposited at low deposition time and solution flow rate on KCl substrate are more suitable for utilization as electrodes in solar cells application. In effect, the deposition time, solution flow rate, surface substrate and annealing temperature are interesting factors for control the quality of the thin films deposited by ultrasonic spray technique.

According to the above analysis, the poor properties of the  $\text{In}_2\text{O}_3$  thin films are mainly resulted from more oxygen incorporation into the crystalline structure. Certain additional oxygen to the sprayed indium oxide is necessary for a good crystallization of the films for most deposition processes. Our perspective is finding a way to improve the properties of the  $\text{In}_2\text{O}_3$  thin films, i.e. to prevent incorporating more oxygen into the films at the beginning of the film growth.

## References

- [1] M. Morezio, *Acta Crystallographica* 20 (1966) 723.
- [2] Z. Galazka, R. Uecker, K. Irmscher, *Journal of Crystal Growth* 362 (2013) 349–352.
- [3] W. SIEFERT. *Thin Solid Films*, 121(1984) 215-282.
- [4] Chin-Chung Yu, Kai-Shun Yang, Ho Chang. *Vacuum* 102 (2014) 63-66.
- [5] Y. Sato, M. Taketomo, N. Ito, Y. Shigesato, *Thin Solid Films* 516 (2008) 5868.
- [6] W.G.Haines,R.H.Bube,J.Appl.Phys.49(1978)304.
- [7] A. Gurlo, M. Ivanovskaya, A. Pfau, U. Weimar, W. Göpel, *Thin Solid Films* 307 (1997) 288.
- [8] V. Marotta, S. Orlando, G.P. Parisi, *Appl. Surf. Sci.* 168 (2000)141–145.
- [9] O. Bierwagen, J.S. Speck, *Journal of Applied Physics* 107 (2010) 113519.
- [10] L. Kong, J. Ma, F. Yang, Z. Zhu, C. Luan, H. Xiao, *Applied Surface Science* 257 (2010) 518.
- [11] J. Joseph Prince, S. Ramamurthy, B. Subramanian, C. Sanjeeviraja M. Jayachandran. *Journal of Crystal Growth* 240 (2002) 142–151.
- [12] G. Korotcenkov, V. Brinzari, A. Cerneavschi,M.Ivanov,A. Cornet, J. Morante, A. Cabot, J. Arbiol. *Sensors and Actuators B* 98 (2004) 122–129.
- [13] *M. Girtan, Surface and Coatings Technology* 184 (2004) 219–224.
- [14] S. Parthiban, E. Elangovan, K. Ramamurthi, R. Martins, E. Fortunato. *Solar Energy Materials & Solar Cells* 94 (2010) 406–412.
- [15] R.W.G. Wyckoff, *Crystal Structures*, Interscience Publishers, vol. 2, (1963), 2.
- [16] A.El Hichou, A.Kachouane , J.L.Bubendorff. *Thin Solid Films* 458(2004)263–268.
- [17] S.Seki, Y.Sawada, T.Nishide, *Thin Solid Films* 388(2001)22.
- [18] Landolt, Bornstein, *Numerical Data and Functional Relationships in Science and Technology, New Series* (Springer, Verlag 11 117 bl.64, 1975).
- [19] A.A. Dakhel. *Microelectronics Reliability* 50 (2010) 211–216.

- [20] G.Frank and H.Kostlin, *Applied Physics A*, 27, (1982) 197.
- [21] J.H.W.DeWit, *Journal of Solid State Chemistry*, 13, (1975), 192-200.
- [22] P. Kofstad: "Non-stoichiometry, Diffusion and Electrical Conductivity in Binary Metal Oxides", Wiley, New York, 1972.
- [23] K.DAOU DI, élaboration et caractérisation de films minces d'oxyde d'indium dopé à l'étain obtenus par voie Sol-Gel, potentialité pour la réalisation d'électrodes sur silicium poreux, doctorate thesis, CLAUDE BERNARD University – LYON 1, 2002.
- [24] R. Botter, T. Aste, and D. Beruto. *Sensors and Actuators B [Chemical]* , 22:27–35, 1994.
- [25] C.M. GHIMBEU. Préparation et Caractérisation de couches minces d'oxydes métalliques semiconducteurs pour la détection de gaz polluants atmosphériques. doctorate thesis, Université Paul Verlaine de Metz. 2007.
- [26] Chander Shekhar, K.I. Gnanasekar, E. Prabhu. *Sensors and Actuators B155* (2011) 19–27.
- [27] A. Luque; S. Hegedus, (Eds.) John Wiley and Sons: New York, 2003; pp.663-700.
- [28] B. O'Regan; M. Gratzel, *Nature* 1991, 353, (6346), 737-740.
- [29] K.Takahashi;M.Konagai, *Amorphous Silicon Solar Cells*. North Oxford Academic Publishers: London, 1983,102-110.
- [30] C. Beneking; B. Rech; S. Wieder; O. Kluth; H. Wagner; W. Frammelsberger; R. Geyer; P. Lechner; H. Rübel; H. Schade, *Thin Solid Films* 1999, 351, (1-2), 241-246.
- [31] Takashi Koida\*, Hitoshi Sai. *Thin Solid Films* 518 (2010) 2930–2933.
- [32] T. Koida, H. Fujiwara, M. Kondo, *Appl. Phys. Express* 1 (2008) 041501.
- [33] A.R. West, 'Solid State Chemistry' John Willey & Sons, Singapore, (2003).
- [34] K. L. Chopra, 'Thin Film Phenomena', McGraw Hill, New York (1969).
- [35] Y. Gao, H. Niu, C. Q. Chen, *Chem. Phys. Lett.*, 367 (2003) (1-2) 141.
- [36] J. H. Park, *Chemical Vapor Deposition*. ASM International, 2001.
- [37] L. E. Scriven. *Mat. Res. Soc. Symp. Proc*, 121 (1988) 717–729

- [38] A. Busnaina, Nanomanufacturing handbook. Taylor & Francis Group, USA, 2007.
- [39] S.MENAKH, Contribution à l'étude des propriétés de films ZnO, magister thesis, Mentouri University, Constantine, 2010.
- [40] J. C. Viguit and J. Spitz, J. Electrochem. Soc.,122 (1975) 585.
- [41] A.MOUSTAGHFIR, Élaboration et caractérisation de couches minces d'oxyde de zinc. Application à la photoprotection du polycarbonate, Doctorate thesis, BLAISE PASCAL University, 2004.
- [42] M. Devika, K.T.R. Reddy, Appl.Phys.100 (2006) 023518.
- [43] B.D. Cullity, Elements of X-ray Diffraction, Addison-Wesley, New York, 1978.
- [44] K.L. Chopra, Thin Film Phenomena, McGraw-Hill, New York, 1969, pp. 270.
- [45] G.B. Williamson, R.C. Smallman , Philosophical Magazine 1(1956) 34–46.
- [46] J.I. Goldstein: “Practical Scanning Electron Microscopy”, in Chap. 3: “Electron Beam-Specimen Interaction”, ed. J.I. Goldstein and H. Yakowitz, PlenumPress, New York, 1975.
- [47] J.Bardeen, F.J. Blatt, L.H. Hall, Proceedings of Atlantic City Photoconductivity Conference in1954, Wiley and Chapman and Hall, New York, 1956.p. 146.
- [48] Lingyi Kong, Jin Ma, Fan Yang, Zhen Zhu. Applied Surface Science257 (2010) 518–522.
- [49] J. I. Pankove, Physical Review, 140 (6A) (1965) 2059-2065.
- [50] D. Redfield, Physical Review, 130 (3) (1963) 914-918.
- [51] F.Zhu, K.Zhang, E.Guenther, Ch.S. Jin , Institute of Materials Research & Engineering, Singapor, 2000.
- [52] M. Mekhnachea, A. Drici. Superlattices and Microstructures 49(2011) 510–518.
- [53] J. Gottesman, W.F.C. Ferguson, J. Opt. Soc. Am. 44 (1954) 368.
- [54] S. Kasap, P. Capper, “Springer Handbook of Electronic and Photonic Materials”, Springer Science + Business Media, Inc, New York, USA, 2006.

- [55] S. Rahman 'Elaboration et caracterisation de couches minces par spray pyrolyse Et Pulverisation Magnetron', Doctorat thesis, University Med Khider of Biskra, 2008.
- [56] G. Korotcenkov, A. Cerneavschi, V. Brinzari, A. Vasiliev, M. Ivanov, . Sensors and Actuators B 99 (2004) 297–303.
- [57] G. Korotcenkov, V. Brinzari, A. Cerneavschi, A. Cornet, J. Morante, A. Cabot, J. Arbiol. Sensors and Actuators B 84 (2002) 37–42.
- [58] Y. Shigesato, D C. Paine. Thin Solid Films, 1994, 238: 44.
- [59] K.H.L. Zhang, A. Walsh, C.R.A. Catlow, V.K. Lazarov, Nano Letters 10 (2010) 3740–3746.
- [60] J.-H. Lee, B.-O. Park. Surface and Coatings Technology 184 (2004) 102–107.
- [61] Z. Qiao, R. Latz, D. Mergel. Thin Solid Films 466 (2004) 250 – 258.
- [62] N.G. Pramod, S.N. Pandey, P.P. Sahay .Ceramics International 38 (2012) 4151–4158 .
- [63] T.P. Rao, M.C. Santhosh Kumar, Applied Surface Science 255 (2009) 4579–4584.
- [64] Thin film materials technology sputtering of Compound materials. William Andrew. 2004.
- [65] A. Amarala, P. Brogueira, C. Nunes de Carvalho, G. Lavareda , Surface and Coatings Technology 125 (2000) 151–156.
- [66] M. Jothibasa, C. Manoharan, S. Ramalingam, S. Dhanapandian, S. Johnson Jeyakumar, M. Bououdina, Journal of Molecular Structure 1049 (2013) 239–249.
- [67] S. Addala, L. Bouhdjer, A. Chala, A. Bouhdjar, O. Halimi, B. Boudine, and M. Sebais. Chin. Phys. B Vol. 22, No. 9 (2013) 098103.
- [68] C.S. Son, S.M. Kim, Y.H. Kim, S.I. Kim, Y.T. Kim, K.H. Yoon, I.H. Choi, H.C. Lopez, J.Korean Phys. Soc.45 (2004) S685.
- [69] H. Kim, J.S. Horwitz, W.H. Kim, Z.H. Kafafi, D.B. Chrisey, J. Appl. Phys. 91 (2002) 537.
- [70] A. Mosbah, S. Abed, N. Bouhssira, M.S. Aida, E. Tomasella. Materials Science and Engineering B 129 (2006) 144–149.

- [71] I.Y.Y. Bu. *Ceramics International* 40 (2014) 3445–345.
- [72] A. Bagheri Khatibani, A. Abdolazadeh Ziabari, S.M. Rozati, Z. Bargbidi, G.Kiriakidis, *Trans. Elect. Electron. Mater.*13 (2012) 111.
- [73] N. Lehraki, M.S. Aida, S. Abed, N. Attaf, A. Attaf, M. Poulain, *Current Applied Physics* 12 (2012) 1283e1287.
- [74] R.A. Street, *Hydrogenated Amorphous Silicon*, Cambridge University Press, 1991, p. 92.
- [75] M.S. Aida, A. Attaf, M.L. Benkedir, *Phil. Mag. B* 73 (1996) 339.
- [76] H. Moualkia, S. Hariech, M.S. Aida, N. Attaf, E.L. Laifa, *J. Phys. D: Appl. Phys.* 42 (2009) 135404.
- [77] S. Ilican, Y. Caglar, M. Caglar, B. Demirci, *J. Optoelectron. Adv. Mater.* 10 (2008) 2592.
- [78] M. Girtan, G. Folcher, *Surface and Coatings Technology* 172 (2003) 242–250.
- [79] Y. Igaski, H. Saito, *J. Appl. Phys.* 70 (1991) 3613.
- [80] J.E. Morris, M.I. Ridge, C.A. Bishop and R.P. Howson: *J. Appl. Phys.* 51,1847 (1980)
- [81] V. Senthilkumar, P. Vickraman, *Curr. Appl. Phys.* 10 (2010) 880.
- [82] A.K. Saxena, S.P. Singh, R. Thangaraj, O.P. Agnihotri, *Thin Solid Films* 117 (1984) 95.
- [83] P. Thilakan, C. Minarini, S. Loreti, E. Terzini, *Thin Solid Films* 388 (2001) 34
- [84] N.G. Pramod, S.N. Pandey, *Ceramics International* 40 (2014) 3461–3468.
- [85] M.A. Majeed Khana,, Wasi Khan, Maqusood Ahamed, Mansour Alhoshan, *Materials Letters* 79 (2012) 119–12.
- [86] J. Melsheimer, D. Ziegler, *Thin Solid Films* 129(1985)35.
- [87] C. Eberspacher, A.L. Fahrenbruch, R.H. Bube, *Thin Solid Films* 136 (1986) 1.
- [88] M.A. Kaid, A. Ashour, *Appl. Surf. Sci.* 253 (2007) 3029–3033.
- [89] D. Beena, K.J. Lethy, R. Vinodkumar, V.P. Mahadevan Pillai, *Applied Surface Science* 255 (2009) 8334–8342.

- [90] H. Kim, J.S. Horwitz, G.P. Kushto, S.B. Qadri, Z.H. Kafafi, D.B. Chrisey, *Appl. Phys. Lett.* 78 (2001) 1050.
- [91] Song D, Widenborg P and Chin W 2002 *Solar Energy Materials & Solar Cells* 73:1.
- [92] A. Bouhdjer, A. Attaf, H. Saidi, H. Bendjedidi, Y. Benkhetta, and I. Bouhaf. *J. Semicond.* 2015, 36 (8).
- [93] L. Bouhdjer, S. Addala, A. Chala, O. Halimi, B. Boudine and M. Sebais. *J. Semicond.* 2013, 34(4):043001-4
- [94] M Devika<sup>1</sup>, N Koteeswara Reddy et al *Semicond. Sci. Technol.* 21(2006) 1495–1501.
- [95] Duy Phong Pham, Bach Thang Phan, Van Dung Hoang et al. *Thin Solid Films* 570 (2014) 16–19.
- [96] Zhaohui Qiao, Dieter Mergel. *Thin Solid Films* 484 (2005) 146–153.
- [97] E. Terzini, *Mater. Sci. Eng. B* 77 (2000) 110.
- [98] W. Seilera, M. Nistor et al. *Solar Energy Materials & Solar Cells* 116 (2013) 34–42.
- [99] M.Jothibasa, C. Manoharan, S. Ramalingam, *Spectrochimica Acta Part A: Molecular and Biomolecular Spectroscopy* 122 (2014) 171–178.
- [100] T. S. Moss, *Proc. Phys. Soc. London, Sect. B* 67, 775 (1954).
- [101] Brus L. *J Phys Chem* 1986;90:2555.
- [102] Allan G, Delerue C. *Phys Rev B* 2007;75:195311.
- [103] Saâd Rahmane, Mohamed Salah Aida, Mohamed Abdou Djouadi, *Superlattices and Microstructures* 79 (2015) 148–155.
- [104] A. Sudha, S.L. Sharma, T.K. Maity. *Materials Letters* 157 (2015) 19–22.
- [105] Cha J-H, Ashok K, Kissinger NJS. *J Korean Phys Soc* 2011;59 (September (3)):2280–5.
- [106] D. Mergel, W. Stass, G. Ehl, D. Barthel, *J. Appl. Phys.* 88 (2000) 2437.
- [107] Kazuhiro Kato, Hideo Omoto, Takao Tomioka. *Thin Solid Films* 520 (2011) 110–116.

- [108] D.R. Gaskell, Introduction to the Thermodynamics of Materials, 4th Edition, Taylor.
- [109] A. Moses EzhilRaja, K.C. Lalithambika. Physica B 403 (2007) 544.
- [110] W.F. Wu and B.S. Chiou, Thin Solid Films, 247(1994) 201.
- [111] W.F. Wu and B.S. Chiou, Semicond. Sci. Technol, 11(1996) 196.

## Publications produced through this work

“Correlation between the structural, morphological, optical, and electrical properties of  $\text{In}_2\text{O}_3$  thin films obtained by an ultrasonic spray CVD process”

A. Bouhdjer, A. Attaf, H. Saidi, H. Bendjedidi, Y. Benkhetta, and I. Bouhaf . Journal of Semiconductors Vol. 36, No. 8. 2015.

“Structural, morphological, optical, and electrical properties of  $\text{In}_2\text{O}_3$  nanostructured thin films”

A. Bouhdjer, H. Saidia, A. Attaf, M.S. Aidab, Mohamed Jlassic, I. Bouhafa, Y. Benkhetta, H. Bendjedidi a. Optik 127 (2016) 7319–7325

“Influence of annealing temperature on  $\text{In}_2\text{O}_3$  properties grown by an ultrasonic spray CVD process”

A. Bouhdjer, A. Attaf, H. Saidi, Y. Benkhetta, M.S. Aida, I. Bouhaf, A. Rhil. Optik 127 (2016) 6329–6333.

# Study of Thin Layers of Indium Oxide ( $\text{In}_2\text{O}_3$ ) Elaborated by Chemical Means

## Abstract:

In this work indium oxide ( $\text{In}_2\text{O}_3$ ) thin films have been grown by ultrasonic spray technique using Indium chloride ( $\text{InCl}_3$ ) as precursor solution. The effect of the deposition time, solution flow rate, surface substrate and annealing temperature on the structural, morphological, optical and electrical properties of these films have been studied.

A number of techniques, as well as X-ray diffraction (XRD), SEM, and UV-visible are used to characterize the physical properties of these films. X-ray diffraction analysis showed that the films are polycrystalline in nature having cubic crystal structure and symmetry space group Ia $\bar{3}$ . On the other hand, the preferred growth orientation change from the (222) plane to (400) plane with the increase of the film thickness or decrease of the oxygen concentration in the film. SEM images show that the films are rough surface and the shape of grains changes with the change of the preferential growth orientation. The transmittance improvement of  $\text{In}_2\text{O}_3$  films was closely related to the good crystalline quality of the films and the optical gap is varied between 3.64 eV and 3.93 eV.

The electrical characterization of our films by the four-point method show that the (400)-plane textured  $\text{In}_2\text{O}_3/\text{KCL}$  films has the lowest resistivity ( $0.8 \times 10^{-3}$  cm).

**Key words:** Indium oxide; thin films; Ultrasonic Spray; optical and electrical properties.

## دراسة خصائص الشرائح الرقيقة لأوكسيد الأنديوم ( $n_2O_3$ ) المحضرة بطريقة كيميائية

\_\_\_\_\_:

قمنا في هذا العمل بتحضير شرائح رقيقة لأوكسيد الأنديوم ( $In_2O_3$ ) بواسطة تقنية الرش فوق الصوتي مستخدمين كلوريد الأنديوم ( $InCl_3$ ) ، وقد تم دراسة تأثير الترسيب، معدل تدفق المحلول. . ودرجة حرارة التـ. ين على الخصائص البنيوية، المورفولوجي الضوئية والكهربائية لهذه الشرائح الرقيقة.

استخدمنا عدة طرق لتشخيص الخصائص الفيزيائية لهاته الشرائح الرقيقة، مثل انعراج أشعة X التي بينت أن الشرائح متعددة البلورات وذات بنية مكعبة و  $Ia3$ ، أيضا الاتجاه البلوري المفضل لنمو الحبيبات يتغير من الاتجاه (222) (400) بزيادة سمك العينة أو نقص نسبة الأكسجين في الشرائح.

أظهرت صور المجهر الالكتروني أن . خشنة، كما أن شكل الحبيبات يتغير بتغير الاتجاه البلوري المفضل للنمو، نفاذية الشرائح الرقيقة لأوكسيد الأنديوم تتعلق كثيرا بالحالة البلورية لهاته الشرائح، وجدنا أيضا أن النطاق الممنوع (Eg) لهاته الشرائح يتغير من 3.64 (ev) 3.93 (ev).

أظهرت الخصائص الكهربائية أن kcl لها ممانعة دنيا ( $0.8 \cdot 10^{-3}$  cm).

### • لمفتاحية:

" اوكسيد الأنديوم، شرائح رقيقة، رش فوق صوتي، الخصائص الضوئية والكهربائية ".

# Etude des couches minces d'oxyde d'indium ( $\text{In}_2\text{O}_3$ ) élaborées par voie chimique

## Résumé:

Dans ce travail nous avons élaboré des couches minces d'oxyde d'indium ( $\text{In}_2\text{O}_3$ ) par la technique spray ultrasonique en utilisant chlorure d'indium comme solution de précurseur. L'effet du temps de dépôt, débit de la solution, surface de substrat et la température de recuit sur les propriétés structurales, morphologiques, optiques et électriques de ces films ont été étudiés.

Un certain nombre de techniques, ainsi que la diffraction des rayons X (XRD), SEM, et UV-visible sont utilisées pour caractériser les propriétés physiques de ces films. L'analyse par diffraction des rayons X a montré que les films sont de nature polycristalline ayant une structure cristalline cubique et un groupe d'espace de symétrie  $Ia3$ . D'autre part, l'orientation de croissance préférée est changée de l'orientation (222) vers la direction (400) avec l'augmentation de l'épaisseur du film ou de la diminution de la concentration d'oxygène dans le film. Images MEB montrent que les films sont surface rugueuse et la forme des grains change avec le changement de l'orientation de croissance préférentielle. L'amélioration de la transmission des films  $\text{In}_2\text{O}_3$  a été étroitement liée à la bonne qualité cristalline des films et l'écart optique varie entre 3,64 eV et 3,93 eV.

La caractérisation électrique de nos films par la méthode à quatre points montrent que les films  $\text{In}_2\text{O}_3$  / KCL a la résistivité la plus faible ( $0,8 \cdot 10^{-3}$  cm).

**Les mots clés :** Oxyde d'indium; couche mince; spray ultrasonique; les propriétés optiques et électriques.